




University of
Stavanger

FACULTY OF SCIENCE AND TECHNOLOGY

MASTER'S THESIS

Study program/Specialization: Petroleum Engineering /Production and Process	Spring semester, 2022 Open
Authors: Imran Abdulhameed Yaser El Taliani	 (signature of authors)
Supervisor: Professor Zhixin Yu	
Title of master's thesis: Catalytic conversion of CO ₂ to methanol over Cu/Zn/Al catalysts promoted with cerium and lanthanum	
Credits (ECTS): 30	
Key words: CO ₂ hydrogenation Methanol Cu-based catalysts Coprecipitation Catalyst characterization	Number of pages: 110 Stavanger, 30/06/2022

Acknowledgements

Firstly, we would like to express our most sincere gratitude and appreciation to our supervisor Professor Zhixin Yu for his professional guidance, continuous support, patience, motivation, enthusiasm, and valuable advice throughout our thesis.

To Kristian Stangeland and Song Lu, thank you for all your assistance. We are extremely grateful for all your guidance and support during the laboratory work and data analysis.

To the engineers and staff in the Department of Energy and Petroleum Engineering, we would not gain such practical experience in the labs without your continuous help and assistance. You were always available to support us in all the tasks which we had.

To all our classmates in Production and Process Engineering, although we worked on different projects, your considerable encouragement is greatly appreciated throughout the whole master's program.

Finally, to our beloved families in Lebanon and Nigeria, without you, we would not have been here. Thank you for your unconditional love and for always being supportive and caring throughout our studies.

Abstract

Carbon dioxide is one of the most prominent greenhouse gases, and the rise in its emissions is causing an increase in the world's temperature, which can have catastrophic effects if it is not controlled. Governments and organizations are working hard to implement sustainable solutions to address the issue of climate change. Among proposed solutions, the capture of CO₂ and its recycling to valuable fuels and chemicals has grabbed the attention of scientists. CO₂ hydrogenation to methanol is a promising technological solution as methanol is an important component in the fuel sector and carbon utilization is an environment friendly way to reduce the emissions.

Heterogenous catalytic systems are applied to convert CO₂ to methanol, and the commercial catalyst, Cu/ZnO/Al₂O₃, is one of the most used catalysts because of its relatively high performance and relatively low cost compared to other heterogenous catalyst. However, promoters were added to this catalyst to improve its performance and make it effective for industrial utilization of CO₂ hydrogenation to methanol. Cerium and lanthanum precursors showed good performance when added to the Cu/ZnO/Al₂O₃ catalyst when the catalyst is prepared with the co-precipitation method. However, it was demonstrated that more promising performance could be obtained when lanthanum was added to the conventional catalyst through a sequential preparation method. In this study, two series of catalysts were prepared by the coprecipitation method using different amounts of cerium and lanthanum as promoters. The performance of the promoted catalysts was compared to a conventional Cu/ZnO/Al₂O₃ catalyst. Furthermore, a La promoted catalyst was also prepared using a sequential preparation method by impregnating the Cu/ZnO/Al₂O₃ catalyst with lanthanum. The catalysts were characterized by XRD, TPR, TEM, N₂ adsorption-desorption, and N₂O chemisorption.

The catalytic performance of the catalysts was tested in a fixed bed reactor at 230°C, 40 bar, and H₂/CO₂/N₂ ratio of 3/1/1. The lanthanum promoted Cu/ZnO/Al₂O₃ catalyst prepared by the sequential preparation method showed the highest methanol selectivity of 49.9% and space time yield of 1357 mmol·gcat⁻¹·h⁻¹. For the catalyst prepared by co-precipitation, the catalysts containing 2% cerium and 4% lanthanum showed the best catalytic performance. It was also observed that the promoted catalysts showed superior performance at different reaction conditions (temperature, pressures, and gas-hour space velocity) compared to the unpromoted catalyst. Furthermore, long-term tests over 72 h indicate that the stability of the catalyst is enhanced for the La and Ce promoted catalysts.

Abbreviations

ALD	atomic layer deposition
BET	Brunauer–Emmet–Teller
BJH	Barret–Joyner–Halenda
DFT	density functional theory
DRIFTS	diffuse reflectance infrared fourier transform spectroscopy
DME	dimethyl ether
GC	gas chromatography
GHG	greenhouse gas
GHSV	gas hourly space velocity
JCPDS	Joint Committee on Powder Diffraction Standards
RWGS	reverse water-gas shift
SA _{Cu}	Cu surface area
SMSI	strong metal support interaction
STY	space-time yield
TEM	transmission electron microscopy
TOF	turnover frequency
TPR	temperature-programmed reduction
XPS	X-ray photoelectron spectroscopy
XRD	X-ray diffraction

Table of Contents

Acknowledgements	ii
Abstract	iii
Abbreviations	iv
Table of Contents	v
List of Figures	viii
List of Tables	x
1 Introduction	1
1.1 Greenhouse gases and energy transition.....	1
1.2 Scope of the Study	4
2 CO₂ hydrogenation to methanol	5
2.1 Thermodynamics	5
2.2 Historical development of catalysts.....	7
2.3 Methanol synthesis catalyst	8
2.3.1 Copper-based catalyst	8
2.3.2 Metal oxides supports and promoters	9
2.3.3 Other supports	17
2.3.4 Bi-metallic Cu based catalysts	18
2.4 Reaction mechanism.....	20
2.5 Catalyst synthesis methods.....	23
2.5.1 Solid-state combustion.....	23
2.5.2 Sol–gel auto-combustion	23
2.5.3 Reduction–precipitation	24
2.5.4 Solid state reaction	24
2.5.5 Co-precipitation	25
2.5.5.1 Aging.....	27
2.5.5.2 Calcination	28
2.5.5.3 Reduction	29
2.6 Catalyst Characterization.....	29
2.6.1 X-ray diffraction (XRD)	29
2.6.2 Temperature programmed reduction.....	32
2.6.3 Transmission electron microscopy (TEM)	33
2.6.4 Chemisorption.....	34

2.6.5 N ₂ adsorption desorption.....	36
2.6.6 Gas chromatography (GC).....	38
2.7 Kinetics of methanol synthesis	40
2.7.1 Kinetic models	40
2.7.2 Power law model.....	41
3 Experimental.....	46
3.1. Materials and equipment	46
3.2 Catalyst preparation.....	47
3.3 Catalyst characterization.....	48
3.3.1 X-Ray diffraction	48
3.3.2 Nitrogen adsorption-desorption	49
3.3.3 Temperature programmed reduction	49
3.3.4 N ₂ O chemisorption.....	49
3.3.5 Transmission electron microscopy	50
3.4 Catalytic activity tests.....	50
4 Results and discussion.....	53
4.1 Characterization of Catalysts.....	53
4.1.1 XRD analysis of as-prepared catalysts.....	53
4.1.2 XRD of calcined catalysts.....	54
4.1.3 XRD of reduced catalysts	55
4.1.4 TPR analysis	56
4.1.5 N ₂ adsorption-desorption	57
4.1.6 N ₂ O chemisorption.....	59
4.1.7 TEM	60
4.2 Methanol synthesis activity tests	61
4.2.1 Activity and selectivity of different catalysts	61
4.2.2 Effect of GHSV.....	64
4.2.3 Effect of temperature	66
4.2.4 The effect of pressure	66
5 Conclusions and future work	70
5.1 Conclusions	70
5.2 Recommendations for future work	71
References	72

Appendices	90
Appendix A: Calculations of catalysts synthesis.....	90
Appendix B: Description of reaction and data collection procedure.....	92

List of Figures

Figure 1.1: Methanol production capacity [5].	2
Figure 1.2: Methanol production by source between years 2020 and 2050 [6].	3
Figure 2.1: Temperature effect on ΔG for CO and CO ₂ hydrogenation reactions [11].	6
Figure 2.2: Pressure and temperature effect on (a) CO ₂ conversion and (b) methanol selectivity at phase and chemical equilibrium (Dashed lines depicts the chemical equilibrium predicted by gas phase thermodynamics) [12].	7
Figure 2.3: ZrO ₂ phases effect on the catalytic performance [56, 59, 61].	12
Figure 2.4: (a) STY of methanol vs reaction time over a period of 100 h (b) product selectivity vs reaction time [64].	13
Figure 2.5: CO ₂ conversion of for three different promoted catalyst systems for hydrogenation of CO ₂ over 12 h time on stream (TOS). Reaction conditions: 250°C, 40 bar and H ₂ /CO ₂ =3, and GHSV = 4000 h ⁻¹ [69].	15
Figure 2.6: Surface reaction sequences for CO ₂ conversion to methanol in the “formate” path and the “RWGS + CO-hydro” path on PdCu(111) [92].	20
Figure 2.7: The pathways CO ₂ hydrogenation to methanol over Cu-based catalysts. [1]	22
Figure 2.8: pH profile during the ageing of Cu/Zn precipitate [117].	28
Figure 2.9: Graphical representation of Bragg’s law [128].	30
Figure 2.10: TEM classification [139].	34
Figure 2.11: The working principle of TEM [139].	35
Figure 2.12: (a) Types of physisorption isotherms; (b) Types of hysteresis loops [146].	38
Figure 2.13: Classification of the various chromatography methods [150].	39
Figure 2.14: Parity Plots for (a) methanol synthesis (b) reverse water gas shift reaction [152].	45
Figure 3.1: Schematic diagram of the CO ₂ hydrogenation experimental setup.	51
Figure 4.1: XRD of the as-prepared samples (a) Ce-promoted; (b) La-promoted.	53
Figure 4.2: XRD of the calcined samples (a) Ce-promoted; (b) La-promoted. (∇) CuO (♦) ZnO (◀) CeO ₂ (*) La ₂ O ₃ .	55
Figure 4.3: XRD pattern of the reduced unpromoted and promoted catalysts. (♦) ZnO (●) Cu ⁰ (■) Cu ₂ O.	56
Figure 4.4: H ₂ -TPR profiles of calcined catalysts.	57
Figure 4.5: N ₂ adsorption-desorption isotherms of calcined samples.	58
Figure 4.6: Pore size distribution of calcined samples.	59

Figure 4.7: TEM images of the reduced-passivated La/CuZnAl catalyst (a-c) at different magnifications and CuZnAl-4La catalyst (d and e).	61
Figure 4.8: CO ₂ conversion and CH ₃ OH selectivity of unpromoted and Ce promoted catalysts	62
Figure 4.9: CO ₂ conversion and Methanol selectivity of promoted CuZnAl catalyst with La	63
Figure 4.10: Effect of GHSV on CO ₂ conversion and Methanol selectivity over CuZnAl-4La catalyst. Reaction conditions: 230°C, 40 bar and H ₂ /CO ₂ /N ₂ ratio of 3:1:1.	65
Figure 4.11: The effect of temperature on CO ₂ conversion and Methanol selectivity for the CuZnAl-0, CuZnAl-4Ce and CuZnAl-4La catalysts.	66
Figure 4.12: Effect of pressure on CO ₂ conversion and selectivity over CuZnAl-4Ce Reaction conditions: 230°C, H ₂ /CO ₂ /N ₂ ratio of 3/1/1.	67
Figure 4.13: CO ₂ conversion and methanol selectivity over 72 h for (a) CuZnAl-0; (b) CuZnAl-4Ce; (c) CuZnAl-4La; (d) La/CuZnAl.....	68

List of Tables

Table 2.1: Comparison of the activity and selectivity of different Cu-based catalyst synthesized under different conditions.....	16
Table 3.1: List of chemicals utilized for catalyst preparation.	46
Table 3.2: List of Gases used during this work.....	47
Table 3.3: Denotations and composition of the prepared catalysts.....	47
Table 4.1: Summary of the N ₂ adsorption-desorption data, crystallite size and particle size of the calcined catalysts.....	60
Table 4.2: Summary of CO ₂ conversion, CH ₃ OH selectivity as well as space time yield of different catalysts.	64
Table 4.3: The effect of GHSV on CO ₂ conversion, methanol selectivity and space time yield of the performance of the CuZnAl-4La catalyst.	65
Table 4.4: Methanol selectivity and STY of reaction at 24 h and after 72 h TOS.....	68

1. Introduction

1.1 Greenhouse gases and energy transition

The dependence on renewable energy resources has increased in the past few years and is predicted to continue to grow in the short and medium-term. However, fossil fuels remain the main source of energy, especially in the transportation and industrial sectors, resulting in high CO₂ emissions [1]. The emission of greenhouse gases (GHGs) from the combustion of fossil fuels is a huge threat to the human environment [2]. The continuous increase in carbon emissions has led to an increase in the earth's temperature, resulting in global warming. This has encouraged many countries to deploy low greenhouse gas emission technologies to limit emissions, such as solar and wind power, as well as carbon storage and sequestration [3]. The CO₂ generated in different sectors can be utilized in the manufacturing of valuable chemicals and energy carriers, which could help limit the environmental problems the global population is experiencing due to global warming.

CO₂ has been used at the industrial scale to obtain different valuable chemical products, such as methanol, urea, and formic acids. Among them, the synthesis of urea and methanol are the predominant consumers of CO₂ in the industry today [1]. Although the current estimates indicate that the development of renewables will be more favoured in the long run, the natural inexistence of these sources in some environments and their intermittency is a drawback for increasing full dependency on them in the energy market. Therefore, the conversion of renewable energy into different energy carriers (e.g., hydrogen, methanol, or ammonia) can help the integration of renewables into various sectors. The advantage of liquid energy carriers such as methanol and ammonia is that it is easier and cheaper to distribute and store compared to hydrogen, which requires significant infrastructure investment [4]. Methanol has several applications and can be an important intermediate chemical utilized in the production of highly demanded chemicals such as formaldehyde, dimethyl ether, and acetic acid. It can also be utilized directly as a fuel [4]. The global production of methanol was 157 million metric tons in 2020. However, this amount is expected to double by 2030, and it may reach 311 million metric tons. This increase is based on over 100 methanol plants that are in the planning phase and have been announced around the world, which will begin production by the end of the decade [1]. Figure 1.1 shows the production capacity of methanol worldwide from 2018 to 2020 and the forecast for 2030.

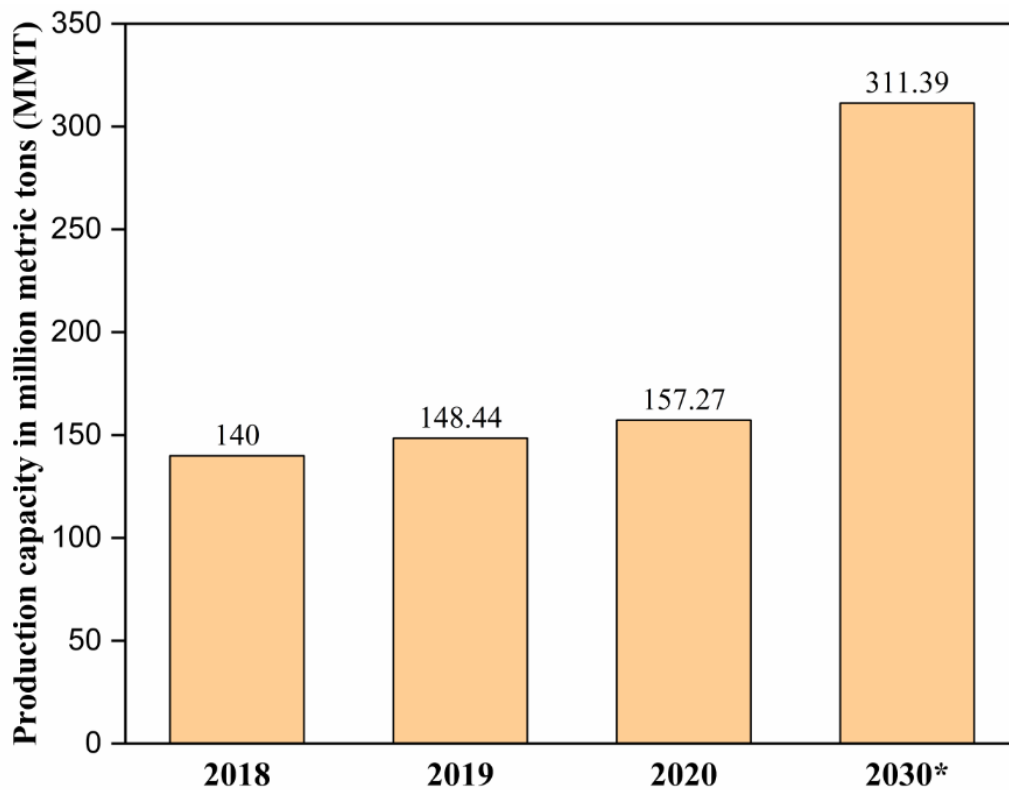


Figure 1.1: Methanol production capacity [5].

The expected increase in methanol production is also related to the diversity of methanol sources in the future. Nowadays, methanol production depends mainly on fossil fuels as its feedstock. However, it is predicted that the production of methanol from captured CO₂ combined with renewable hydrogen (e-methanol) and bio sources (bio-methanol) will increase significantly in the upcoming years, thereby contributing to the overall methanol production in the next decades. Figure 1.2 compares methanol production in 2020 to the production expected in 2050 from different feedstocks.

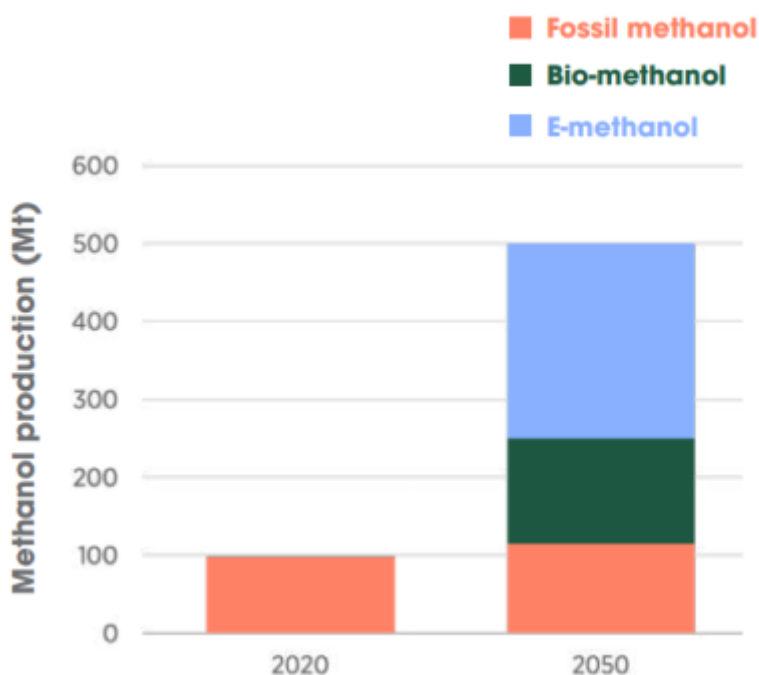


Figure 1.2: Methanol production by source between years 2020 and 2050 [6].

Renewable methanol synthesis could be a very important industrial catalytic reaction because it has the potential to play a significant role in energy production and distribution for achieving the goals related to a sustainable environment [7]. Renewable methanol could reduce GHG emissions from many sectors since CO₂ is the main driver of the global challenges faced today [8].

Syngas (CO₂/CO/H₂/H₂O) is used commercially to produce methanol [7]. Both theoretical and experimental studies have been performed on the catalytic hydrogenation of CO₂, which show that the production of methanol in the absence of CO is more challenging. Different types of catalytic systems have been employed, including heterogeneous, homogeneous, electrochemical and photocatalysis. Currently, the use of heterogeneous catalysts is preferred in the synthesis of renewable methanol at an industrial scale. The studies on heterogeneous catalysts focus on different types of catalysts, such as Cu-based catalysts, Pd-based catalysts, Co nanoparticles, and In-based catalysts [8]. The studies typically focus on enhancing the activity and methanol selectivity. The higher amounts of water and production of by-products, especially CO, are typically limiting the activity and selectivity of the catalysts. The use of promoters to limit the effect of water and CO production is a promising approach to enhance the performance of the catalyst for CO₂ hydrogenation to methanol.

1.2 Scope of the Study

In this thesis, we firstly review the recent improvements in heterogeneous catalysts and the research on enhancing the process for the direct hydrogenation of CO₂ to methanol. The focus is on the enhancement of the conventional Cu/ZnO-based catalysts and the promising new catalytic systems that have been investigated for methanol synthesis from CO₂ [1]. The first part of the thesis highlights the important studies that focused on developing active and selective catalysts based on mechanistic investigations as well as advanced synthesis and catalyst design. Furthermore, a summary of the most promising catalytic systems to develop enhanced heterogeneous catalysts for methanol synthesis from CO₂ is presented.

In the second part of the thesis, we investigate different copper-zinc-alumina (CuZnAl) catalysts synthesized by the co-precipitation method. Two series of catalysts were prepared, using Ce and La as promoters. The content of Ce and La in the promoted catalysts was 2%, 4%, and 6%. Additionally, another La promoted catalyst was prepared by sequential impregnation. Activity tests were conducted to study the performance of the synthesized catalysts for CO₂ hydrogenation. Stability tests were conducted to investigate the influence of the promoters on catalyst deactivation. The effect of pressure, temperature, and gas hourly space velocity (GHSV) was also studied. The catalyst was characterized by X-ray diffraction (XRD), N₂O chemisorption, Transmission electron microscopy (TEM), Brunauer-Emmett-Teller (BET), and temperature programmed reduction (H₂-TPR) analysis.

2. CO₂ hydrogenation to methanol

2.1 Thermodynamics

The CO₂ compound is thermodynamically stable and has relatively low reactivity. Therefore, it is essential to overcome the thermodynamic barrier if the compound is to be converted into methanol [9]. The main reactions involved in methanol synthesis are the conversion of CO₂ and CO into methanol (Eq. 2.1 and Eq 2.2) and the reverse water-gas shift (RWGS) reaction (Eq 2.3). Thermodynamically, synthesizing methanol from CO₂ is favored at lower temperatures and high reaction pressures. At increased temperatures, the endothermic RWGS reaction is more favorable (>200°C), which can lead to increased production of CO [10]. Furthermore, other compounds are highly favorable at the typically employed reaction conditions (e.g., hydrocarbons and other oxygenates). Therefore, highly selective catalysts are needed to limit the amount of by-products in methanol synthesis.



Suresh et al. [11] carried out a thermodynamic feasibility analysis on the reactions above using the equilibrium reactor model on Aspen Plus software. They utilized the predictive SRK-EOS to support the non-ideal characteristics in the calculation of the Gibbs Energy. Since the reactions are heavily dependent on temperature, a sensitivity analysis of the effect of this parameter on the equilibrium constant (K) was done in the temperature ranges from 25°C to 500°C under a pressure of 1 bar. Figure 2.1 shows the effect of increasing temperature on ΔG. Hydrogenation of CO₂ and CO at increased temperatures led to an increase in the ΔG values, which proves that the reactions are exothermic, while in the case of the so-called RWGS reaction, the ΔG values followed a declining trend with increased temperature, and this is typical of an endothermic reaction. Therefore, the synthesis of methanol from CO₂ hydrogenation is thermodynamically favored at lower temperatures, but the challenge is the inertness of CO₂, which typically requires higher temperatures to reach sufficient reaction rates.

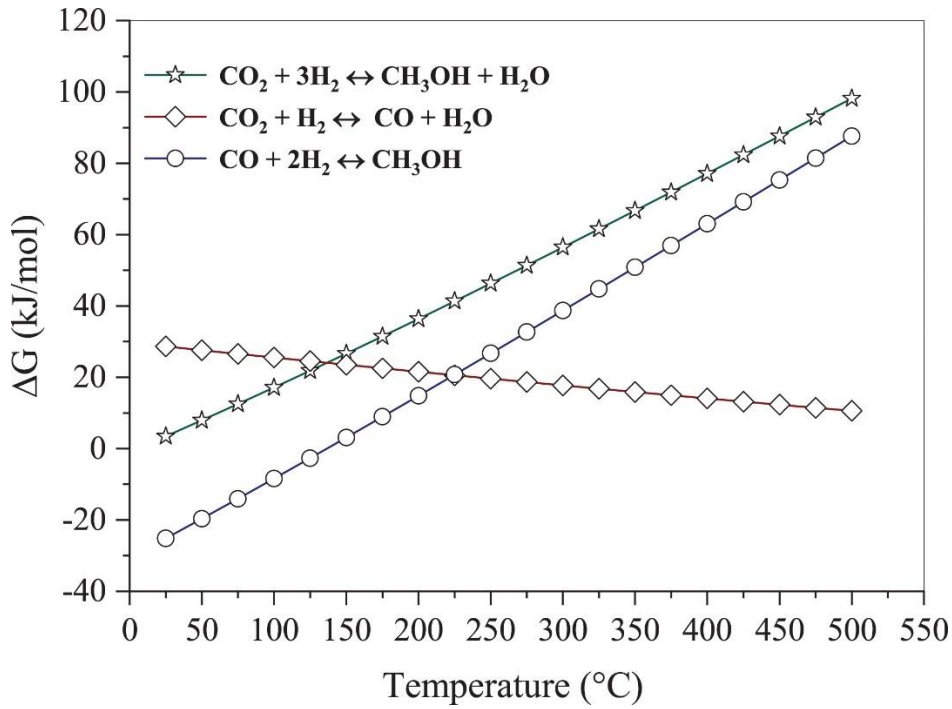


Figure 2.1: Temperature effect on ΔG for CO and CO₂ hydrogenation reactions [11].

Stangeland et al. [12] extensively studied the effect of pressure and temperature on the CO₂ conversion and methanol selectivity based on a stoichiometric H₂/CO₂ ratio of 3/1. Their findings agree with that of Suresh et al. [11] and show that significant conversion of CO₂ can be achieved at lower temperatures and higher pressures. Figure 2.2a and b show the CO₂ conversion and methanol selectivity at different reaction conditions, respectively. The CO₂ conversion lines in Figure 2.2a merge at higher temperatures, and this is because the RWGS reaction is endothermic and is not affected by the reaction pressure [12].

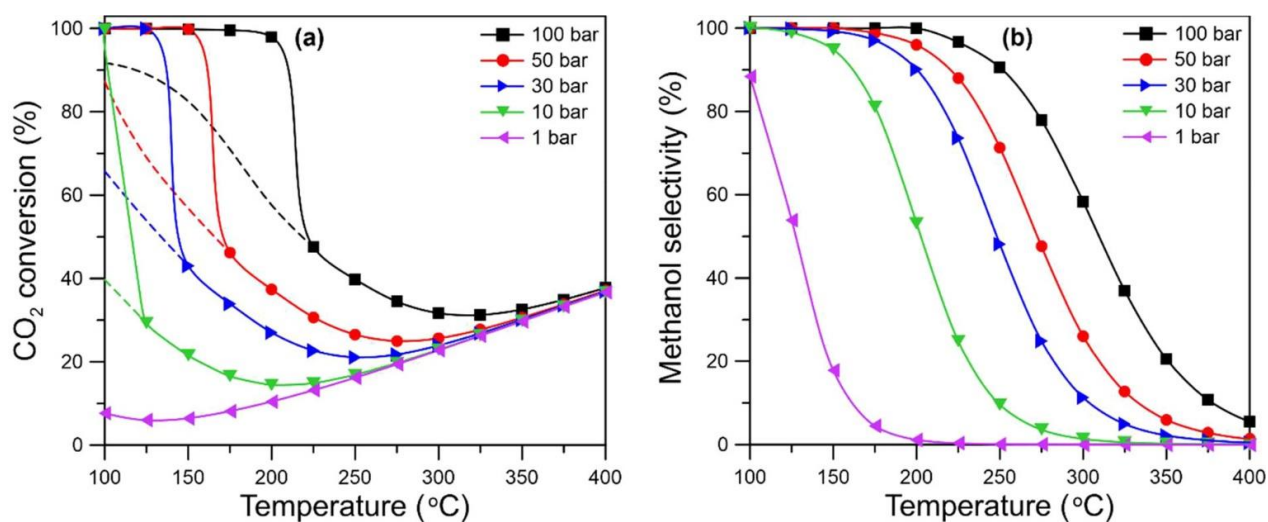


Figure 2.2: Pressure and temperature effect on (a) CO₂ conversion and (b) methanol selectivity at phase and chemical equilibrium (Dashed lines depicts the chemical equilibrium predicted by gas phase thermodynamics) [12].

2.2 Historical development of catalysts

Cu-based catalyst has been mostly used throughout history. The utilization of Cu-based catalysts for synthesizing methanol by the CO/CO₂ hydrogenation route is as old as the beginning of the process itself [13]. The foremost patent for methanol synthesis based on Cu-catalyst was filed by Patart in 1921 [14]. However, due to the catalyst's susceptibility to sulfur poisoning, it did not gain attention for commercial adaptability. Later, during the late 1960s, Imperial chemical industries developed the widely adopted Cu/ZnO catalyst which was effective at pressures between 50-100 bar and temperatures around 200-300°C for methanol synthesis with syngas (CO+H₂) as the feedstock [15]. As a result of the development and industrialization of the gas purification systems, which enabled the syngas from crude oil, natural gas and coal to be free from sulfur poisoning [16], interest in Cu-based catalysts aggrandized with the development of a ternary Cu-based catalyst that was synthesized by in situ reductions (Copper Oxide (CuO)-Zinc Oxide (ZnO)- Chromium Oxide (CrO) [17]. Eventually, significant studies and research realized that alumina could replace CrO to increase the catalysts longevity. The copper-zinc-alumina catalyst was prepared by co-precipitating soluble copper and zinc salts with an alkaline carbonate solution. The mixed solution of carbonates is subjected to heating to form a mixture composed of oxides. Finally, the resultant product is mixed with aluminum oxide [18].

As far back as 1930, the concept of the possibility of methanol synthesis from CO₂ being the only feedstock was known. It was also proposed that synthesizing methanol from CO and H₂O may not be direct, particularly when arriving at a steady state. The formation of CO and H₂O from the reaction of H₂ and CO₂ over methanol catalysts was eminent at atmospheric pressure [19]. This reaction was confirmed in 1932 alongside the consistent methanol formation over unsupported zinc–copper–aluminum catalyst under high temperatures and certain pressures [20]. However, despite the catalyst not being particularly active, it paved an idea for the course of the reaction. In 1945, Ipatieff and Monroe [21] conducted an experiment to study the actual reaction of CO₂ and hydrogen over copper-zinc-alumina catalysts compared to other studies that relatively dismissed the statement because of the prior understanding that the CO₂ reduces to CO especially at high pressures and the reaction follows that which is typical of syngas (CO + H₂) [22, 23]. They observed that catalysts with copper or alumina separately did not catalyze the formation of methanol from CO₂ and hydrogen. Therefore, it is necessary to have both in a mixture for the catalyst to be active. The catalyst with the highest activity had a Cu content ranging between 8-28% and achieved a conversion of over 90% at 409 atm and 282°C. Similarly, when CO was utilized as the carbon source under the same conditions as the former, the methanol conversion was between 39-43%, where only 10-15% and 32-41% of CO converted to methanol and DME [21].

Comprehensive research on the hydrogenation of CO₂ to methanol and for a more selective, stable and active catalyst gained momentum in the 1980s [13]. It is understood that the formation of methanol in this process takes place mainly from CO₂, while CO plays the role of scavenger for surface oxygen [15, 25, 26]. The bulk amount of CO₂ emitted from the production and transportation industries has made the requirement for environmental cleaning paramount to deter global warming and meet up with the climate goals [27, 28]. Due to this challenge and the demand for clean energy, significant research efforts have been devoted to improving the process of synthesizing methanol with CO₂ as the sole feedstock [15]. However, the major constraint is the lack of effective catalysts.

2.3 Methanol synthesis catalyst

2.3.1 Copper-based catalyst

CO₂ hydrogenation has been under extensive investigation by theoretical and experimental methods for the past decades. To increase the viability of methanol via CO₂ hydrogenation, it

is necessary to develop a catalytic system that offers high selectivity towards methanol, improved activity and restricts the production of bi-products [29]. The most efficient catalyst utilized at the industrial level for methanol synthesis is the ternary copper, zinc oxide, and aluminum oxide (Cu/ZnO/Al₂O₃) catalyst. However, these catalysts are optimized for methanol production via the syngas route. Therefore, catalyst's efficiency requires further improvements to be more suitable in methanol synthesis from CO₂ [30].

2.3.2 Metal oxide supports and promoters

Currently, the commercial synthesis of methanol is done over Cu/ZnO/Al₂O₃ catalysts utilizing syngas as the feedstock at 50-100 bar pressure and temperature range of 220-350°C. The conventional catalyst comprises 50-70 atomic% of CuO, 20-50% ZnO and 5-20% Al₂O₃ (promoter) [13]. High methanol selectivity and activity are the general targets for effective catalyst development. These properties are related to the surface area of Cu, which is partly achieved via a uniform and periodic distribution of Cu and ZnO nanoparticles. For decades the nature of the active site has been debated. Some researchers have proposed that metallic Cu⁰ is the active site [31, 32], while others have suggested that Cu⁺ dissolved in ZnO and stabilized by promoters also contributes [33, 34]. In addition, Frost and Liao [35, 36] proposed that Cu at the Schottky junction, which is at the interface between metallic Cu and ZnO, as the active site. Another model by Topsoe [37, 38] suggests that the strong metal support interaction (SMSI) plays a vital role in methanol synthesis. Under typically applied reduction conditions, the model is based on Zn atoms migrating to the copper surface, thereby generating active sites for methanol synthesis. Another study combining theoretical modelling and experimental investigations reported that the Zn decorated Cu surface serves as the active site for synthesizing methanol using CO₂ as feed. [39]. It has also been observed that ZnO acts as a structural promoter, which limits the sintering of Cu, enhances the lattice oxygen vacant sites, and supports an active electron pair towards activating key intermediates in methanol synthesis. Furthermore, the improved dispersion of Cu by addition of the Al₂O₃ promoter aids the enhancement of both the activity and stability [40–42].

To improve the efficiency of the Cu/ZnO catalysts, different types of modification can be done by adding a variety of stabilizers and promoters. Stangeland et al. [43] investigated the effect of indium oxide (In₂O₃), where they observed that the methanol selectivity increased when In was added to the conventional Cu/Zn/Al₂O₃ catalyst, but the activity was reduced. Furthermore, when long-term stability tests were performed over 72 hours, the CO₂ conversion over the In

promoted catalyst remained relatively stable. The Cu crystallite size of the In promoted catalyst slightly increased from 12 to 14 nm, while that of the unpromoted catalyst increased from 13 to 20 nm. This resulted in a lower deactivation and improved stability of the former catalyst as compared to the latter. Matsumura & Ishibe [44] also confirmed that the presence of In on the surface of Cu during methanol reforming process over a Cu/ZnO-based catalyst limited CO formation, thereby improving the selectivity.

Several studies have also been carried out where CeO₂ was introduced as a support and co-support for the catalysts for CO₂ hydrogenation to methanol [45–50]. It was observed to have a stronger adsorption affinity for CO₂ due to its oxygen vacancies and strong basicity. When introduced as a support, it facilitates spillover of atomic hydrogen and enhances dispersion of Cu particles [46, 49]. Despite the positive effect of ceria, it had an adverse influence on the surface area of the catalyst, which reduced the activity [51]. Furthermore, a study by Rodriguez et al. showed that combining Cu metal and the oxide sites in the Cu-CeO₂ interface generates active sites favorable for the reaction pathways for the methanol synthesis from CO₂ [49]. The application of combining theoretical and experimental methods was used to demonstrate the hydrogenation of CO₂ over an inverse CeO_x/Cu(111) surface, where complementary surface analysis by X-ray photoelectron spectroscopy (XPS) determined Ce₂O₃/Cu (111) as the active phase of the catalyst. It was also realized that the inverse catalyst was much more active for methanol synthesis than Cu(111) and ZnO/Cu(111). Additionally, a decrease in the activation energy for the conversion process was observed, which declined from 25 kcal/mol on Cu(111) to 16 kcal/mol on ZnO/Cu(111) and lastly, 13 kcal/mol on CeO_x/Cu(111) [13]. After the surface analysis was carried out using ambient pressure infrared reflection absorption spectroscopy and ambient pressure XPS, it was realized that formates and carboxylates are formed during the reaction. Thus, CeO_x-Cu rich in Ce³⁺ sites was proposed to be the active catalyst, which enhanced the stability of the carboxylate species that is a key intermediate for methanol production [10]. In the ternary CuZnCeO_x, CeO_x promotes the spillover of atomic hydrogen and enhances Cu particles dispersion, whereas ZnO helps to increase the dispersion of the CeO_x nanoparticles. As a result, the CuZnCeO_x catalyst has been shown to be better than the catalyst containing only CuZnO_x [50]. However, it was observed that the CuZnCeO_x catalyst has a higher selectivity towards CO [52].

The effect of gallium oxide (Ga₂O₃) has also been studied, and it was observed that its small particle size enhanced the formation of an intermediary phase of Cu between Cu⁰, Cu₂⁺ and Cu⁺ to some extent [53]. The catalysts derived from Ga modified hydrotalcite demonstrated

improved dispersion of the Cu particles and the creation of active Cu-ZnO sites, which significantly increased the efficiency of Ga modified Cu-based catalyst for methanol synthesis via CO₂ hydrogenation [54]. Li et al. [55] suggested that adding Ga³⁺ to the Cu/ZnO catalyst's precursor sped up the reduction of ZnO to Zn⁰ via the formation of an “electronic heterojunction of ZnO-MGa (M= Cu or Zn)”, where the formation of CuZn is due to the interaction between Cu nanoparticles and reduced Zn⁰. The hydrotalcite-derived catalysts were able to preserve their morphology in ultrafine layers after calcination treatment, which changes the phase to amorphous. These amorphous phases are characterized by metallic Cu crystals, which are small, properly dispersed and have a large surface area containing sparse amounts of Zn atoms [55].

Amongst the promoters for Cu based catalysts, ZrO₂ is by far the most investigated after ZnO. However, it is often combined with ZnO in ternary catalysts [56]. Rungtaweivoranit et al. analysed Cu confined in Zr based metal organic framework (MOF) using XPS [57]. This indicated that there is a strong interaction between Cu and ZrO₂ due to the existence of several Cu oxidation states and the increased interfacial contact surface between Cu and ZrO_x. The binary catalyst promoted by ZrO₂ had better performance relative to the conventional Cu/Zn/Al₂O₃ catalyst [57]. Besides from the high thermal stability of ZrO₂ when subjected to reduction and oxidization, its surface basicity and hydrophobicity properties makes it a good support [56]. Sloczynski et al. [58] studied the effect of ZrO₂ on the conventional catalyst and reported an improvement of the Cu surface area and an alteration of the Cu⁺/Cu⁰ ratio. Additionally, uniform dispersion of CuO on the ZrO₂ surface can lead to the formation of a large interface that is favorable for methanol synthesis [56].

ZrO₂ occurs in various crystal structural phases (polymorphs): monoclinic m-ZrO₂ and amorphous, a-ZrO₂ and t-ZrO₂. At low temperatures, ZrO₂ assumes the a-ZrO₂ and t-ZrO₂ crystal structure, and it later converts to m-ZrO₂ at higher temperatures [13]. However, after a-ZrO₂ was impregnated with a Cu solution, a significant amount of the Cu species was impregnated into a-ZrO₂ after calcination [59]. Thus, facilitating the formation of a mixed oxide of Cu-Zr mixed oxide. Systematic investigations on the effect of the different ZrO₂ polymorphs, including the -a, -t and -m phases on the Cu structure, interactions between Cu-ZrO₂ and adsorption-desorption of CO₂ and H₂ were carried out alongside a study of the catalytic performance of the catalysts that are based on the different polymorphs (Cu/a-ZrO₂, Cu/t-ZrO₂ and Cu/m-ZrO₂) [60]. By employing various analytical techniques, the surface area of Cu was found to increase in the trend: Cu/a-ZrO₂ > Cu/t-ZrO₂ > Cu/m-ZrO₂. This trend is also in correlation with the methanol yield, and the highest methanol yield was obtained on the Cu/a-

ZrO₂ catalyst. Tada et al. [59] also compared the interfacial sites of the different ZrO₂ polymorphs. They found that a higher amount of active interfacial sites of Cu/a-ZrO₂ relative to Cu/t-ZrO₂ and Cu/m-ZrO₂ could be obtained when the prepared amorphous Cu-Zr-O oxides were reduced without the formation of Cu crystalline particles. The adsorption of methanol on Cu/a-ZrO₂ and Cu/m-ZrO₂ was weaker, which might be responsible for the higher methanol selectivity by suppressing unwanted methanol decomposition. A comparison of the effects of the different ZrO₂ phases on the catalytic performance is portrayed in Figure 2.3 [56, 61, 59]. It is largely agreed that the amorphous ZrO₂ promotes the stabilization of small Cu particles, and the interaction with these small particles increases the CO₂ conversion and methanol selectivity of the catalyst.



Figure 2.3: ZrO₂ phases effect on the catalytic performance [56, 59, 61].

However, after comparison of the methanol turnover frequency (TOF_{methanol}), the Cu/t-ZrO₂ showed higher TOF than that of Cu/a-ZrO₂. This might be related to a strong Cu-ZrO₂ interaction and an increased surface concentration of atomic hydrogen [60].

Ro et al. [62] conducted methanol synthesis via CO₂ hydrogenation over Cu/ZrO₂ catalyst prepared by the atomic layer deposition (ALD) and controlled surface reaction (CSR) methods. The formation of Cu-ZrO₂ interfacial sites enhanced the TOF. The oxidation states of the Cu and ZrO₂ species were determined by X-ray absorption near edge structure (XANES) study. It was confirmed that Cu⁰ and Zr⁴⁺ were the main oxidation state for the species. Furthermore, it

was proposed that an interface of Cu-ZrO_x is created because of the diffusion of some of the Cu atoms into the ZrO₂ structure, where the valence state of Cu and Zr was Cu⁺ and Zr^{δ+} (δ < 4). Zhu et al. [63] and Rungtaweeworant et al. [57] conducted a study on Zr constructed metal organic framework (MOF) structure (UiO-66). The results from their characterization showed that molecular interactions with both metals and oxides are necessary. These interactions led to highly improved synergistic effect on activity and selectivity. Zhu et al. [63] further showed that materials that consisted of atomically dispersed Cu-O-Zr sites or isolated Cu particles only favored the RWGS reaction. On the other hand, the MOF structure (UiO-66) in which the missing linker defects are occupied by Cu particles developed a higher fraction of metallic Cu interfaced to ZrO₂ nodes. This led to a high adsorption capacity for CO₂ and increased the activity and selectivity during low temperature methanol synthesis. An et al. [64] also conducted a study where MOFs were utilized, in which pre-assembled bipyridine (bpy) and Zr₆(μ₃-O)₄(μ₃-OH)₄ sites present in UiO-bpy MOFs was used to anchor infinitesimal Cu/ZnO_x nanoparticles, thereby deterring the phase separation between Cu and ZnO_x by MOF cavity confinement of Cu/ZnO_x NPs. The Cu/ZnO_x@MOF catalysts outperformed the conventional Cu/ZnO/Al₂O₃ catalyst with significantly higher space time yield (STY) of about 2.59 g_{MeOH} kg_{Cu}⁻¹ h⁻¹. After long term tests of over 100 h, the catalyst remained relatively stable, and it also had 100% selectivity for methanol (Figure 2.4).

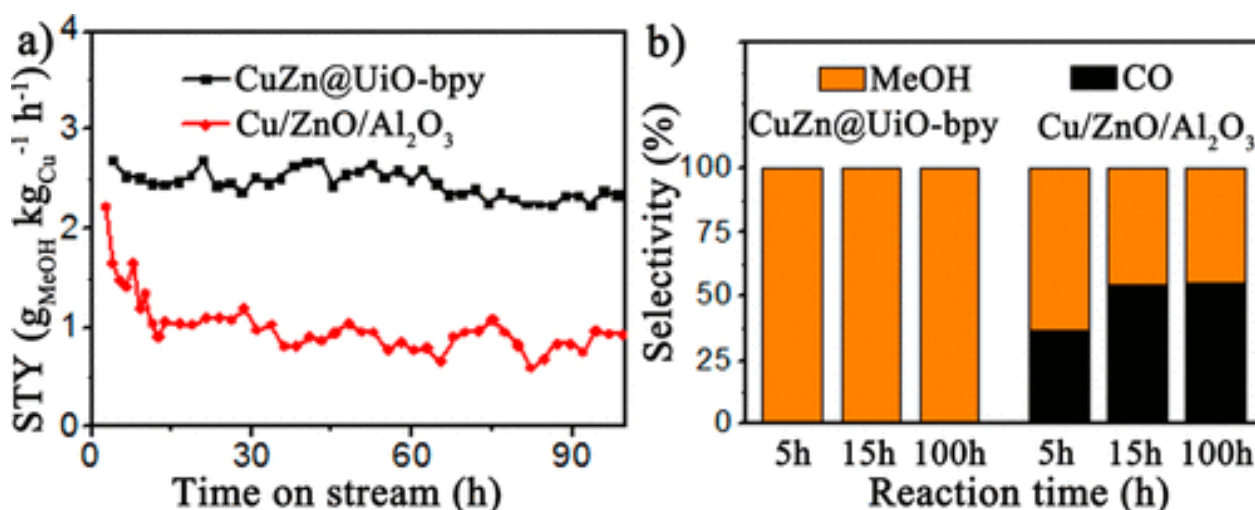


Figure 2.4: (a) STY of methanol vs reaction time over a period of 100 h (b) product selectivity vs reaction time [64].

Enhancement of the activity and stability of the Cu/ZrO₂ catalysts can be achieved by modifying the preparation methods and the addition of other specific additives such as gallium. Fornero et al. [65] introduced gallium (Ga) in the form of gallium oxide (Ga₂O₃) as a promoter to the catalyst with ZrO₂ as support. The promoter resulted in a catalyst five times more active than the unpromoted catalyst. In addition, reports from Toyir et al. [53] and An et al. [64] supported the claims of Fornero et al. [65], where they realized that Ga₂O₃ seemed to enhance the activity per unit surface area of the methanol synthesis catalyst. Catalysts derived from hydroxycarbonate precursors can be modified by Ga³⁺ to obtain precursors with hydrotalcite-like structures. These catalysts showed significant improvement on Cu particles dispersion and the creation of active Cu-ZnO_x sites, thereby enhancing the effectiveness of the Cu-ZnGa catalyst system for methanol synthesis [64]. A reason for this improvement can be linked to the ability of the hydrotalcite derived catalysts to sustain their morphology in ultrafine layers even after heat treatment at elevated temperatures.

Song et al. [66] studied the effect of adding some rare earth elements (Sm, Ce and La) as promoters to the binary (Cu/ZnO) and ternary (Cu/ZnO/Al₂O₃) catalysts. The catalysts were synthesized by co-precipitation and calcined at 500°C. After long term activity tests, all the catalysts had a similar trend in regard to the CO₂ conversion, which eventually reached a steady state period after 12h. However, the catalyst promoted by La (CuLaZnAl) had the highest CO₂ conversion of about 25%, whereas the CuZnAl catalyst had a conversion of 22% which was the lowest. The trend of the conversion for the different catalysts is depicted in Figure 2.5. In partial contrast to Song et al. [66] findings, Kourtelesis et al. [67] reported that the addition of La₂O₃ to the reference catalyst led to a reduction in CO₂ conversion and an increase of methanol selectivity. The promoted catalyst exhibited higher methanol yield than the unpromoted catalyst (over 30%). The increase in yield is attributed to the relatively large specific surface area and high porosity of the catalyst, the formation of active sites with adequate strength, which improved the adsorption of CO₂ and intermediates favoring the hydrogenation steps. The promoted catalyst preserved significant parts of the copper in its metallic form under the reaction conditions [67]. Furthermore, the exposure of the promoted catalyst to CO₂/H₂ reaction mixture led to the formation of oxygenated surface species, particularly the methoxy and formate species. The methoxy species that are formed by stepwise hydrogenation of formate are regarded as key intermediates for methanol production [68]. On the other hand, the production of CO from the formate species could also occur via the reverse water-gas shift reaction or decomposition [67].

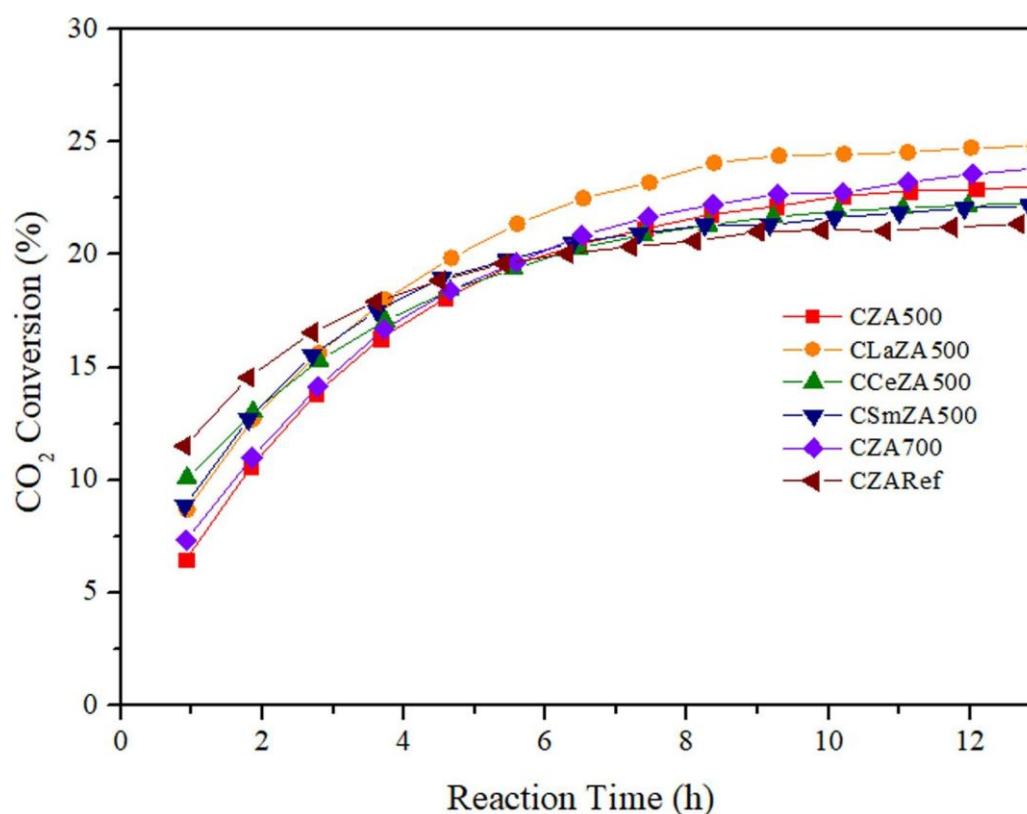


Figure 2.5: CO₂ conversion of for three different promoted catalyst systems for hydrogenation of CO₂ over 12 h time on stream (TOS). Reaction conditions: 250°C, 40 bar and H₂/CO₂=3, and GHSV = 4000 h⁻¹ [69].

Magnesium oxide (MgO) as a promoter in the ternary CuZnAl based catalyst for methanol synthesis dates back to the 1990s [70]. Reports from different studies proved that MgO had a positive effect on the stability of the catalyst but decreased the catalytic activity [71–73]. When the addition of Mg was investigated on a Cu/Zn/Zr catalyst for CO₂ hydrogenation to methanol, it was found that Mg improved the adsorption properties of the catalyst [74]. Sharma et al. [75] synthesized a highly stable MgO promoted catalyst by the hydrothermal method. They showed that there was a significant increase in methanol yield, and this is attributed to the synergistic interaction between the small Cu particles and the MgO/ZnO support, which increased the Cu dispersion and Cu surface area. Furthermore, an enhanced adsorption site for CO₂ was developed adjacent to the Mg atoms, and this is as a result of the formation of defective ZnO crystals with Mg atoms [73, 75].

Table 2.1: Comparison of the activity and selectivity of different Cu-based catalyst synthesized under different conditions.

Catalyst	Preparation method	T (°C)	P (Bar)	H ₂ /CO ₂ molar ratio	XCO ₂ (%)	S _{MeOH} (%)	Ref
Cu/ZnO/Al ₂ O ₃	Oxalate gel CP*	210	20	3/1	11.6	75	[76]
Cu/ZnO/Al ₂ O ₃ / In ₂ O ₃	CP	250	30	3/1	7.3	52	[43]
Cu/ZnO	CP	250	30	3/1	~11	-	[77]
Cu/AlCeO	CP	260	30	3/1	~17	85	[45]
Cu/ZrO ₂	IW*	260	80	3/1	15	86	[62]
CuZnCeO _x	Parallel flow CP	240	20	3/1	13	40	[52]
Cu/ZnO/Ga ₂ O ₃	CP	240	45	2.8/1	27	50	[55]
Cuo/ZnO/ZrO ₂	CP	340	30	3/1	5.6	64	[78]
Cu/ZnO/Al ₂ O ₃ / ZrO ₂	CP	190	50	3/1	10.7	81.8	[79]
CuZnO@UiO- bpy	DSM *	250	40	3/1	3.3	100	[64]
Cu/ZnO/Al/ La ₂ O ₃	CP	250	40	3/1	11	43.3	[66]
Cu-MgO/ZnO	HT*	200	30	3/1	8.7	99	[75]
CuO/ZnO/TiO ₂	CP	220	30	3/1	14.8	51	[80]

*CP, co-precipitation; IW, incipient wetness; DSM, double solvent method; HT, hydrothermal.

Recently, new studies have been carried out to understand the influence of promoting the Cu/Zn/Al catalyst with Mg, particularly by the co-precipitation and fractional precipitation synthesis methods [81–83]. The method of preparation has shown to have significant effects on the catalysts properties as well as their performance during methanol synthesis. Brunauer-Emmett-Teller (BET) analysis was used to characterize the catalysts, and this showed that the catalysts synthesized by co-precipitation had higher BET surface area and Cu dispersion. However, the catalytic activity of the catalyst was decreased. On the other hand, the catalysts synthesized by fractional precipitation enhanced the substitution of Cu by Zn in the sub-carbonate precursor, thereby enhancing the catalytic performance [81]. Dasireddy et al. [82] eventually suggested that in the catalysts prepared by co-precipitation, Mg-Al hydrotalcite was formed, which had a negative effect on methanol production.

Titanium oxide (TiO_2) has also been extensively studied and the results have demonstrated that a relatively high performance of TiO_2 promoted catalyst can be achieved [50, 80, 84]. Xiao et al. [80], while using the co-precipitation prepared various catalysts containing $\text{CuO}/\text{ZnO}/\text{TiO}_2$ with different TiO_2 loadings. Upon TiO_2 promotion of the CuO/ZnO catalyst, the copper species were into an amorphous-like structure, which improved the reduction of CuO . Furthermore, when the TiO_2 loading was increased, the metallic Cu surface area (SA_{Cu}) of the promoted catalyst increased but decreased when TiO_2 loading was over 10%. Therefore, a loading of 10% TiO_2 was the optimum for producing an effectively promoted catalyst. In addition, the methanol yield increased linearly relative to the increment of the SA_{Cu} , which indicated that when TiO_2 was added to the catalyst, it only enhanced the SA_{Cu} but not the intrinsic activity. Similarly, Bao et al. [84] developed a series of Cu/TiO catalysts and demonstrated that a higher specific surface area of Cu is very effective for CO_2 hydrogenation, and the presence of sufficient amount of Ti^{3+} enhanced the CO_2 adsorption/activation. Both resulted in higher TOF of methanol formation [85]. Titanium nanotubes (TNT) support has also been incorporated into $\text{CuO}/\text{ZnO}/\text{CeO}_2$ catalysts. This resulted in the promotion of the CuO reducibility, improvement of metallic Cu dispersion and increase of the specific surface area. The promoted catalysts prepared by deposition precipitation with different TNTs content had higher CO_2 conversion and methanol selectivity compared to the unpromoted catalyst [50]. The increased CO_2 conversion and improved selectivity could be attributed to the specific surface area of Cu and the number of basic sites.

2.3.3 Other supports

Generally, silica (SiO_2) is characterized with a large surface area and porosity, a relatively high thermal stability and adequate dispersion capacity but weak interactivity with metals [86]. However, when it is exposed to steam at high temperatures, its thermal stability is weakened because it transforms to $\text{Si}(\text{OH})_2$. The incorporation of varying amounts of silica in the Cu/ZnO catalysts dramatically improved the stability of the catalyst, as it reduced the crystallization of ZnO [53]. Kunkes et al. [87] synthesized Pd/SiO_2 and Cu/SiO_2 catalysts using incipient wetness impregnation of silica gel with Pd and Cu nitrate solutions to obtain metal loadings around 10 wt%. The formation rates of methanol were higher for the Cu/SiO_2 catalyst (2.1%) when compared to the Pd/SiO_2 catalyst (0.3%). It has been suggested that the silica-based catalyst had relatively higher selectivity for methanol and higher activity when compared to the conventional ZnO -based catalysts. This could be because of the larger surface area of the silica-based catalysts [88]. Grandjean et al. [89] reported that the effect of SiO_2 on the Cu-based

catalysts can be improved if other metal oxides are introduced and silica serves as a co-support or promoter. Jiang et al. [90] synthesized a micro-spherical SiO₂ support using the spray-drying technique. They developed a series of SiO₂ promoted Cu/ZnO catalysts with different weight percentages of Cu and ZnO by the ammonia-evaporation synthesis method. They showed that it was possible to deposit Cu and Zn ions within the pores of SiO₂ and high distribution, which is affected by metal loading. The specific surface area increases with the metal loading, which was ascribed to the porous structure of SiO₂. However, when the metal loading exceeded 47.91%, the catalysts' specific surface area began to decrease. This led to a slight reduction of CO₂ conversion, which could be due to the blockage of the pores [90]. The combination of different characterization techniques (CO-adsorption in situ Fourier-transform infrared spectroscopy analysis, X-ray diffraction, X-ray Auger electron spectroscopy and X-ray photoelectron spectroscopy) proved that the formation of both Cu⁺ and Cu⁰ species are facilitated by SiO₂ [90].

Similar to SiO₂, carbon materials also have very large surface area, and they are very stable at higher temperatures. They have good mechanical strength, significant hydrogen uptake which facilitates H₂ dissociation. These properties are favourable for CO₂ hydrogenation at lower temperatures with improved selectivity. However, due to low CO₂ conversion, its application as a catalyst is not commercially applicable [91]. Deerattrukul et al. [91] synthesized Cu/Zn catalyst supported on reduced graphene oxide (rGO). They found that 10 wt% of the Cu/rGO exhibited the most promising activity for CO₂ hydrogenation, achieving conversion and methanol selectivity of 26% and 51% respectively. The highest STY attained was 424±18 mg_{methanol} at 250°C and 15 bar. In addition, MOFs were also studied as supports for the catalysts. It has been reported that the MOF supported catalyst exhibited over 99% methanol selectivity [57, 63, 64]. Despite the promising properties and activity, limited conversion rates and instability at higher temperatures still hinders its industrial applicability [90, 91].

2.3.4 Bi-metallic Cu based catalysts

Several researchers have reported that the bimetallic Cu-based catalysts also exhibit very good performance in CO₂ hydrogenation to methanol [90, 92, 93]. Noble metals such as palladium have favorable properties that promote hydrogen activation and palladium supported on metal oxides possess significant high activity [48, 49, [94]. Preliminary studies proved that the supported Pd nanoparticles were indeed involved in the methanol synthesis process. Nie et al. [92] focused on Pd-Cu catalysts and provided significant insight about the chemistry of the

reaction. Jiang et al. [94] observed a synergistic effect when methanol production was conducted over a Pd-Cu bimetallic catalyst supported on amorphous silica, where the Pd/(Pd+Cu) atomic ratios were maintained within the range of 0.25 to 0.34. The methanol formation rate over the bi-metallic catalyst (Pd-Cu/SiO₂) was two times higher than that of the monometallic Pd and Cu catalysts.

The modification of the conventional Cu/ZnO catalyst surface with Pd is an efficient way for developing catalysts with improved activity. This is as a result of to the so-called hydrogen spillover mechanism [95]. The effect of hydrogen spillover is the development of a catalyst surface that has high tendency to facilitate the hydrogenation process. Kugai et al. [96] showed that the noble metal Pd improves activity of the Cu sites. The effect of the increment of Pd loading was noticed as the Cu dispersion and surface concentration on the catalyst surface was enhanced up to a certain point. Furthermore, it is believed that because of the intersection of Pd and Cu, which resulted in strong electronic perturbations and shrinkage of the Cu-Cu bond, a well dispersed Cu species is formed. Similarly, Choi et al. [97] developed a Pd-Cu/CeO₂ catalyst and reported that the interaction with Pd, which is highly dispersed on the CeO₂ support, suppressed Cu particles aggregation. A XPS analysis showed that, peaks for Cu 2p electrons in the Pd-Cu/CeO₂ catalysts are located at a lower binding energy compared to Cu/CeO₂ catalysts. This means that the Cu sites in the former catalyst is richer in electrons and therefore, donating electrons to Cu will enable the stabilization of Cu in a more reduced state [98]. Nie et al. [92] after conducting first principle calculations determined that the stepped PdCu(111) surface which had Pd atoms on the top was better than the flat Cu-rich PdCu₃(111). This is because the former is favored for CO₂ and H₂ activation as well as CO₂ hydrogenation to methanol. Furthermore, CO₂ hydrogenation experiments over SiO₂ supported bimetallic catalysts revealed that the composition of Pd-Cu(0.5) is dominated by PdCu alloy phase which resulted in improved methanol selectivity relative to the PdCu₃-rich Pd-Cu(0.25) [92]. The surface reaction sequences in both the “formate and RWGS + CO-hydro” pathways on the PdCu(111) surface is depicted in Figure 2.6.

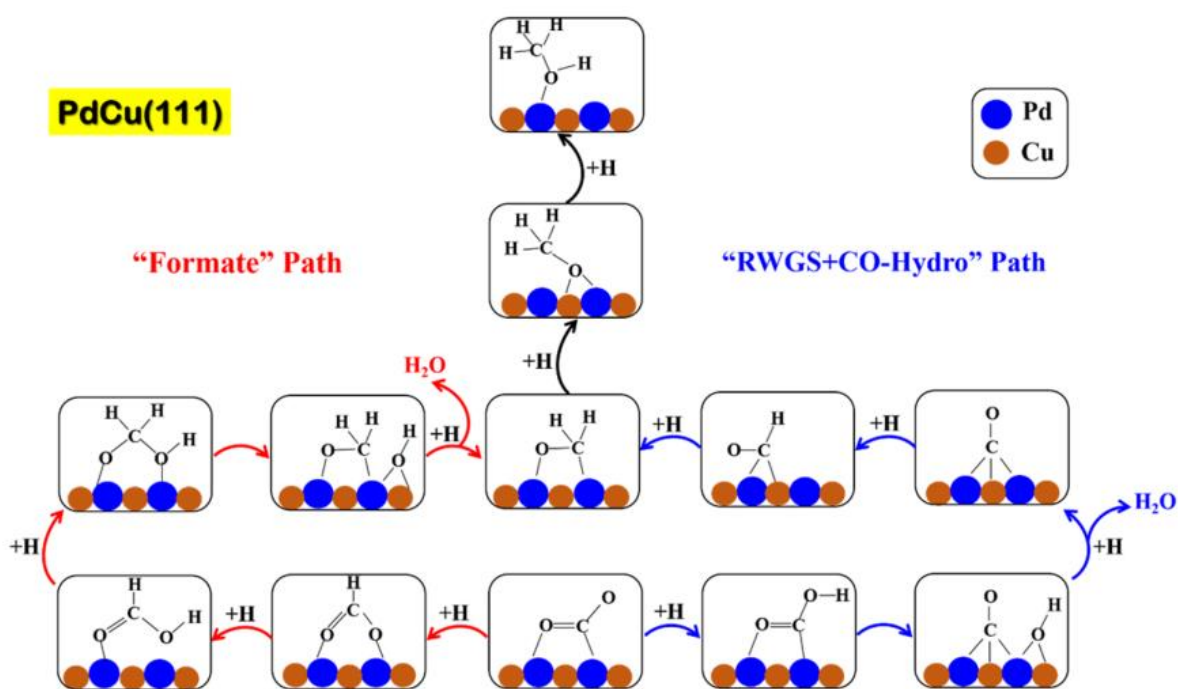


Figure 2.6: Surface reaction sequences for CO₂ conversion to methanol in the “formate” path and the “RWGS + CO-hydro” path on PdCu(111) [92].

Additionally, kinetic studies and in situ DRIFTS analysis were used to understand the origin of the bimetallic promoting effect. It was revealed adsorbed species and surface site balance could be altered by alloys. These alloys also decrease the activation barrier for the formation of methanol, thus, improving methanol formation [99]. Liang et al. [100] synthesized Cu-Zn bimetallic catalyst supported on Al foam by the hydrothermal method. Under 250°C, 3 Mpa and high WHSV of 20,000 mL g_{cat}⁻¹h⁻¹, a methanol yield of 7.81 g g_{Cu}⁻¹h⁻¹ was obtained with 9.9% CO₂ conversion and 82.7% methanol selectivity.

2.4 Reaction mechanism

Understanding the mechanistic details is a key component for improving the catalyst design criterion when it comes to CO₂ hydrogenation catalysts [13]. The active sites in the Cu-ZnO catalysts are linked with partial or fully reduced Cu and the synergic contact with ZnO or moderately reduced ZnO_x [1]. The formation of Cu-ZnO interface is critical for the activity. Several options are proposed from different studies and amongst them are; (i) the ZnO enhances the dispersion of reduced Cu, thereby increasing the number of active sites, (ii) the ZnO promotes the Cu²⁺ reducibility, (iii) the active sites of Cu⁺ is stabilized on the surface of ZnO,

or (iv) the basic sites of ZnO that are in close contact with the Cu-metal sites are essential to catalyze hydrogenation of carbon oxides [15, 82, 101, 102]. Thus, the formation of interfaces between Cu-ZnO can be a determining factor if highly active catalysts for methanol synthesis from CO₂ hydrogenation are to be obtained [77, 103, 104]. These important interphases are formed during the course of reduction of the catalyst precursors, where an optimization of the reduction variables tend to play a pivotal role in producing catalysts with optimum activity [77]. In addition to the interfaces between Cu-ZnO, the exposed faces of the ZnO that is in contact with the Cu species also influences the catalytic behavior of the Cu/ZnO systems. It was confirmed after the synthesis of ZnO with different nanomorphology that the (002) face of the ZnO had the best catalytic activity for the synthesis of methanol. This is due to the fact that the face was more polar and it presented higher concentration of oxygen vacancies [105].

Conversely, understanding the reaction mechanism that operates on Cu/ZnO catalysts will further enable the development of improved catalysts for this process. In this regard, two widely accepted mechanistic pathways have been suggested from previous studies for the hydrogenation of CO₂ to methanol over Cu-based catalysts [7, 22, 106]. The first pathway (Figure 2.7) features the reverse-water-gas-shift (RWGS) and CO hydrogenation mechanism, where the CO₂ is initially converted to CO and later proceeded by hydrogenation of CO to methanol through formyl (HCO) and formaldehyde (HCOH) intermediates. The second pathway is associated with the formate mechanism, in which formate intermediates (HCOO) are produced during the hydrogenation of CO₂ which eventually produces methanol via C–O bond cleavage and *HCO or *H₂CO intermediates [15]. Formaldehyde, the intermediate product which is common in both mechanisms can be hydrogenated to form methoxy and subsequently to methanol [82].

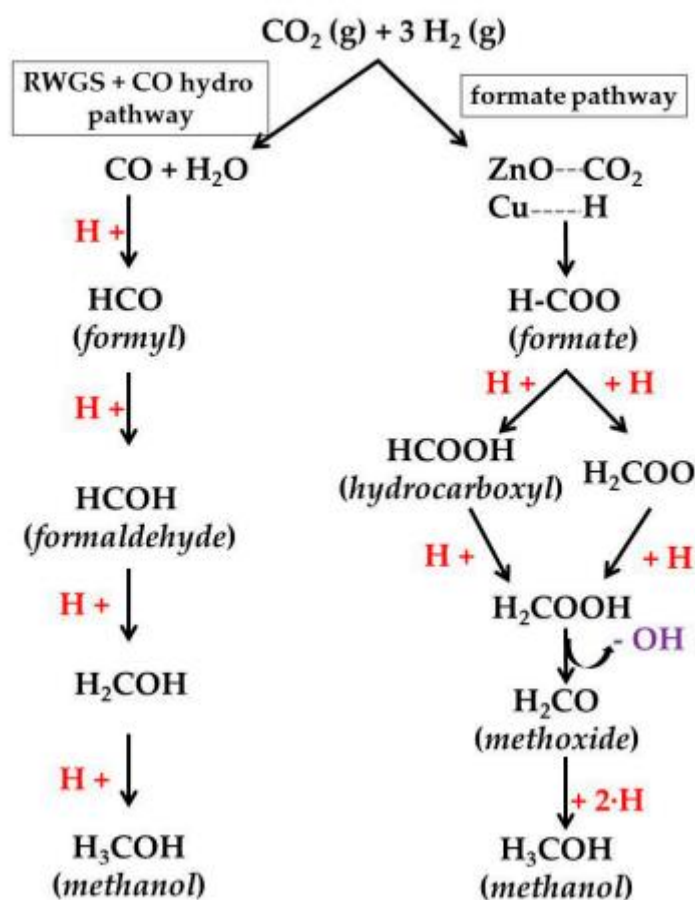


Figure 2.7: The pathways CO₂ hydrogenation to methanol over Cu-based catalysts. [1]

Kinetic investigation has identified the hydrogenation of formate (HCOO) and dioxomethylene (H₂COO) species as the limiting steps for the methanol synthesis via the formate pathway [15, 105, 107]. Meanwhile, if the synthesis proceeds through the RWGS and hydrogenation of CO pathway, the limiting steps will be the hydrogenation of CO and formyl (HCO). Potentially, both reaction pathway may operate on a real Cu/ZnO-based catalyst. Therefore, when Cu/ZnO catalyst is utilized, the CO₂ hydrogenation activity might also be affected by (i) the CO hydrogenation barrier, (ii) the barrier of dioxomethylene hydrogenation, and (iii) the CO binding energy. In an ideal scenario, the Cu-based catalyst used in CO₂ hydrogenation to methanol is supposed to hydrogenate dioxomethylene easily without restrictions and bond CO abstemiously. Thus, this will be strong enough to promote the required CO hydrogenation as compared to CO desorption but less likely to deter CO poisoning. In this regard, production of methanol from both pathways can be expedited [107].

Density functional theory (DFT) calculations has shown that CO₂ hydrogenation is more favored through the formate pathway via *HCOOH, *H₂COOH, and *CH₃O intermediates rather than the RWGS related pathway for methanol synthesis [13]. Furthermore, the existence of CO₂ enhances the reaction rate of syngas conversion to methanol, thereby indicating that methanol is produced mainly via the formate route [108]. Consequently, the new Cu/ZnO catalysts should be able to enhance the capacity of the methanol synthesis sites and either suppress the active sites favoring the RWGS reaction or enhance the hydrogenation of by-product CO to methanol.

2.5 Catalyst synthesis methods

To achieve high catalytic activity, the catalyst should meet some desirable properties such as large surface area and effective Cu-ZnO interphase. Several methods have been utilized to prepare commercial catalysts where the preparation approaches and conditions have valuable influence on the catalytic performance [13, 109]. Numerous synthesizing methods have been studied by researchers, such as the solid-state combustion, solid state reaction, reduction–precipitation, sol–gel auto-combustion, and co-precipitation. However, among all the aforementioned catalyst synthesis methods, the coprecipitation method is preferred in the industry [13]. A brief overview of the different methods used in catalyst synthesis for methanol production are discussed below.

2.5.1 Solid-state combustion

Solid state combustion was used to prepare a series of Cu-ZnO catalysts using metal nitrates and citric acid. This method requires an argon atmosphere where the novel citric acid solid state combustion will take place, and thereby the preparation of the metallic Cu-ZnO catalyst will happen without the need for further reduction. Consequently, the catalyst can be used directly in methanol synthesis. This method is very advantageous due to the simple way of catalyst preparation which does not require a lot of produced water, which is environmentally friendly. Usually, reduction and catalyst engineering process have high costs. However, these extra costs are reduced by this method[110].

2.5.2 Sol–gel auto-combustion

Methanol synthesis is an extremely exothermic reaction, so its efficiency is limited by thermodynamics. This aggrandized the researchers to develop low temperature process for methanol synthesis [111]. One of the processes proposed was the solid-state combustion for

catalyst preparation discussed earlier [110]. The sol-gel auto combustion was also considered as an attractive method for the same cause of developing a low temperature process. The following technique was based on a combination between the chemical sol-gel process and subsequent combustion processes [111]. The preparation process began with the mixing of metal nitrates and citric acids, and the mixture was added to distilled water. Eventually, the solution was adjusted with ammonia to obtain a pH of 7. Stirring and refluxing ensured the binding of the citric acid with the metal ions. Evaporating and drying take place to form porous polymeric xerogel. Finally, the product was calcined between the temperature range of 250-450°C under argon flow and then auto combusted to produce porous and loose pure Cu/ZnO catalyst [111]. In comparison to the one-step synthesised Cu/ZnO catalyst discussed earlier, the sol-gel auto combustion method has lower activity and methanol selectivity [110].

2.5.3 Reduction–precipitation

The conventional gas phase reduction process of the copper-based catalysts has some drawbacks [112]. The disadvantage includes the intense heating effect, uncontrollable reducing conditions, and the time consuming of the operation [112, 113]. An attractive technique was introduced where NaBH₄ was used to reduce copper-based catalysts, which proved to be fast, economical, and easy to operate. The presence of NaBH₄ showed an effect on the catalytic performance as it produced smaller Cu particles compared to the conventional co-precipitation method. The variation of the NaBH₄ content had an influence on the activity of the catalysts as well [112].

2.5.4 Solid state reaction

The solid-state reaction was a method introduced to reduce the cost and complexity of the catalyst synthesis process. In this method the catalyst is prepared through a chemical reaction between hydrated metallic salts and citric acid ligand which will obtain a complex of metal citrate. Calcination is a very important step in the solid-state reaction for the preparation of the copper-based catalyst. It was shown that the calcination temperature has a strong influence on the physicochemical properties and the catalytic activity [109]. The dispersion of copper species will decrease as the calcination temperature increases. The solid-state reaction is preferred due to its simplicity, time efficiency, and being a solvent free method. However, this method produced catalysts with low BET surface area, which is a major hindrance to the catalytic activity [109].

2.5.5 Co-precipitation

The Cu/ZnO/Al₂O₃ catalyst is mostly prepared by co-precipitation which is known as the conventional method [13]. Co-precipitation is a typical preparation method for catalyst precursors [114]. A mixture solution of copper and zinc nitrate in deionized water is prepared, then sodium carbonate is added as a precipitating agent for the successful co-precipitation of Cu/Zn hydroxycarbonate precursor [115]. During co-precipitation, it is decisive to keep the synthesis parameters as required to obtain a more effective catalyst. The most significant parameters are PH and temperature. Some studies proposed that the best temperature range is between 60-70°C, and pH between 6-7 [114]. Other important parameters that should be maintained are composition, concentration, and aging time [115].

The co-precipitation method includes three stages. It begins with the precipitation of the precursors in the form of hydroxycarbonates [1]. For example, the mixed Cu/Zn/Al hydroxycarbonate could be coprecipitated to be the precursor for the Cu/ZnO/Al₂O₃ catalyst. The formation of the hydroxycarbonate is an important step in the catalyst synthesis since the properties developed in the early stages of preparation will affect the efficiency of the catalyst [1, 114]. The second stage will be controlled calcination of these hydroxycarbonate precursors to obtain highly dispersed CuO–ZnO species with some residual carbonates. These residual carbonates accounts for maintaining high porosity and surface area. The final step is to reduce the oxidized phases to get active sites. Some properties are favoured when it comes to the final catalyst such as high Cu surface area, good interaction between Cu and ZnO, and minimal presence of Na that was utilized in the coprecipitation stage [1].

The best hydroxycarbonate phase to obtain the optimal catalyst for CO₂ hydrogenation to methanol is still under investigation [116]. The hydroxycarbonate phases can be aurichalcite, zincian malachite, hydrotalcite, and the amorphous zincian georgeite phase. The zincian georgeite is formed by co-precipitating acetate salts with ammonium carbonate. The addition of zinc into the georgeite phase and small aging prevents crystallisation into zincian malachite or aurichalcite [116]. However, the low temperature coprecipitation permits the synthesis of pure zinc malachite precursor with high Zn content, which allows the maximizing of the dispersion of Cu and oxygen defect sites on the ZnO surface [117]. The catalytic performance was very high for catalysts derived from the zinc malachite phase, especially when huge amount of Zn content is incorporated into the structure of malachite [1]. The performance also depends on the morphology of the precursor particles and the degree of Zn substitution of Cu in the zincian malachite phase [114]. Additionally, the presence of amorphous zincian georgeite can

also be advantageous for the catalytic performance over the single-phase zinc malachite. In this process, the hydroxycarbonate precursors will change in the preparation step where it will begin in the georgeite phase and later evolve into malachite. The transition from the georgeite to malachite is defined as of the meso-structuring. Nano-structuring is also possible which is the transformation from aged precipitate to calcined product [1, 114].

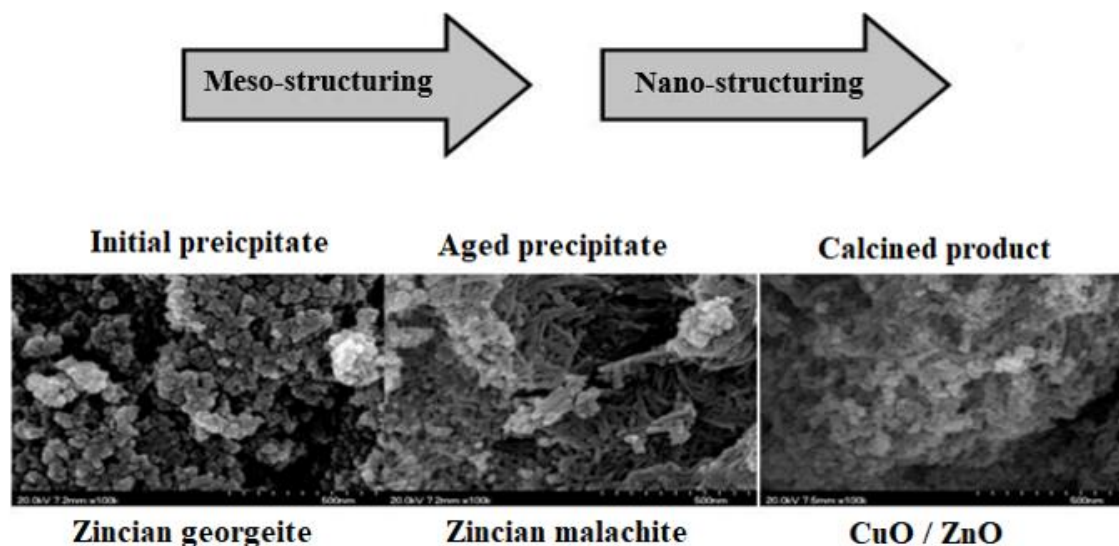


Figure 2.8: Scanning electron microscope images of the materials obtained at different stages during the preparation of Cu/ZnO/Al₂O₃ catalysts [1].

Catalysts can also be derived from hydrotalcites [118]. The hydrotalcite precursors can be formed by the nucleation and growth of the metal hydroxide layer because of the mixing between an aqueous solution, where two metallic salts are used to obtain a base and an anion. An easy method of obtaining higher dispersion between the metallic copper and the Zn or/and Al₂O₃ is using precursors containing Cu/Zn/Al with a hydrotalcite structure. The catalysts resulting from the hydrotalcite (HT)-like hydroxycarbonate precursors - have well inter-dispersed mixed metal oxides with high surface area, in addition to small and uniform particle sizes. These factors can lead to high catalytic activity [118].

An alternative precursor is aurichalcite. It is usually found as a secondary mineral in copper and zinc deposit, and its composition show Cu/Zn ratio in the range from 1:9 to 2:3. The catalysts are synthesized by thermal decomposition of aurichalcite [119]. Usually, XRD is used to study the crystalline components of the precursor materials in relation to other mineral phases

(malachite, aurichalcite...). The following figure shows the difference in crystal structure between malachite and aurichalcite [120].

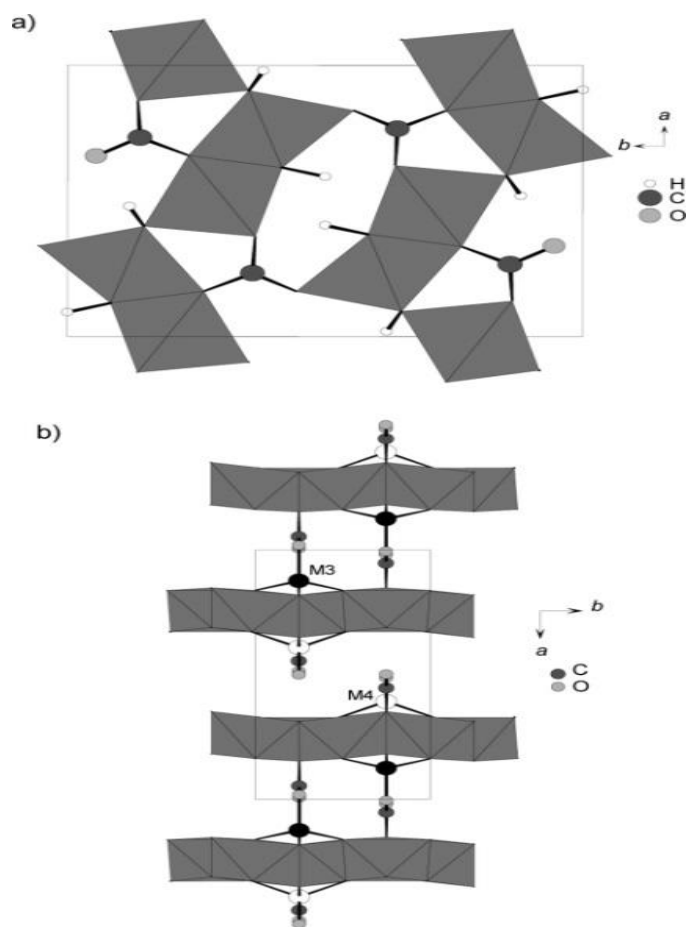


Figure 2.9: a) The malachite crystal structure viewed along [001] and b) aurichalcite crystal structure viewed along [001] [120].

2.5.5.1 Aging

The composition of the precursor is an important factor to define the properties of the catalyst. Aging is a very critical stage in the catalyst synthesis as well [120, 121]. It is considered as a post synthesis process usually done after the completion of the precipitation phase by stirring the precipitate in its mother liquid for a defined period in the same reaction vessel. Many processes could occur during the aging period, such as the change in the morphology, particle sizes, and the chemical composition of the solid precipitate [120]. It is very important to study the effect of aging temperature for the copper-based catalyst obtained by co-precipitation [121]. XRD analysis showed that the variation in aging temperature can have an influence on the ratio and the crystallinity of the precursor phases such as zincian malachite and aurichalcite [120, 121]. The aging temperature will become more important in the precipitation stage because of

the rearrangement of the structures during the aging process. Aging time and pH are very important variables in the aging process so they must be carefully monitored. The aging is usually done for hours. However, in the first half hour of aging, three important events happen which are; a light drop in the pH, increase in turbidity, and the colour change. These changes are due to the crystallization from amorphous to crystalline precipitate [122]. Figure 2.8 shows the drop in pH after the start of aging.

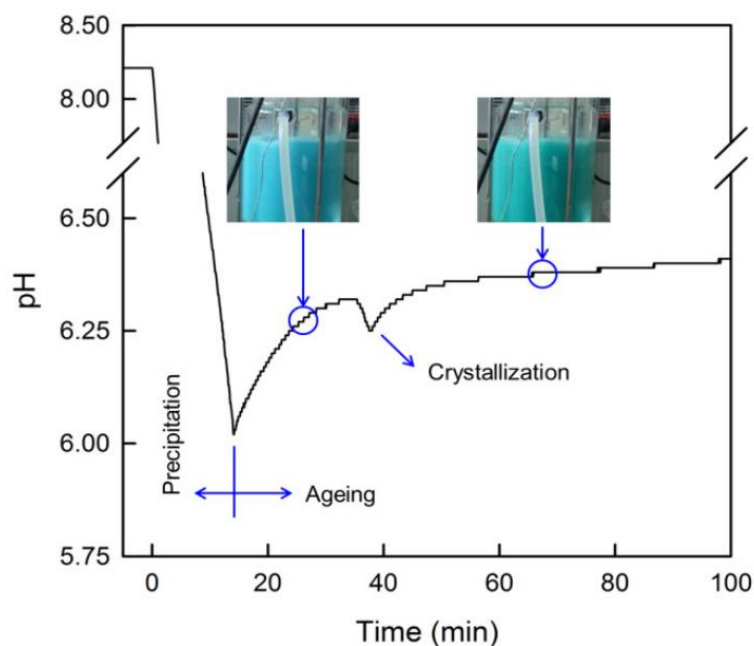


Figure 2.8: pH profile during the ageing of Cu/Zn precipitate [117].

The precipitation process takes place in the pH range of 6-7 to have a homogenous precipitation, and the temperature should be in the range of 60-70°C. The temperature and pH are almost the same in the aging phase with a slight drop in pH due to crystallization [122]. The drawback of the aging process is that the composition may differ when compared to that after precipitation [120].

2.5.5.2 Calcination

Calcination is a thermal and chemical process applied to the prepared catalyst after the aging process. The catalyst is heated at constant temperature in the presence of synthetic air or oxygen, and the goal is to transform the composition from hydroxides to metal oxides. The calcination temperature has big influence on the catalysts, and it may have different effect related to the origin the catalysts obtained. For aurichalcite, Fujita et al. [123] discussed that the decomposition of precursor will take a short period when calcination is applied with faster

heating rate. However, the decomposition of the precursor will happen slowly over a longer period when calcination is applied with slower heating rate. Therefore, a decrease in the crystalline size of CuO can occur when calcination takes place at slower heating rate. The results were different compared to the catalyst obtained from zincian-malachite where decomposition took place at lower temperatures. Therefore, the size of CuO is practically unchanged irrespective of the heating rate for the calcination [124]. It was also discovered that calcination at mild heating rates can lead to a better dispersion of CuO and ZnO, therefore stopping the aggregation of oxides and giving a higher dispersion of the metal particles in the reduced catalyst [123, 124]. Therefore, sufficient temperature is required to allow the formation of metal oxides, and at the same time the temperature should not be very high because it can lead to sintering and decrease of the catalyst surface area [123].

2.5.5.3 Reduction

Reduction takes place after calcination in the catalyst activation process. Catalysts require a reducing agent to be activated and for which hydrogen is commonly used. The reduction step converts the metal oxides to active metal species. A very critical parameter in reduction is temperature because it affects the surface area and dispersion. Hydrogen temperature programmed reduction (H_2 -TPR) with a linear heating rate is used conventionally to study the reducibility of the CuO/ZnO/ Al_2O_3 catalyst [125]. Reducing the catalyst for longer periods and at lower temperature will result in higher Cu dispersion and eventually higher catalytic performance [124]. Moreover, due to the significant temperature impact, more active and homogenous catalysts can be obtained where local heating can be avoided in the reduction process [125]. Nevertheless, mild temperature reduction can play a role in preventing the Cu particles from excessive sintering throughout the autocatalytic reduction in the fixed bed reactor [125].

2.6 Catalyst Characterization

2.6.1 X-ray diffraction (XRD)

The X-ray diffraction is an analytical technique widely used to characterize the crystalline phases of various materials, usually for analysis of mineralogy and determination of the properties of unknown materials [126]. Intensities from the different peaks obtained are evaluated and correlated to an already developed database of materials in order to identify the

crystalline structure, defects and content of the sample or material being investigated [127]. The process of characterization is done by irradiating a sample with incident X-rays, which then creates a reflection of several waves depending on the structures that are present in the sample. While crystals are seen as arrays of atoms, ions or molecules packed in a repetitive ordered pattern, X-rays could be well-thought-out to be waves of electromagnetic radiation. The crystal atoms scatter (diffract) incoming photons, fundamentally by interacting with the electrons of the atoms (elastic scattering) [128]. To gain understanding of the reason the cleavage phases of crystals reflect x-ray beams at specific angles of incidence, two English physicists in 1913, Sir W.H Bragg and Sir W.L Bragg defined the x-rays diffraction and interference in a crystal as probable reflections at the atomic planes of the crystal lattice. The calculation of the several positions of the various reflections could be realized using the optical path difference $2s$, where $s = d \sin \theta$, between two rays reflected at adjacent interplanar spacings. As in visible light optics, maxima are produced for different integer multiples of λ [128]. From this definition, the Bragg's law described in Eq. 2.4 was developed.

$$n \lambda = 2 \times d \times \sin \theta \quad (2.4)$$

where;

d interplanar spacing generating the diffraction

θ Bragg angle

2θ : angle between incident and reflected beam

n order of interference $n = 1, 2, 3 \dots$ normally $n = 1$ (called: refraction order of $n=1$)

λ wavelength

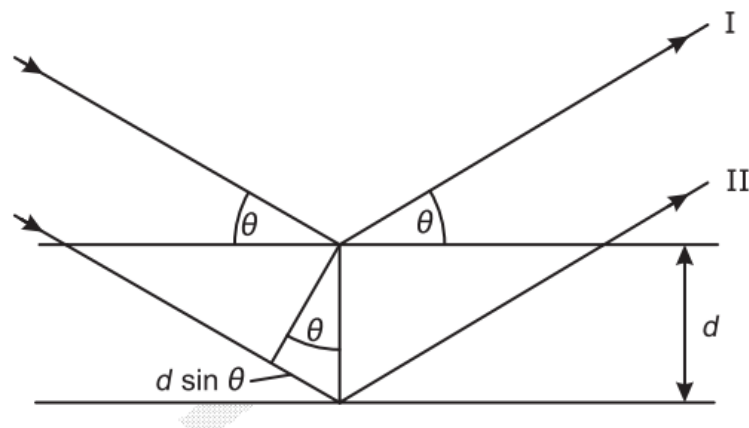


Figure 2.9: Graphical representation of Bragg's law [128].

Furthermore, the interplanar spacing d can be determined by employing the Scherrer equation Eq. 2.5 [129].

$$d = \frac{k\lambda}{B\cos\theta} \quad (2.5)$$

where;

B width total at half maximum peak (r)

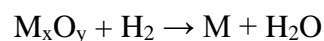
k numerical factor ascribed to the crystalline shape factor

The x-ray diffractometers used in this analysis consist of three main elements; the x-ray tube, a holder for the samples and an x-ray detector [130]. X-rays are formed in a cathode ray tube, where a filament is subjected to heat to produce electrons. The electrons are further focused on a target by the application of a voltage, thereby bombarding the targeted material with electrons. Eventually, when the electrons attain adequate energy to displace the inner shell electrons of the material being targeted, the production of characteristic x-ray spectra is witnessed. In addition, these spectra are composed of several components, the most prevalent being K_α and K_β [126]. The K_α component consists of $K_{\alpha 1}$ and $K_{\alpha 2}$, where the former has a relatively shorter wavelength and doubles the intensity of the latter. These wavelengths are characteristics of some specific target materials (Cr, Fe, Cu, Mo).

There are several x-ray diffraction (scattering) techniques: single crystal XRD, powder x-ray diffraction (PXRD) and other special x-ray techniques such as high resolution XRD, pair distribution function (PDF) analysis, and small angle x-ray scattering (SAXS). However, PXRD is the most commonly used technique that utilizes a stable wavelength. The diffraction of the lattices can be obtained because of the random placement by investigating the sample through 2θ angles. Exclusively, PXRD is the only technique that can be utilized when there is no single-crystal specimen, which is the case in most materials [131]. Furthermore, the location of the diffraction patterns obtained from PXRD analysis gives information on the size and shape of the composition and the intensities on the other hand are used to determine the atoms position in the sample [132]. In addition, the XRD peak intensity line with the recorded interplanar spacing data saved in an already developed database, referred to as the joint committee on powder diffraction standard (JCPDS), while making use of the strongest peak intensity line as a function of the weight of phases in a sample can be employed for quantification of phases [133]. Similarly, the arrangement of the atoms and crystalline size of a sample can be identified by considering the intensities of the beams. Moreover, there are various elements which could affect these intensities: addition of atoms, the affinity to atom's order and the quantity of crystals oriented in the Bragg's angle [131].

2.6.2 Temperature programmed reduction (TPR)

Temperature programmed reduction (TPR) is a method utilized for the characterization of metal oxides and mixed metal oxides that are dispersed on a support. It characterizes the oxido-reduction properties of both bulk and supported catalysts by determining how easily CO or hydrogen reduces the oxidation state of solids, particularly catalysts [134]. In addition, the obtained TPR profiles give qualitative details regarding the oxidation state of the reducible species. During the analysis, a reducing gas mixture, primarily composed of hydrogen, is flowed over the mixed oxide (M_xO_y) while the temperature is linearly increased. As the reaction between the reducing gas (H_2) and the M_xO_y occur, the formation of metal (M) and water is realized, while the H_2 concentration in the gas mixture decreases [135].



The measurement of change in the composition of the reactive mixture leaving the reactor is continuously monitored to determine the reduction rate. This check is achieved with the aid of a thermal conductivity detector (TCD) which measures thermal conductivity of the flowing gas. Furthermore, gases which have significant difference in terms of thermal conductivities, such as argon and nitrogen, are mostly utilized as carrier gases to ensure that clearer signals are recorded by the detector. However, in order to maintain optimum sensitivity of the detector, the hydrogen concentration in the mixture should be <10%. This is because the change in thermal conductivity is only proportional to the mole fraction at low concentration of the reactant gas in the mixture. It is also important to note that the TPR analysis can be used to study coke deposition on catalysts [136].

Typically, in a H_2 -TPR experiment, a weighed mass of the catalyst powder sample (<2.0g) is placed on a quartz wool inside the reactor. If necessary, the sample is pre-treated with flowing oxygen to obtain a well-defined oxidation state. The sample is then cooled back to the start temperature and the O_2 flow is switched to an inert gas (Ar or N_2) and eventually to the reducing gas mixture. After the stabilization of the detector system, the linear temperature increment and measurement initializes [137]. In order to prevent excess H_2 concentration gradients across the catalyst, it is paramount that the reaction is carried out under differential conditions. However, the H_2 concentration difference between the inlet and outlet of the reactor has to be detected with a level of accuracy. The parameters which determine the shape of the H_2 consumption peaks and position of the maximum rate are: the initial amount of reducible species n_0 , heating rate β (K/s), the reducing gas mixture flow rate F (cm^3/s) and H_2 concentration in the carrier

gas c_o ($\mu\text{mol}/\text{cm}^3$). A characteristic number K was defined to relate the parameters and to also facilitate the selection of appropriate values.

$$K = \frac{no}{Fco} \quad (2.6)$$

Here, the values of K is determined to be between the ranges of 55-140 (s) for heating rates of $0.1 < \beta < 0.3$ K/s, in order to acquire optimum reduction profiles [138].

2.6.3 Transmission electron microscopy (TEM)

Among the different nanomaterial characterization techniques, the transmission electron microscopy (TEM) is the most popular and widely utilized [139]. It is a high-resolution technique employed to obtain chemical knowledge and images of nanomaterials at spatial resolutions equivalent to the level of atomic dimensions. This analysis relies on the interaction between an electron beam, in which incident light is transmitted, and a thin foil sample. The electrons are transformed to elastically or inelastically dispersed electrons after interaction between the beam and sample. The distance ratio between the objective lens, the sample and the image plane are viewed as magnified by the lens. TEM provides precise particle size of both bright field images and dark field images, and also other significant details regarding the nanoparticles, since the analysis uses energetic electrons to provide data on the morphology, composition and crystallography of the specimen [139].

TEM can be classified based on the method of sample preparation. In negative-stain TEM, the nanoparticles are adsorbed onto an electron microscope support and a heavy metal stain is applied. Despite the easy applicability of this TEM variation, it suffers from wide adaptability in nanomaterials research due to limitations related to collapse of particles, aggregation and nonuniform deposition of the samples during preparation. In addition, it is often difficult to control the adsorption of the particles on the electron microscope [140]. Hacker et al. [141] developed a simpler variation of the negative stain, where they premixed the nanoparticles in a hydrophilic support medium prior to the introduction of the heavy metal stains. This method made it feasible to control aggregation and patchy distributions as well as particle collapse when retaining the structure of the nanoparticles. Another classification of the TEM is the freeze-fractured TEM. Here, the sample is placed between two copper holders. Afterwards, it is vitrified by rapid freezing and the specimen is visualized. The freeze-fractured method offers some advantages over the negative-stain TEM in the sense that drying is not needed. However, insufficient freezing and redeposition of the solvent molecules may present artifacts [140].

Lastly, for cryogenic TEM, a suspension of the nanoparticle is rapidly frozen at cryogenic temperatures and the sample is visualized at the frozen state. This method presents several advantages when compared to the other methods. It does not require the usage of heavy-contrast and particularly, it allows preservation of the aggregation state and hydration [140].

Figure 2.10 and Figure 2.11 depicts the classification and working principle of the TEM analysis respectively. The principle of TEM is based on optical microscopy. Here, electrons are replaced by photons, electromagnetic lenses are used instead of glass lenses, and the images are visualized from a screen rather than an eyepiece. The TEM technique provides very powerful magnification and information related to compound and element structures [142].

2.6.4 Chemisorption

The method of chemisorption is highly suited for the determination of exposed active sites, because the adsorbate molecule forms a chemical bond on the surface of the adsorbent [143]. Unlike physical adsorption, this process results in the formation of strong chemical bonds that are often irreversible between the molecules of the adsorbate and the metal surface with relatively higher heats of adsorption. The heats of chemical adsorptions are equal to 20 Kcal/mol and due to intermolecular repulsive forces, this can vary significantly with coverage [144].

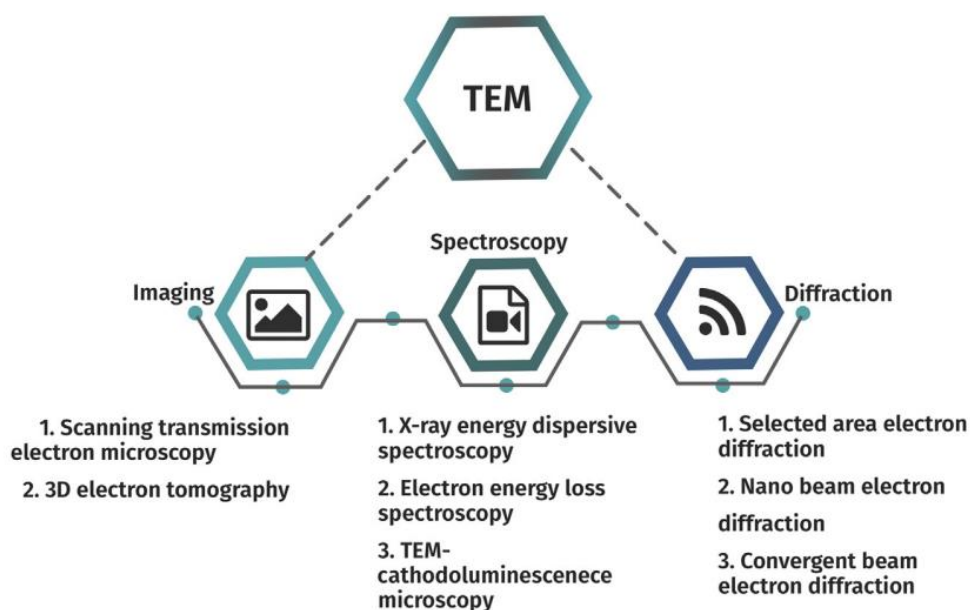


Figure 2.10: TEM classification [139].

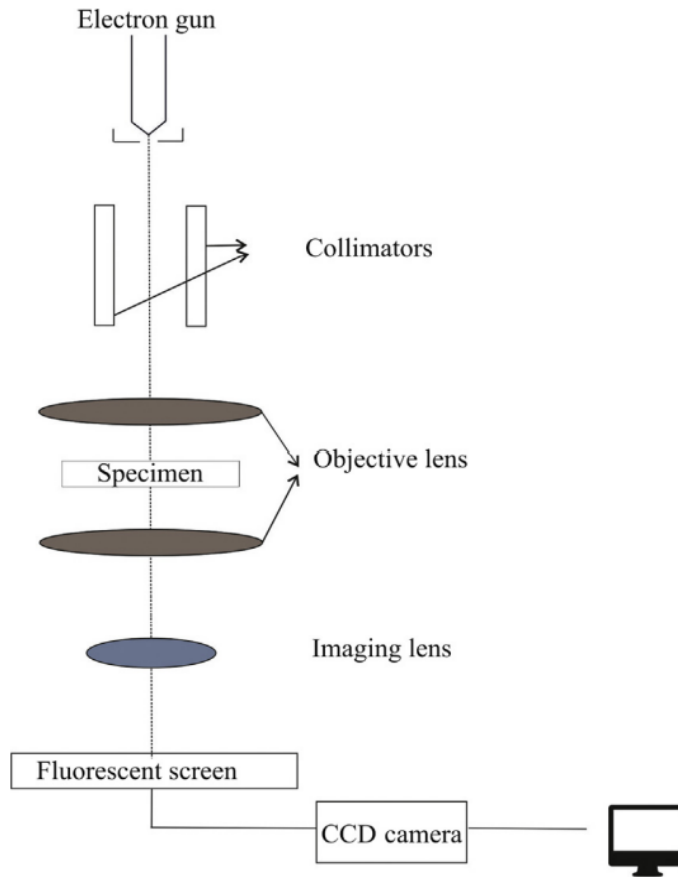


Figure 2.11: The working principle of TEM [139].

Chemisorption can determine the metal dispersion, which is equivalent to the ratio of the surface atoms to the total number of atoms. Furthermore, as a decrease of the surface to volume ratio of the particles is observed, increase in dispersion is equally realized. To calculate the dispersion, experimental determination of the monolayer uptake of the adsorbate, quantity of surface atoms covered by each chemisorbed gas molecule and the catalyst's metal content is required. Eq. 2.6 could be employed for the calculation of dispersion (D).

$$D = \frac{N_m * S * M}{100 * W} \quad (2.6)$$

Where N_m is the quantity of adsorbed molecules, S is the adsorption stoichiometry (e.g $S = 2$ for H_2 on Cu), M and W are the molecular weight and the loading of metal respectively. Additionally, the quantity of gas adsorbed by the sample in the chemisorption process can be used to obtain the monolayer capacity V_m . By employing Langmuir's model (Eq. 2.7), determination of the active sites on the surface from the isotherm can be realized, where V_m (mL at STP) is the monolayer volume and L represents the Avogadro's constant ($6.022 \times$

10^{23} /mol). Eq. 2.8 expresses the total active area A_m , where A_x represents the cross-sectional area of metal atom. Moreover, the dispersion $\gamma\%$ can be calculated by the ratio of exposed metal atoms to the total metal content (N_t) (Eq 2.9) [145].

$$N_a = \frac{V_m}{22414} LS \quad (2.7)$$

$$A_m = \frac{N_a A_x}{W} \quad (2.8)$$

$$\gamma\% = \frac{N_a}{N_t} * 100\% \quad (2.9)$$

2.6.5 N₂ adsorption desorption

Gas adsorption-desorption is the most common method utilized for the characterization of the surface area and pore size of porous materials. Among all the gases and vapors which are readily accessible and can be used as adsorptives, the effectiveness of nitrogen has remained unmatched. [146]. According to the strength of interaction, the process of adsorption can be classified into two categories of chemical (chemisorption) and physical (physisorption) adsorption. To determine surface area, physisorption is the most efficient approach because the adsorption is realized at lower heat, preventing violent or disruptive changes to the surface of the sample during measurement. Unlike the former, physical adsorption could result in surface coverage by multiple layers of the adsorbate. In addition, since no activation energy is required, the equilibrium is rapidly achieved. Thus, the pores can be filled stepwise from micropores to monolayer and multilayer. Analysis of the adsorption and desorption data harnessed is then used to determine the pore size, pore volume and distribution [147].

As is well known, the Brunauer – Emmett – Teller (BET) theory is the most adopted theory used for the determination of the surface area of porous materials. This theory is based on a simplistic model of physisorption. As in Langmuir theory, the surface of the adsorbent is viewed as an array of equivalent sites on which molecules adsorption occur in a random pattern [146]. It is believed that the occupation probability of a site is not dependent on the occupancy of the neighboring sites and there are also lateral exchanges between the adsorbed molecules. The molecules present in the first layer serve as sites for the molecules in the second layer; these are also successively sites for molecules in the third layer and so on for molecules in the upper

layers. Despite that no lateral interactions are allowed; it is assumed that all the layers above the initial layer have liquid-like characteristics. After considering a multi-layer adsorption for the BET theory, the BET equation (Eq. 2.10) was deduced.

$$\frac{1}{W \left(\frac{P}{P_0} - 1 \right)} = \frac{1}{W_m C} + \frac{C-1}{W_m C} \left(\frac{P}{P_0} \right) \quad (2.10)$$

Where P and P_0 are the equilibrium and the saturation pressure of adsorbates at the temperature of adsorption respectively, C represents the BET constant relating the adsorbate and adsorbent interactions. Through measurement, W_m (weight corresponding to the BET monolayer) can be determined from the plots of $1/[W \times (P/P_0 - 1)]$ versus P/P_0 obtained from the accumulated gas quantity adsorbed versus gas pressure at certain temperatures which are dependent on the adsorbate (i.e., 77 K for nitrogen).

According to the classification of IUPAC, the sorption isotherms are of six different types; type I to VI, presented in Figure 2.12 a and b [146]. From the figures, the type IV isotherm is typical for mesoporous materials and the most characteristic feature of this isotherm is the hysteresis loop which can be related to the presence of pore condensation. The BET theory is not only considered as simple but also highly effective since it has the ability to account for the various isotherm types. Thus, it is the most universally applied for surface area determination.

To measure the pore volume and pore size distribution, the Barrett-Joyner-Halenda (BJH) method is commonly utilized. The results are obtained directly from the gas adsorption isotherms and modified Kelvin equation. Eventually, the relationship between the volume of capillary condensate and pressure can be determined by the correlation of vapor depression to capillary radius [145].

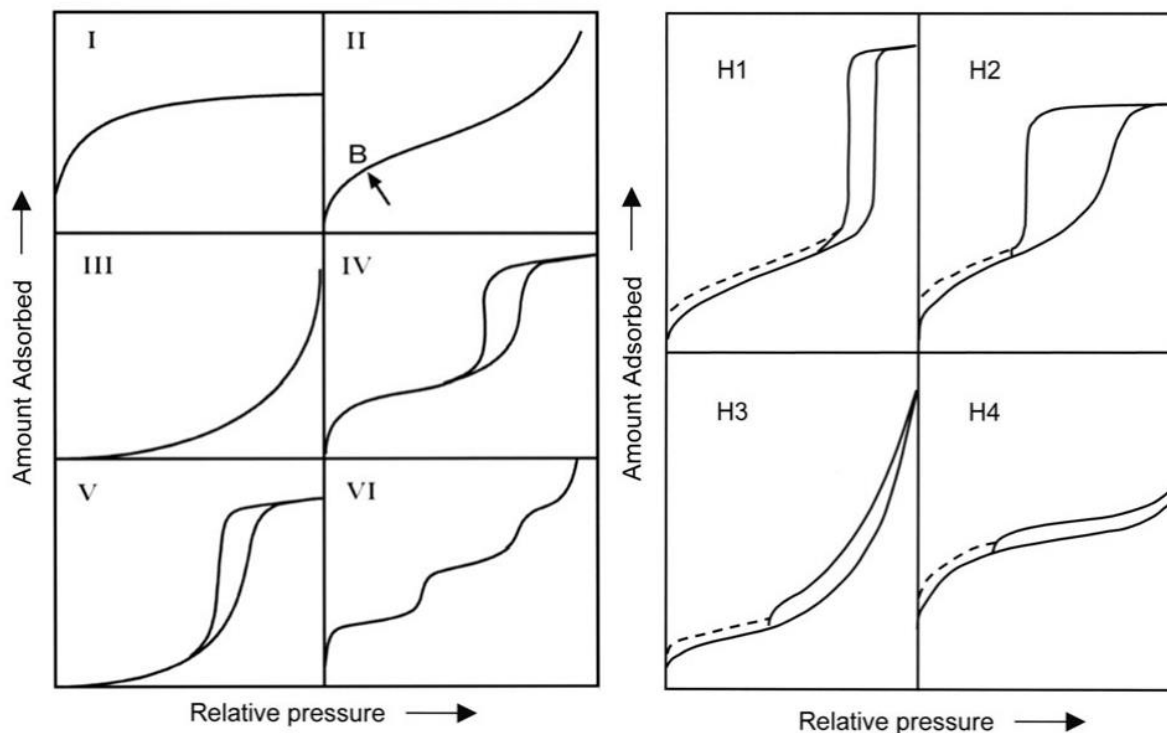


Figure 2.12: (a) Types of physisorption isotherms; (b) Types of hysteresis loops [146].

2.6.6 Gas chromatography (GC)

Gas chromatography is a widely adopted dynamic method for the separation and determination of the composition of volatile compounds. This method is relatively fast and simple, and the analysis is applicable to several organic and inorganic substances. This analysis is a physical separation method, where the components of a sample is split to two phases: a stationary bed characterized with a relatively larger surface area and a gas which travels through the stationary bed. The sample is vaporized and transported through the column by the carrier gas (mobile gas phase). According to the solubilities of the samples at given temperatures, they equilibrate into the stationary liquid phase. Eventually, the sample components (analytes or solutes) split from one another because of their different relative pressures and affinities for the stationary bed. Similarly, the International Union of Pure and Applied Chemistry (IUPAC) defined chromatography as a separation method where the components to be separated are split to two phases, a stationary phase and a mobile phase that travels in a definite path. A method of chromatography referred to as “Elution chromatography” is that where the sample is continuously fed into the system as a finite slug due to continuous passes of the mobile phase through the chromatographic bed [148].

Furthermore, during the GC analysis, the detector and carrier gas are not necessarily required for the separation itself. However, they are typically used in modern versions of the technique [149]. The different chromatography processes are named in accordance with the physical state of the mobile phases. Thus, in the liquid chromatography (LC), the mobile phase is a liquid, while that of gas chromatography (GC) is a gas. Subsequently, there are also other sub-classifications used to categorize the different types of chromatography which is related to the state of their stationary phase [150]. The categorizations of the different chromatography types are depicted in Figure 2.13. Consequently, the usage of gas as the mobile phase requires the development of a system that is leak-free. This is usually achieved with a metal tube or glass considered to be the column. As the solutes leave the column when traveling through the detector, output signals are recorded as a chromatogram.[149]

To determine the quantity of solutes in a sample, the chromatogram data has to be analyzed, peak heights are measured, and calculations are carried out in desired units. There are five methods of quantitative analysis, namely area normalization, area normalization with response factors, standard addition, internal standard and external standard [150]. However, the most used method in analyzing gases is the external standard.

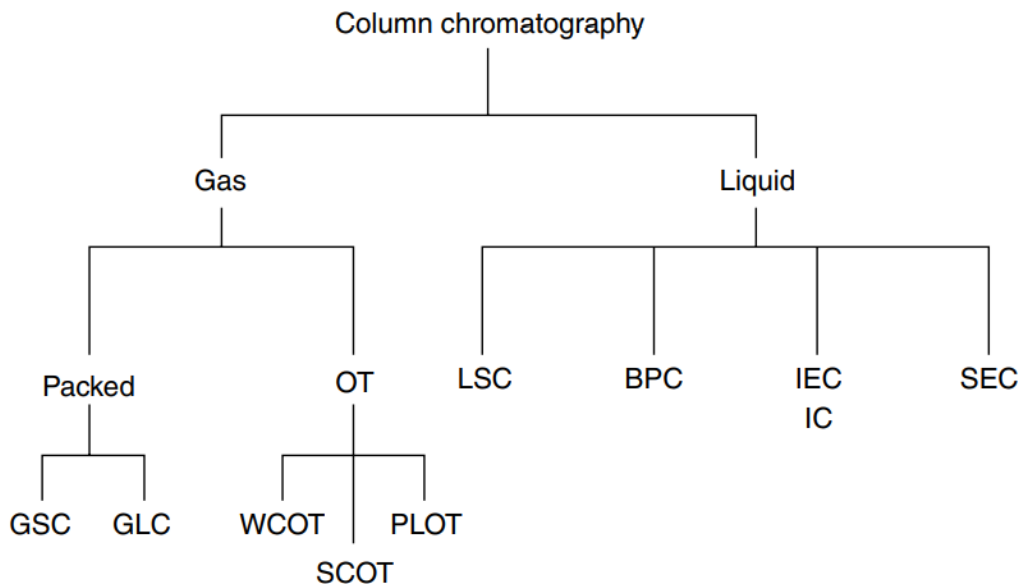


Figure 2.13: Classification of the various chromatography methods [150].

2.7 Kinetics of methanol synthesis

Methanol production from carbon dioxide is accomplished through two different reactions: carbon dioxide hydrogenation and the water gas shift reaction. The preferred reaction is the hydrogenation of carbon dioxide which takes place in parallel to the RWGS that produces carbon monoxide [151]. Numerous kinetic models have been reported to describe the methanol synthesis [151, 152]. The studies are differentiated by altering the pressure and the temperature of the reaction, thermodynamic and kinetic parameters, feedstock composition and the catalysts [151]. Initially, the models were exclusive for methanol production from carbon monoxide and hydrogen, and they were not used for pure CO₂ feed streams. Later, more complex models have been introduced considering that methanol can be produced from CO₂ hydrogenation [152]. Diverse kinetic models were used, where they were focused on the rate determining step concluded from the reaction's mechanism.

2.7.1 Kinetic models

As a definition, a kinetic model is a mix between the kinetic rate equation and respective kinetic parameter set [153]. Kinetic modelling is an interesting subject in heterogeneous catalysis and different kinetic models can be applied depending on the level of understanding of the reaction. Power laws and Langmuir–Hinshelwood–Hougen–Watson models (LHHW) are mainly used to describe the methanol synthesis reaction [154].

Van den Bussche and Froment [155] proposed a steady state kinetic model for methanol synthesis on the Cu/ZnO/Al₂O₃ catalyst. The model considered CO₂ resulting from the water gas shift reaction as the main source of carbon. This model contradicts the first models developed on the same catalyst which considered CO as the only source of carbon in the reaction. The dissociative adsorption of CO₂ and H₂ was the rate determining step [154, 155].

Another kinetic model was developed for the same commercial catalyst Cu/ZnO/Al₂O₃. The model focused on the adsorption of both CO and CO₂ on different types of the active sites of copper, and it showed similar contributions of CO and CO₂ hydrogenation. The model considered the two hydrogenation reactions in addition to the water gas shift reaction, and it proposes that higher methanol production depends on temperature and CO fraction. This model is based on the Langmuir–Hinshelwood–Hougen–Watson (LHHW) mechanism [153, 156].

LHHW and power models are commonly used as the simplest case, and power laws are usually used when there is limited information on the mechanism of the chemical reaction [154]. The

power law requires several assumptions, and it usually considers the CO₂ hydrogenation reaction and the reverse water gas shift reaction [152]. The model includes a comparison between the experimental data and modelled data, and assumptions are used to reduce the differences among them. The power law model will be discussed further in the following section.

Microkinetic models were also used for methanol synthesis. It was found that this model could explain many of the significant kinetic dependencies of the RWGS reaction over the copper-based catalysts. This model focuses on exploring the chemistry of a reaction more than the reaction rate which is vital in the reactor design calculations [157]. Grabow & Mavrikakis [158] proposed a new microkinetic model for methanol synthesis and water gas shift reaction on the same commercial catalyst Cu/ZnO/Al₂O₃. The model was extensive and included 49 elementary steps that allowed a variety of diverse reaction mechanism and took into consideration the formation of by-products. The biggest advantage of this model is its ability to estimate reaction rates at different conditions such as temperature, pressure, and feed composition [158]. Based on the study by Peter et al. [154], the LHHW and the power law gave higher precise methanol synthesis rates than that of the microkinetic model.

2.7.2 Power law model

Power law model is widely used in kinetics of methanol synthesis because it is a simple model and does not require a lot of information or hypothesis about the reaction mechanism [152, 157]. The power law model focuses on thermodynamic equilibrium, and it is established through sixteen elementary steps [151]. It uses a series of equations that include thermodynamics, activation energy, and catalytic activity. As stated above, it also depends on assumptions and considers two reactions which are CO₂ hydrogenation and reverse water gas shift reaction [152]. It is not restricted to the model parameters. However, precautions should be taken when using it to describe the data because there are many possibilities for fitting the data [154]. The basis of the power law is the implementation of a theoretical and experimental analysis for the chemical reaction and the goal is to decrease the gap between them. It helps in detecting quantitative data about the chemical reaction which can be used later to advance the catalytic process.

The model is divided into two sections: theoretical and experimental. The following equations and formulas are extracted from the study of Kobl et al. [152].

The reverse reactions are considered in this approach, and an additional factor is added to both kinetic equations. The new factor, which is the thermodynamic equilibrium, β_j , is calculated by the outlet partial pressures and the thermodynamic equilibrium constant (K_j). The inclusion of this factor is necessary since these reactions are limited by thermodynamic equilibrium.

β_j is the thermodynamic equilibrium where j is the reaction index. Two reactions are considered (i) CO₂ hydrogenation to methanol (j = methanol) and (ii) reverse water gas shift reaction (j =CO).

$$\beta_{\text{methanol}} = \frac{P_{(\text{methanol},\text{out})} \times P_{(\text{H}_2\text{O},\text{out})}}{K_{(\text{methanol})} \times P_{(\text{methanol},\text{out})}^3 \times P_{(\text{CO}_2,\text{out})}} \quad (2.11)$$

$$\beta_{\text{CO}} = \frac{P_{(\text{CO}_2,\text{out})} \times P_{(\text{H}_2\text{O},\text{out})}}{K_{\text{CO}} \times P_{(\text{H}_2,\text{out})} \times P_{(\text{CO}_2,\text{out})}} \quad (2.12)$$

Quantitative interpretations were excluded by Graaf et al. [159]. However, some changes were applied so that the study will focus on the H₂/CO₂ feed instead of the H₂/CO feed implemented in the original study.

$$K_{\text{methanol}} = (K_{\varphi_{\text{methanol}}} \times K_{P_{\text{methanol}}}) * K_{\text{CO}} \quad (2.13)$$

$$K_{\text{CO}} = K_{\varphi_{\text{CO}}} \times K_{P_{\text{CO}}} \quad (2.14)$$

The two factors K_P and K_φ are partial pressure coefficient and fugacity coefficient respectively.

$$\text{Where } K_{P_{\text{methanol}}} = \frac{Y_{\text{methanol}}}{Y_{\text{CO}} \times Y_{\text{H}_2}} \quad (2.15)$$

$$K_{P_{\text{CO}}} = \frac{Y_{\text{H}_2\text{O}} Y_{\text{CO}}}{Y_{\text{CO}_2} \cdot Y_{\text{H}_2}} \quad (2.16)$$

Y is the mole fraction of the components.

The methanol synthesis reaction will take place at 30 bar, and it will occur in non-ideal gas conditions. However, the partial pressures were not modified for these non-ideal conditions. Even though the correction would have led to better results, but these non-ideal conditions will

not cause huge effect unless the total pressure exceeds 100 bar. In addition to that, the fugacity correlation can be neglected [159–161]. Therefore, $K_{\phi_{methanol}} = K_{\phi_{CO}} \approx 1$.

Another important factor is temperature because the reaction rate is highly dependent on it. Thus, some parameters were considered to account for the temperature sensitivity in the model. The activation energy factor Ea , and pre-exponential factor k , were added to the model to account for this constraint [152].

Additionally, it can be assumed that the partial pressures of the reactants are homogenous over the whole catalyst bed. Two additional parameters n_j and m_j were introduced and defined according to the inlet pressures of H_2 and CO_2 respectively.

Taking all these assumptions into consideration, Eq. 2.17 and 2.18 were formulated for the $TOF_{methanol}$ and TOF_{CO} from the power law expressions:

$$TOF_{methanol} = K_{methanol} \exp\left(\frac{-Ea_{methanol}}{RT}\right) p_{H_2}^{n_{methanol}} p_{CO_2}^{m_{methanol}} (1 - \beta_{methanol}) \quad (2.17)$$

$$TOF_{CO} = K_{CO} \exp\left(\frac{-Ea_{CO}}{RT}\right) p_{H_2}^{n_{CO}} p_{CO_2}^{m_{CO}} (1 - \beta_{CO}) \quad (2.18)$$

As discussed earlier, the power law model is well-defined by the implementation of both theoretical analysis and experimental analysis for the chemical reactions. Some parameters must be explained to have a better understanding of the experimental approach. The index factor (j) is common between the theoretical and experimental analysis.

First parameter n_j is the amount of the component consumed throughout the experimental period: $n_j = \int_0^{t_R} F_j dt$ where F_j is the molar flow rate, and t_R is the time of the experiment.

Additionally, conversion of the reactants CO_2 and H_2 should be taken into account. It is calculated throughout the experiment period. The selectivity can be determined from the carbon content present in the product. Conversion and selectivity are presented by the following equations:

$$X_{CO_2} = \frac{n_{CH_3OH} + n_{CO}}{n_{CO_2,in}} \times 100 \quad (2.19)$$

$$X_{H_2} = \frac{2n_{CH_3OH} + n_{H_2O}}{n_{H_2,in}} \times 100 \quad (2.20)$$

$$S_{CH_3OH} = \frac{n_{CH_3OH}}{n_{CH_3OH} + n_{CO}} \times 100 \quad (2.21)$$

$$S_{CO} = 1 - S_{CH_3OH} \quad (2.22)$$

TOF values are calculated from the experimental data by considering an equally active surface area and assuming that the two reactions occur at the copper surface [162]. Parameters included in the TOF equations are: n : number of moles of methanol; m_{cat} : mass of the catalyst; t : reaction time; N_A : Avogadro's number = $6.022 \times 10^{23} \text{ mol}^{-1}$; N_S : number of surface copper atoms per unite surface area = $1.46 \times 10^{19} \text{ atoms m}^{-2}$ supposing equal areas of exposed (100), (110), and (111) planes.

TOF can be experimentally calculated by Eq. 2.23 and 2.24:

$$TOF_{CH_3OH} = \frac{n_{CH_3OH} \times N_A}{m_{cat} \times SA_{Cu} \times N_S \times t} \quad (2.23)$$

$$TOF_{CO} = \frac{n_{CO} \times N_A}{m_{cat} \times SA_{Cu} \times N_S \times t} \quad (2.24)$$

Finally, correlation should be done between the power law model and the experimental data. The theoretical TOF versus experimental TOF can be plotted as shown in Figure 2.14. The figures known as parity plots are plotted for both reactions of methanol synthesis and RWGS over a CuZA catalyst. They represent a quantitative comparison between theoretical and experimental data. It can be deduced from the example in the figures that most of the experimental data points are defined by the model with an error less than 10% which shows a good precision of the power law model [152].

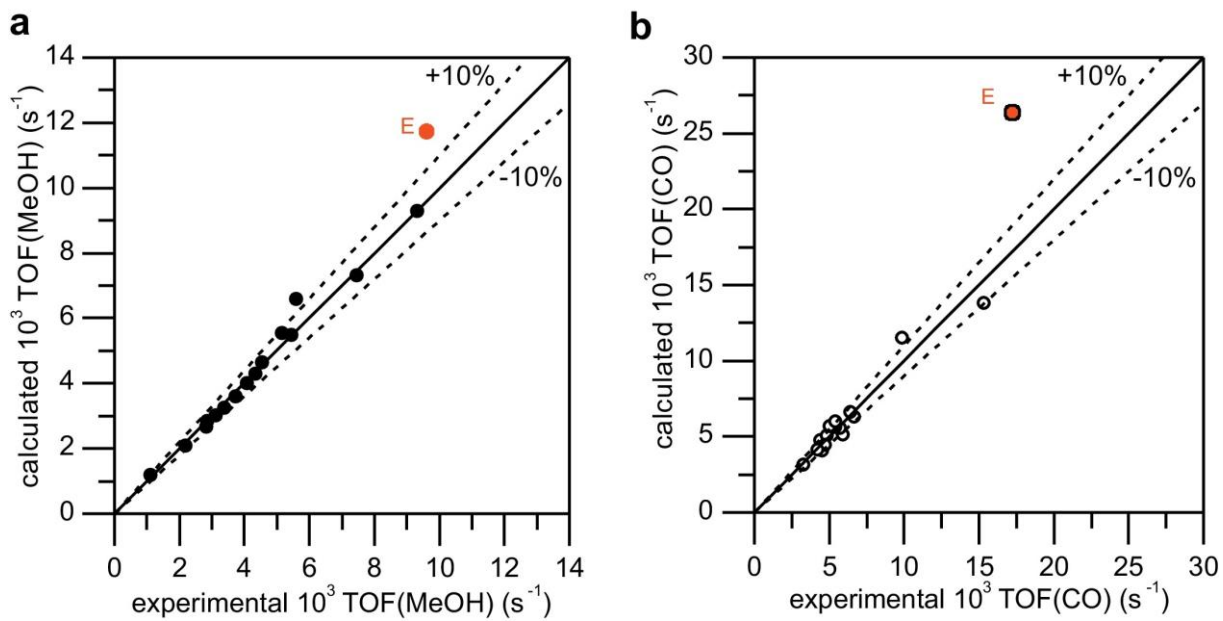


Figure 2.14: Parity Plots for (a) methanol synthesis (b) reverse water gas shift reaction [152].

In conclusion, the comparison between the theoretical and experimental analysis is critical to recognize what is the reaction mechanism, and to test the validity of the assumptions.

3. Experimental

3.1. Materials and equipment

The chemicals used in this experiment were utilized as received and no further purification was performed. Table 3.1 summarizes the chemicals used for catalyst preparation. Furthermore, the gases utilized in this thesis work are summarized in Table 3.2.

Table 3.1: List of chemicals utilized for catalyst preparation.

No	Materials	Chemical formula	Manufacturer	Molecular weight (g/mol)	Purity
1	Copper (II) Nitrate Trihydrate	$\text{Cu}(\text{NO}_3)_2 \cdot 3\text{H}_2\text{O}$	ACROS ORGANICS	241.59	$\geq 99\%$
2	Zinc Nitrate hexahydrate	$\text{Zn}(\text{NO}_3)_2 \cdot 6\text{H}_2\text{O}$	ALFA AESAR	297.49	$\geq 99\%$
3	Aluminum Nitrate Nanohydrate	$\text{Al}(\text{NO}_3)_3 \cdot 9\text{H}_2\text{O}$	EMSURE	375.13	$\geq 98.5\%$
4	Lanthanum(III) Nitrate Hexahydrate	$\text{La}(\text{NO}_3)_3 \cdot 6\text{H}_2\text{O}$	ALFA AESAR	433.01	99.9%
5	Cerium(III) Nitrate Hexahydrate	$\text{Ce}(\text{NO}_3)_3 \cdot 6\text{H}_2\text{O}$	ALFA AESAR	434.23	99.9%
6	Sodium Carbonate	Na_2CO_3	EMSURE	105.99	$\geq 99.9\%$
7	Sodium Hydroxide	NaOH	EMSURE	40.0	$\geq 99.2\%$
8	Silicon Carbide	SiC	ALFA AESAR	40.1	$\geq 98.8\%$
9	Nitric Acid	HNO_3	ANALAR NORMAPUR	63.01	$\geq 65\%$

Table 3.2: List of Gases used during this work.

No	Materials	Chemical formula	Manufacturer	Molecular weight (g/mol)	Purity
1	Carbon dioxide	CO ₂	Yara Praxair	44	99.999%
2	Helium	He	Yara Praxair	2	99.999%
3	Hydrogen	H ₂	Yara Praxair	2.008	99.999%
4	Nitrogen	N ₂	Yara Praxair	28	99.999%
5	Synthetic air	N ₂ ,O ₂	Yara Praxair	28.9	99.999%

3.2 Catalyst preparation

The co-precipitation method was used to prepare two series of catalysts promoted by Ce and La. The reference catalyst synthesized was CuZnAl and is denoted as CuZnAl-0. The other catalysts containing La and Ce is denoted by CuZnAl-YCe and CuZnAl-YLa respectively, where Y represents the weight percentage of Ce and La. In addition, a new La promoted catalyst that was developed by the sequential preparation method is denoted by La/CuZnAl. Table 3.3 summarizes the catalysts prepared and their composition.

Table 3.3: Denotations and composition of the prepared catalysts.

Denotation	Cu/Zn/Al/promoter molar ratio	Catalyst Compositions (wt.%)
CuZnAl-0	0.6/0.3/0.1	60 Cu - 30 Zn – 10 Al
CuZnAl-2La	0.6/0.3/0.08/0.02	60 Cu - 30 Zn – 8 Al – 2 La
CuZnAl-4La	0.6/0.3/0.06/0.04	60 Cu - 30 Zn – 6 Al – 4 La
CuZnAl-6La	0.6/0.3/0.04/0.06	60 Cu - 30 Zn – 4 Al – 6 La
CuZnAl-2Ce	0.6/0.3/0.08/0.02	60 Cu - 30 Zn – 8 Al – 2Ce
CuZnAl-4Ce	0.6/0.3/0.06/0.04	60 Cu - 30 Zn – 6 Al – 4 Ce
CuZnAl-6Ce	0.6/0.3/0.04/0.06	60 Cu - 30 Zn – 4 Al – 6 Ce
La/CuZnAl	0.6/0.3/0.06/0.04	60 Cu - 30 Zn – 6 Al – 4 La

The preparation method for the catalyst developed by the co-precipitation method was based on a procedure described by Behrens and Shlögler [163]. For each synthesis, stoichiometric portions of Copper (II) Nitrate Trihydrate, Zinc Nitrate Hexahydrate, Aluminum Nitrate Nonahydrate, and one of the promoters (Lanthanum (III) Nitrate Hexahydrate or Cerium (III) Nitrate Hexahydrate) were dissolved in 138 ml of distilled water. This mixture is referred to as the cationic solution and had a metal concentration of 1 M. In another beaker, 25 g of sodium carbonate was dissolved in 196 ml of distilled water, and this mixture is referred to as the anionic solution and has a concentration of 1.2 M. After that, 200 ml of deionized water was added to a new beaker and the two solutions (anionic and cationic) were placed in funnels above the beaker. The solutions were added dropwise simultaneously to the water in the beaker while stirring at 300 rpm. During the process of mixing, the pH was held constant at 6.5 using a pH meter, since the control of the pH during coprecipitation is a key factor in catalyst synthesis [1]. The second step after preparing the mixture was to age it overnight at 65°C under stirring at 300 rpm. The aging time is important as it can modify the interfacial contact between Cu and the oxide components in the final catalyst [164]. The third step was washing the catalyst in which the catalyst was placed on a filter paper and rinsed several times using vacuum filtration. After washing, the residue on the filter paper (filter cake) was dried overnight in the oven at 80°C. Eventually, after drying of the catalyst, it was crushed and calcined at 350°C with a temperature ramp rate of 2°C/min for three hours.

In addition, an La promoted CuZnAl catalyst was prepared by the sequential preparation method. Calcined CuZnAl catalyst and La precursor was dissolved in 400 mL of water and mixed overnight. After that, the solution was dried overnight, crushed, and calcined again at 350°C with a temperature ramp rate of 2°C/min for one hour.

3.3 Catalyst characterization

3.3.1 X-Ray diffraction

The catalysts (as-prepared, calcined, and reduced) were subjected to X-ray diffraction study using a Bruker-AXS Microdiffractometer D8 Advance with CuK α radiation source. 2 θ range is elected in 10-90° to record the patterns, with a step interval of 1°/min. The catalysts were finely crushed to make the surface as smooth as possible before analysis. Bragg's law equation (Eq. 2.4) and the Scherrer equation (Eq. 2.5) were used to quantify the structural properties.

3.3.2 Nitrogen adsorption-desorption

The Micrometrics Tristar 3000 instrument utilizing liquid nitrogen at -196°C was used for the adsorption-desorption experiment. Prior to the analysis, the samples were degassed using the Micrometrics VacPrep 061 sample degas system at 180°C overnight under vacuum condition. The specific surface area (SSA) and pore size distribution were estimated using the BET and BJH methods discussed in section 2.5.7, respectively [145–148]. In addition, the total pore volume (PV) was determined from the adsorbed gas quantity at P/P₀ of 0.99.

3.3.3 Temperature programmed reduction

H₂-TPR measurements were carried out by utilizing a Micromeritics Autochem II ASAP 2920 analyzer that is equipped with a thermal conductivity detector (TCD). The calcined samples (~30 mg) were degassed at 200°C in helium flow for 30 minutes to remove any trace of CO₂ and H₂O if present. Eventually, the temperature was cooled down to 50°C and the reducing gas mixture (10 vol% H₂ in argon) at 50 ml/min flowed over the samples. Finally, the temperature was ramped up to 550°C at a rate of 10°C/min and the TPR profiles were recorded.

3.3.4 N₂O chemisorption

The Cu surface area was measured by dissociative N₂O adsorption utilizing the same equipment as for the TPR (Micromeritics Autochem II ASAP 2920). Prior to the adsorption of N₂O, 100 mg of each of the samples were heated to 200°C (ramp rate 5°C/min) for 30 minutes under He flow. Subsequently, it was reduced in 10 vol% of H₂ in argon at 300°C for 120 minutes, and further purged with helium until the temperature was 50°C. The adsorption of N₂O was performed in a 1% N₂O/He mixture at 50°C according to a procedure by Van Der Grift et al. [165, 166]. Afterwards, the physisorbed N₂O was removed by purging the sample with He for 60 minutes. To determine the amount of N₂O consumed, the catalysts were firstly reduced with 10% H₂–90% Ar from 50 to 400°C (ramp rate of 10°C/min), and H₂ TPR analysis was performed. The Cu surface area (SA_{Cu}) was calculated from the amount of H₂ consumed by employing Equation 3.1.

$$SA_{Cu} (m^2 \cdot g_{cat}^{-1}) = \frac{Y \times SF \times N_A}{C_M \times W_{cat}} \quad (3.1)$$

Where Y denotes H_2 consumed in moles after N_2O chemisorption, N_A is the Avogadro's number (6.022×10^{23}), SF represents the stoichiometric factor, which is 2, W_{cat} is the weight of catalyst (g) and C_M is the number of surface Cu atoms per unit surface area (1.47×10^{19} atoms/ m^2).

3.3.5 Transmission electron microscopy

The morphology of the reduced samples was investigated by TEM, utilizing a JOEL JEM-2100F equipment operated at 200 kV. For sample preparation, the catalyst powders which were reduced and passivated were dispersed in ethanol by ultrasonication for 20 minutes on a holey carbon-coated grid.

3.4 Catalytic activity tests

A fixed-bed tubular reactor made of a stainless-steel tube having an internal diameter of 0.5 cm and a length of 50 cm was used in this study. The schematic of this setup is represented in Figure 3.1. The reactor was supplied with feed gases of CO_2 , H_2 and N_2 which were regulated by mass flow controllers (F-201CV, Bronkhorst). The pressure regulator for each gas feed line was set to 50 bar and a pressure gauge and back-pressure valve (Tescom) were installed to measure the pressures at pre-entry and post outlet lines of the reactor. To avoid condensation of liquid products, all the post-reactor lines were heated to $120^\circ C$. Heating up of the reactor was achieved by utilizing an electric oven, and the temperature was modulated by a temperature regulating unit (Eurotherm 328). A thermocouple (type K) was placed close to the middle of the reactor to measure the temperature.

The catalysts for the activity tests were crushed and sieved to 40-60 mesh. They were further mixed with silicon carbide (SiC) at a weight ratio of 1:10. A quartz wool plug was inserted into the tubular reactor to ensure the catalyst bed is kept in place. Prior to the activity tests, the catalysts were reduced in 50 vol% (H_2/N_2) under 50 mL/min flowrate at $300^\circ C$ for 3 hours with a heating rate of $5^\circ C/min$. After reduction, the reactor was cooled down to ambient temperature under N_2 flow. Subsequently, the reactor was pressurized with the reaction mixture after cooling, followed by a temperature ramp up to the desired reaction temperature. Typically, the mixture consisted of 50-100 mL/min flow of $H_2:CO_2:N_2$ at the ratio of 3:1:1.

Analysis of the products were performed using online Agilent 7890 B gas chromatography (GC) which has two channels that were fitted with TCD detectors. For the separation of H_2 , N_2 and CO , a Mols 5A (diameter 1 mm, length 1.5 m and thickness 80/100 μm) and a HayeS Q

(diameter 1 mm, length 0.25 m and thickness 80/100 μm) was used, while a GS-carbon plot column was used to separate the remainder products, mostly CO_2 , C1-C3 hydrocarbons, and C1-C3 oxygenates. Prior to the start of the experiment, calibration of the gaseous components was carried out using a gas mixture with predetermined composition.

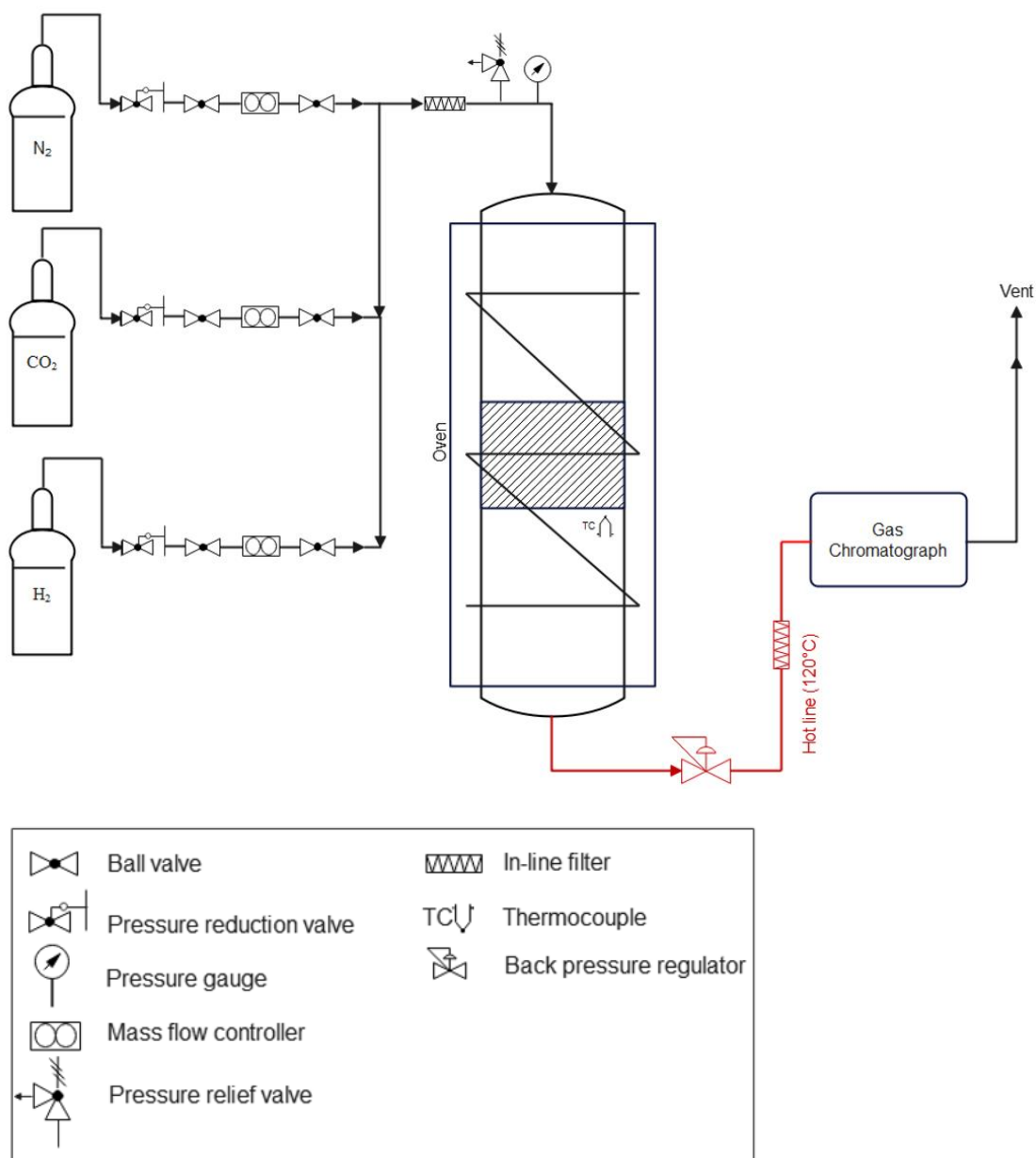


Figure 3.1: Schematic diagram of the CO_2 hydrogenation experimental setup.

CO₂ conversion (X_{CO_2}) was determined using N₂ as the internal standard. The calculation of X_{CO_2} is based on Equation 3.2

$$X_{CO_2}(\%) = \left[1 - \frac{\text{moles } CO_{2,out}}{\text{moles } CO_{2,in}} \times \frac{\text{moles } N_{2,in}}{\text{moles } N_{2,out}} \right] \times 100 \quad (3.2)$$

The product selectivity (S_i) and space-time yield for methanol ($STY_{methanol}$) was calculated using Equation 3.3 and 3.4 respectively.

$$S_i(\%) = \frac{\text{moles product}_{i,out}}{\sum \text{moles product}_{i,out}} \times 100 \quad (3.3)$$

$$STY_{methanol} \left(\frac{\text{mmol}}{\text{g}_{cat} \cdot \text{h}} \right) = \frac{F_{CO_2,in} \times X_{CO_2} / 100 \times S_{methanol} / 100}{W_{cat}} \quad (3.4)$$

where F_{CO_2} (mmol/h) is the molar flow rate of CO₂ at the reactor inlet and W_{cat} (g) is the weight of catalyst.

Furthermore, the TOF of methanol was calculated based on the number of Cu surface atoms determined from N₂O chemisorption analysis using Eq. 3.5.

$$TOF_{methanol} \left(\frac{\text{molecules}_{methanol}}{\text{sec ond} \cdot \text{Cu}_{site}} \right) = \frac{R_{methanol} \times N_A}{S_{Acu} \times C_M} \quad (3.5)$$

where $R_{methanol}$ (mol.g⁻¹.s⁻¹) represents the methanol production rate.

4. Results and discussion

4.1 Characterization of Catalysts

4.1.1 XRD analysis of as-prepared catalysts

XRD patterns of the as-prepared promoted Ce and La catalyst precursors are presented in Figure 4.1a and b, respectively. The pattern for CuZnAl-0 is included in the figures for reference. As anticipated, the diffractograms of the catalyst display typical malachite-like structure as the dominant phase. The peaks located at 2θ of 11.99° , 14.83° , 17.58° , 18.88° , 24.10° , 29.48° , 32.161° and 35.627° represent the (110), (020), (120), (200), (220), (230), (21-1) and (240) planes characteristics of $\text{Cu}_2+2(\text{CO}_3)(\text{OH})_2$ (JCPDS 041-1390). The shift in the (21-1) peak in the 2θ range of $31-33^\circ$ could be as a result of successful Zn incorporation into the malachite structure [120]. In addition, the absence of clearly resolved peaks that correspond to Al_2O_3 and CeO_2 , and La_2O_3 in the XRD patterns could be due to the low amount of these oxides, and this indicates that they exist in a microcrystalline or amorphous state. Similar results have been reported for both Ce and La modified CZA catalysts which were synthesized by the co-precipitation under similar conditions [66, 67, 167].

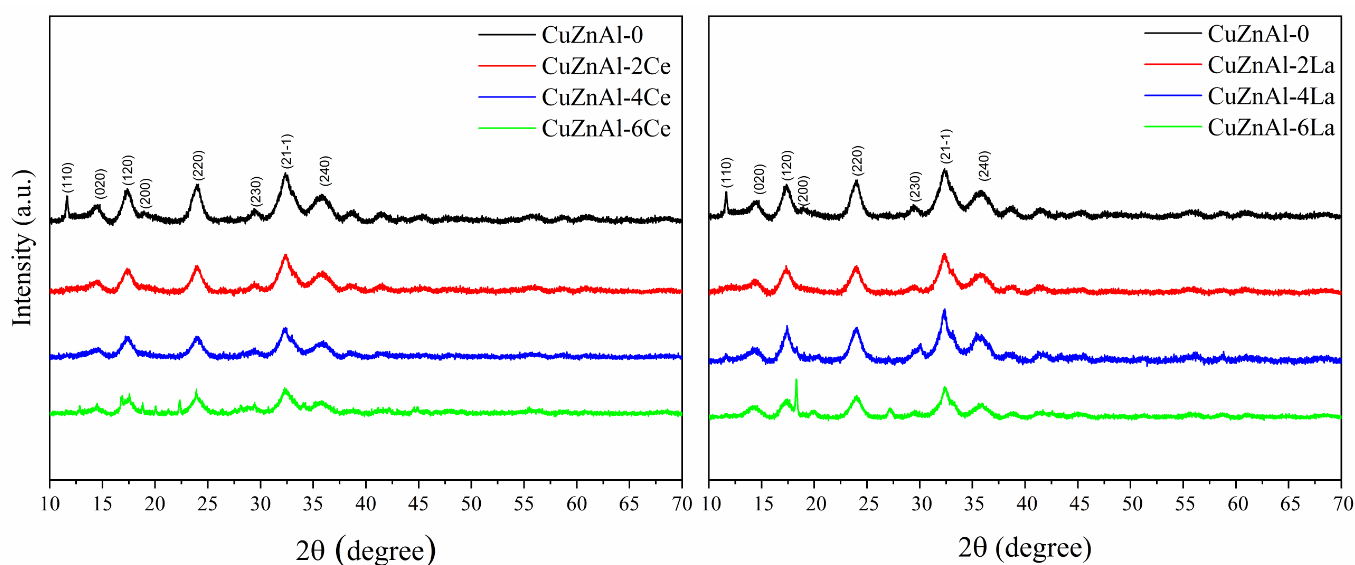


Figure 4.1: XRD of the as-prepared samples (a) Ce-promoted; (b) La-promoted.

4.1.2 XRD of calcined catalysts

The XRD patterns of the calcined Ce and La promoted catalysts are shown in Figure 4.2a and b, respectively. The pattern for CuZnAl-0 is included in the figures for reference. Upon calcination at 350°C for 3.5 hours, it was evident that the malachite structure was no longer retained [168], and a composition of mixed oxides of ZnO, CuO and CeO₂ (Figure 4.2a) and La₂O₃ (Figure 4.2b) can be detected. There were no peaks of Al-containing species detected, and this indicates that Al is present in an amorphous phase. From Figure 4.2a, the crystalline size of Cu decreased as the Ce content increased, proving that the addition of Ce promoted Cu dispersion. The peaks centered at 2θ of 32.51°, 35.42°, 38.71°, 48.72°, and 61.53° indicated the presence of CuO and corresponded to (110), (002), (111), (20 $\bar{2}$) and (11 $\bar{3}$) planes. In addition, the diffraction peaks of both CeO₂ and ZnO were identified from the XRD pattern of the calcined sample (Figure 4.2a). The peaks located at 2θ of 28.68° and 56.78° corresponded to the (111) and (311) diffraction peaks of cubic CeO₂, and the peak at 2θ of 66.38° indicated the presence of hexagonal ZnO, which corresponded to the (200) plane [169–171]. However, it was observed that as the Ce loading was increased, the peak of CuO and ZnO began to shrink. Therefore, Ce seems to decrease the crystallinity of CuO and ZnO.

Similarly, from Figure 4.2b, the most notable peaks are that of CuO and ZnO. The peak of La₂O₃ was also observed at 2θ of 29.16°, which corresponded to the (002) plane of hexagonal La₂O₃. The La₂O₃ peak expanded as the La content increased. Furthermore, for all the promoted catalyst systems, the addition of the promoters led to increased dispersion of Cu nanoparticles. This is aided by the ZnO particles which help in physically spacing the Cu nanoparticles and promoting dispersion [172].

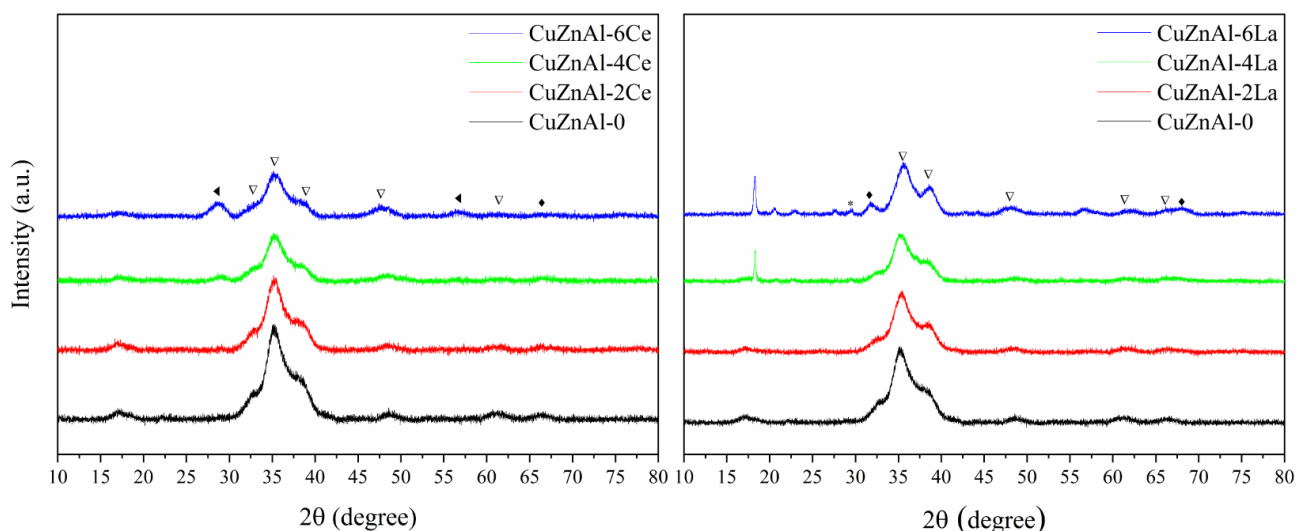


Figure 4.2: XRD of the calcined samples (a) Ce-promoted; (b) La-promoted. (∇) CuO (\blacklozenge) ZnO (\blacktriangleleft) CeO₂ (*) La₂O₃.

4.1.3 XRD of reduced catalysts

The XRD patterns of the reduced-passivated unpromoted and promoted samples are presented in Figure 4.3. The dominant diffraction peaks at 2θ of 43.32° , 50.45° , and 74.13° are typical of metallic copper corresponding to (111), (200), and (220) planes (PDF #85-1326). The peak at 36.4° indicates that parts of the Cu are present as Cu₂O for the catalysts prepared by co-precipitation. Furthermore, the crystallite size is significantly larger for the La promoted catalyst prepared by sequential impregnation. [173]. In addition, the peaks at 2θ of 31.77° , 36.25° , 56.60° , 62.86° , and 67.96° are characteristic of hexagonal ZnO. The diffractograms did not reveal any characteristic peak of the other metals Ce or La: therefore, these species are amorphous or highly dispersed. The calculated crystallite particle size using the diffraction peak around 2θ of 43° , which represents Cu₂O, is 6.4 nm for both CuZnAl-0 and CuZnAl-4Ce catalyst and 4.5 nm for CuZnAl-4La. On the other hand, Cu₂O was not detected for the La/CuZnAl catalyst, and the Cu crystallite had a significantly larger size (12.4 nm) compared to the Cu₂O of the other catalysts representing metallic Cu. Furthermore, it can be seen that the crystallite size of the catalysts prepared by co-precipitation is relatively similar.

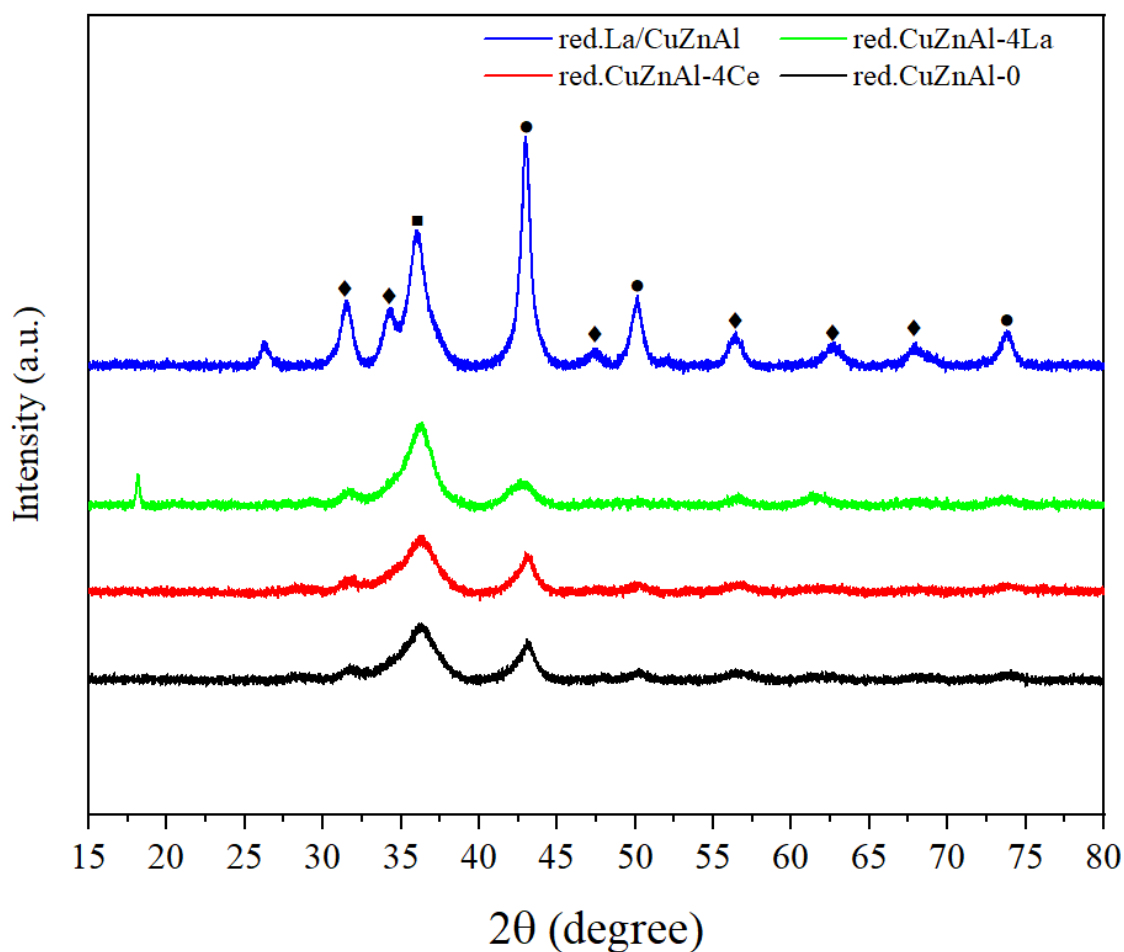


Figure 4.3: XRD pattern of the reduced unpromoted and promoted catalysts. (◆) ZnO (●) Cu⁰ (■) Cu₂O

4.1.4 TPR analysis

The reduction characteristics of the calcined samples were determined by TPR measurements. Figure 4.4 exhibits the TPR profiles of the calcined samples. The reduction peaks observed lie between 160 and 250°C, and this is attributed to the reduction of the CuO species [164]. It can be seen that the main reduction peak of the promoted catalysts shifted to lower temperatures compared to that of CuZnAl [174]. This might be related to the higher dispersion of CuO for the promoted catalysts as observed by XRD. Some of the catalysts were characterized with two peaks, with one occurring at a lower temperature and the other at a higher temperature. The low-temperature peak could have arisen from the finely-dispersed CuO crystallites, while the higher temperature peaks might be ascribed to the reduction of larger CuO crystallites [175]. It is also possible that the reduction of CuO occurs in a two-stage process (CuO→Cu₂O→Cu) where the La and Ce oxide partially stabilize the Cu₂O phase [176]. The reducibility was better for the CuZnAl-4Ce and CuZnAl-4La catalysts which had 4% loading as compared to those

with 2% and 6% for both Ce and La. By peak integration, the amount of hydrogen consumed corresponding to the reduction of CuO to Cu was calculated and is given in Table 4.1. It can be observed that the H₂ consumption decreases with increasing promoter content for the catalyst prepared by co-precipitation. On the other hand, the H₂ consumption is higher for the La/CuZnAl catalyst, which might be related to the enhanced reducibility of CuO and possibly due to the partial reduction of surface La₂O₃.

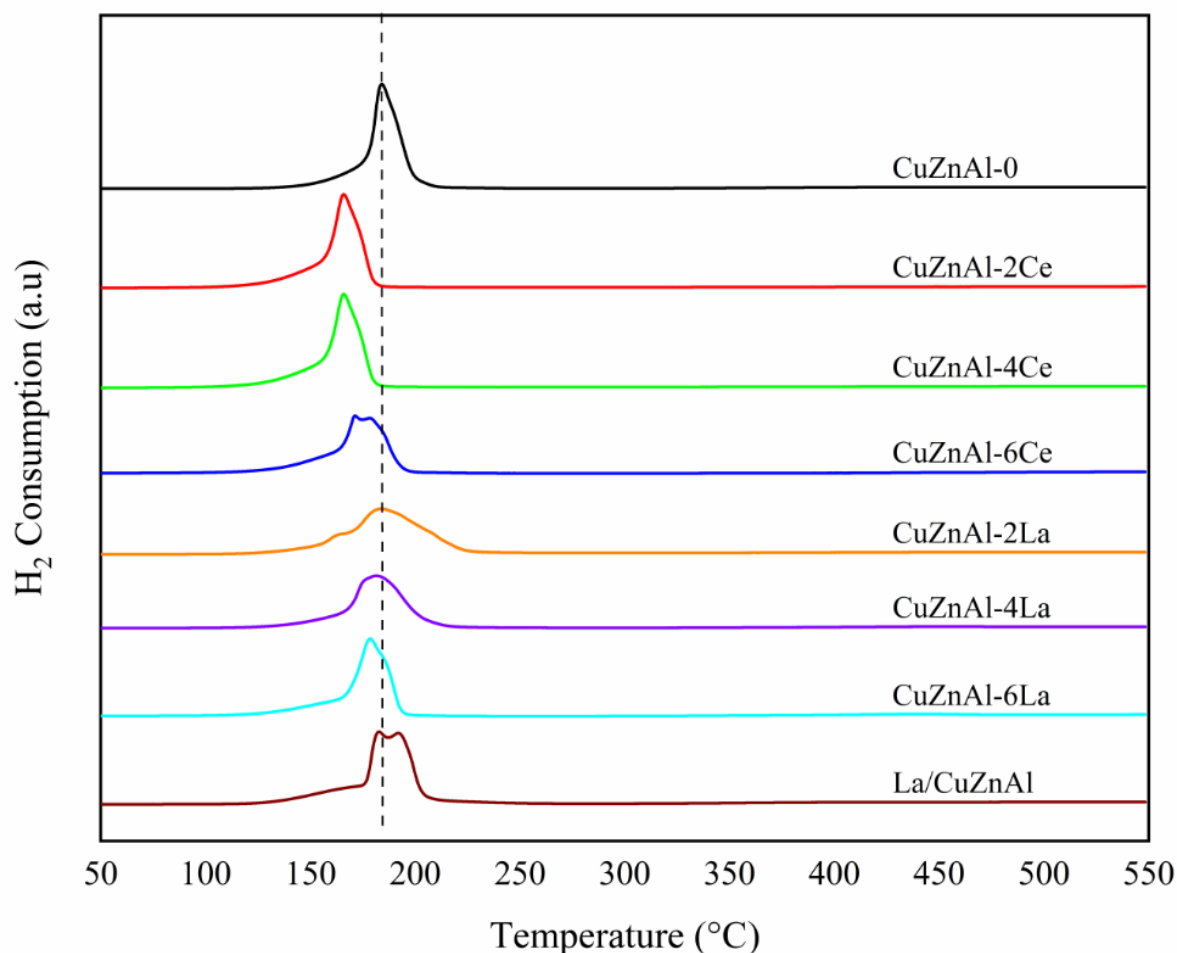


Figure 4.4: H₂-TPR profiles of calcined catalysts.

4.1.5 N₂ adsorption-desorption

The N₂ adsorption-desorption isotherms are summarized in Figure 4.5. The adsorption-desorption isotherms of the samples are typical of type IV with a type H3 hysteresis loop (P/P_0 between 0.4-1.0) according to IUPAC definitions [177]. This indicates that the pores of the catalysts were of mesoporous structure, and this can also be ascertained from the pore size distributions (2-50 nm) [178]. It has been reported that the residual carbonate structures remained after the calcination process [179]. The pore size distribution and a summary of all

the textural properties of the samples are presented in Figure 4.6 and Table 4.1. It can be seen that the catalysts exhibit similar pore size distributions. The reference catalyst (CuZnAl-0) exhibited a comparable BET area as the promoted catalysts; therefore, promotion with Ce and La does not lead to a notable change in the BET surface area. There were only slight changes when the promoters' loadings were increased. Furthermore, the BET surface area is accompanied by smaller variations in the pore sizes of the catalyst. The pore volume seemed to be higher for the La promoted system (0.68-0.78 cm³/g) when compared to the Ce promoted system (0.59-0.71 cm³/g). The pore volume decrease with the increase in pore diameter could be explained by the potential plugging of the catalyst pores by the promoters [180].

The promoted catalyst with 2% La loading exhibited the largest surface area (139 m²/g) among all the catalysts. Increasing the La ratio resulted in a notable decrease in the surface area to 119, 106 and 101 m²/g for this catalyst system. Similarly, for the Ce promoted catalysts, when the Ce loading was increased, the surface area of the catalyst slightly decreased from 131 m²/g to 126 and 124 m²/g. This agrees with the findings of Ali et al. [181] and Jiang et al. [90], who reported that the surface area of the catalysts increased with a certain promoter loading. Beyond this optimum amount, increasing the metal loading further resulted in the reduction of surface area, which might be related to the blockage of the pores by the metal particles.

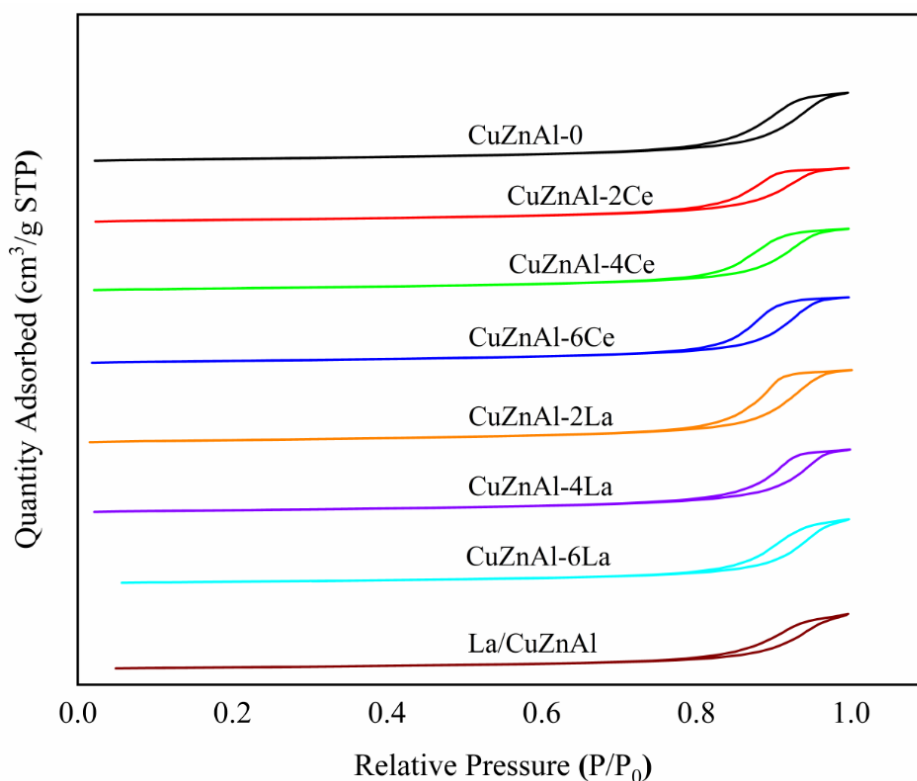


Figure 4.5: N₂ adsorption-desorption isotherms of calcined samples.

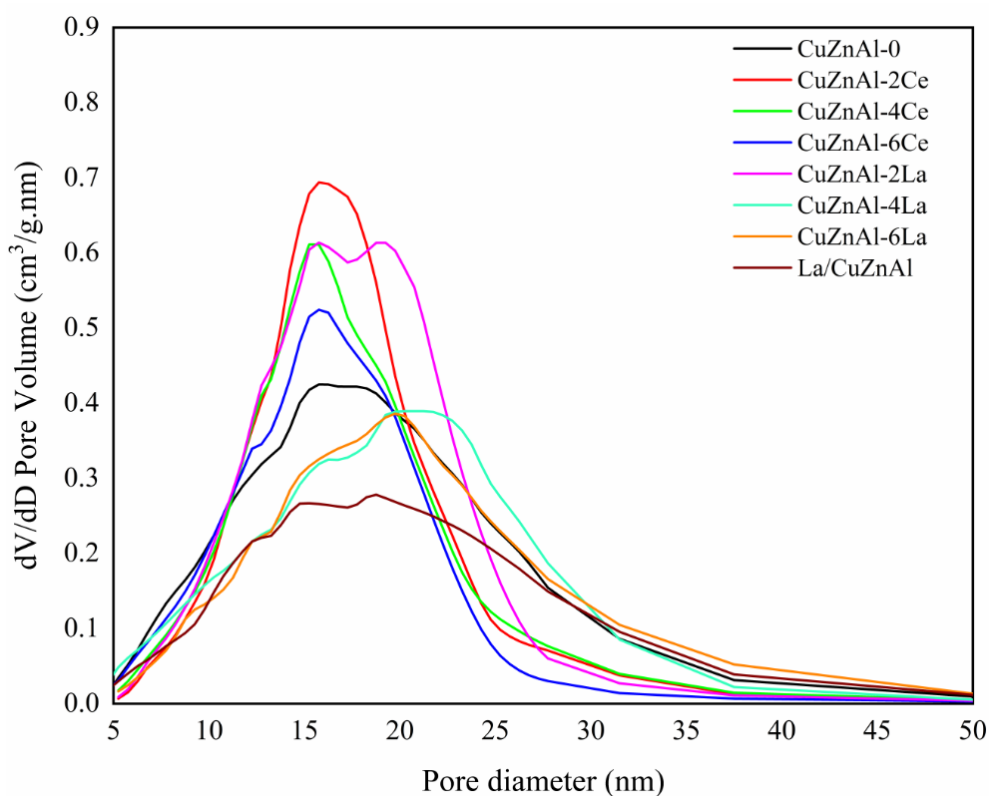


Figure 4.6: Pore size distribution of calcined samples.

4.1.6 N₂O chemisorption

The Cu surface area (SA_{Cu}) of the catalysts was estimated by dissociative N₂O adsorption. A summary of the SA_{Cu} is presented in Table 4.1. Apparently, the promotion of the catalyst with Ce and La enhances SA_{Cu} and the copper dispersion. Impregnating 2% and 4% Ce onto the reference catalyst increased the SA_{Cu} from 41 m²/g to 53 and 61 m²/g, respectively. However, when 6% Ce was doped into the catalyst, the SA_{Cu} was reduced to 51 m²/g. A similar trend was observed with La impregnation. The addition of 2% and 4% of La increased the SA_{Cu} to 48 and 51 m²/g, whereas 6% La addition yielded a reduced SA_{Cu} (48 m²/g). In addition, the La/CuZnAl catalyst had an SA_{Cu} of 52 m²/g, which is the largest for the catalysts promoted with La. It appears that modification of the reference catalyst with Ce and La increased the accessible copper surface when the content of CeO₂ and La₂O₃ was less than 4 wt %. Eventually, increasing the Ce and La content might have resulted in a coverage of the Cu surface by CeO₂ and La₂O₃. Thus, this led to a decrease of the copper surface area, which is also consistent with

the XRD results. Consequently, there is an optimum promoter loading, beyond which further increasing of promoters would no longer enhance the dispersion of Cu or the Cu surface area.

Table 4.1: Summary of the N₂ adsorption-desorption data, crystallite size and particle size of the calcined catalysts.

Catalyst	BET Surface Area (m ² /g)	BJH Pore Volume (cm ³ /g)	Pore Size (nm) ^a	H ₂ consump (mmol/gcat) ^b	SA _{Cu} (m ² /gcat) ^c
CuZnAl-0	134	0.73	16.3	7.0	41
CuZnAl-2Ce	131	0.71	15.5	7.2	53
CuZnAl-4Ce	126	0.67	15.4	6.6	61
CuZnAl-6Ce	124	0.59	14.4	6.1	51
CuZnAl-2La	139	0.78	15.7	7.0	48
CuZnAl-4La	119	0.66	16.6	6.1	51
CuZnAl-6La	106	0.68	12.6	6.1	48
La/CuZnAl	101	0.58	17.8	7.5	52

^a Estimated from BJH analysis

^b Estimated from the amount of H₂ consumed during H₂-TPR

^c Determined by dissociative N₂O adsorption

4.1.7 TEM

The TEM images of the reduced-passivated La/CuZnAl and CuZnAl-4La catalyst are displayed in Figure 4.7 a-e. The catalysts consist of agglomerated particles of a narrow size, which is consistent with previously reported CuZnAl-based catalysts [43]. The porosity of the catalysts is related to the inter-particle spaces. Both catalysts exhibit comparable particle sizes, which indicates that the preparation method had a negligible influence on the particle size distribution. As the Cu element accounts for the largest portion in the precursor, the larger particles probably consist mostly of Cu, whereas the smaller ones can be mainly assigned to ZnO particles.

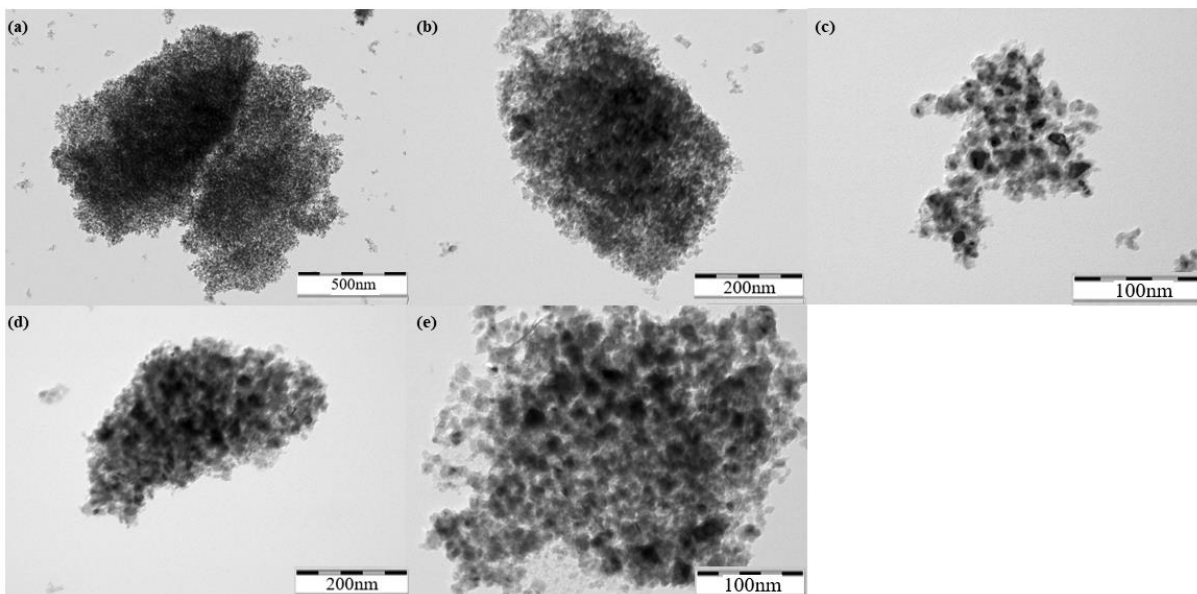


Figure 4.7: TEM images of the reduced-passivated La/CuZnAl catalyst (a-c) at different magnifications and CuZnAl-4La catalyst (d and e).

4.2 Methanol synthesis activity tests

4.2.1 Activity and selectivity of different catalysts

Methanol synthesis over the catalysts was performed under the pressure of 40 bar and temperature of 230°C. The catalyst tested were the i) unpromoted catalyst CuZnAl-0, ii) three promoted catalysts with cerium CuZnAl-Ce (2%,4%,6%), and iii) three promoted catalysts with lanthanum CuZnAl-La (2%,4%,6%). The reactions were performed using 80 mg weight of the catalyst and 100 mL/min gas flow with a H₂/CO₂/N₂ ratio of 3/1/1. The CO₂ conversion and methanol selectivity were studied normally for 24 h. There were some fluctuations which were observed while recording the data, and this might be due to unstable gas flow rate or small temperature variations. The CO₂ conversion and the methanol selectivity over the unpromoted and Ce promoted catalysts are presented in Figure 4.8, while results over the La promoted catalysts are shown in Figure 4.9. It was found that the La and Ce promoted catalysts did not yield any dramatic effect on the CO₂ conversion and methanol selectivity. It can also be seen that the activity and selectivity of the catalyst slightly decreased over 24 h. The higher Cu surface area of promoted catalysts indicates that the number of active sites decreased for the

promoted catalysts. This might be due to a decrease in the number of interfacial sites, which is essential in the conversion of CO₂ to methanol [67].

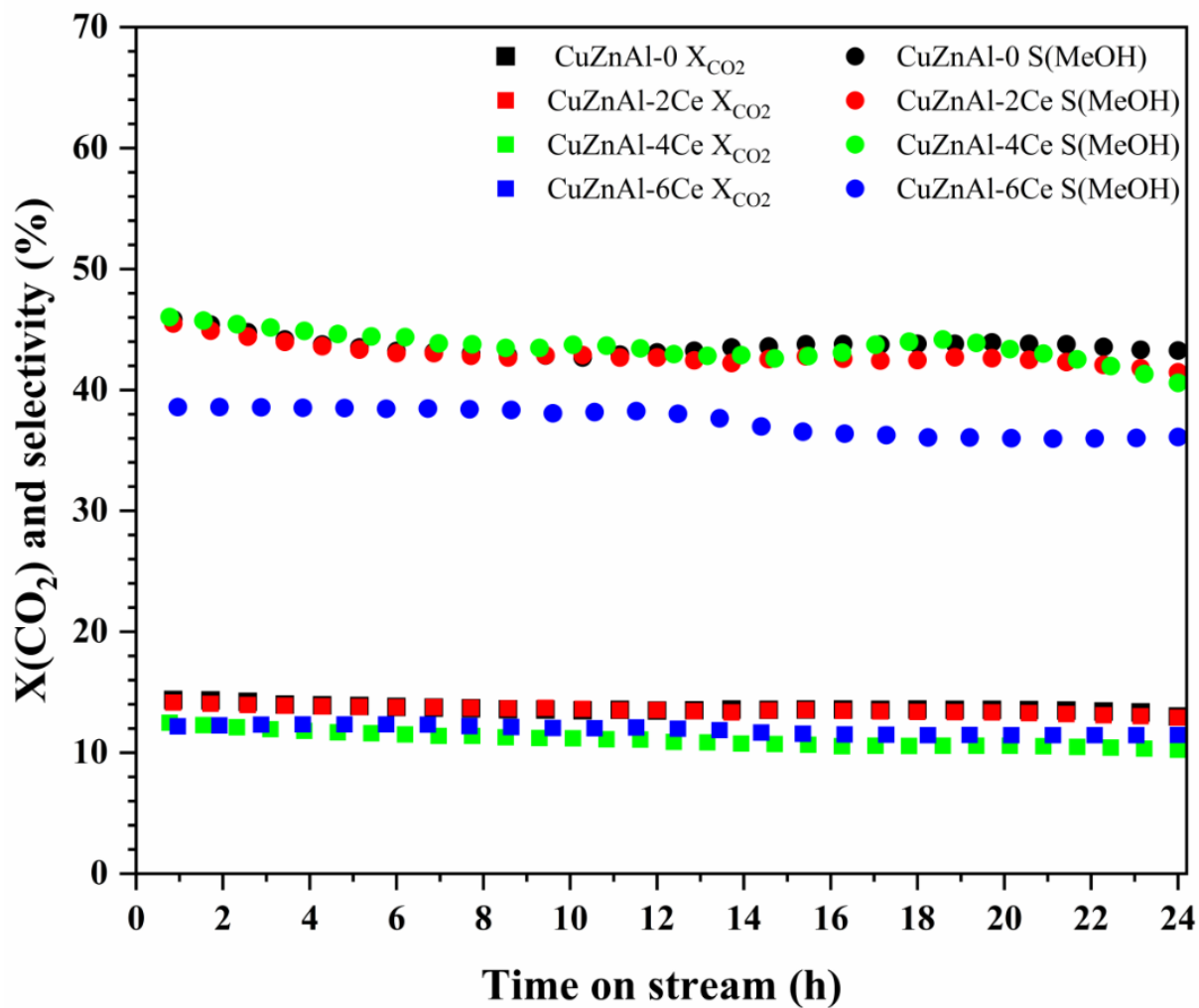


Figure 4.8: CO₂ conversion and CH₃OH selectivity of unpromoted and Ce promoted catalysts

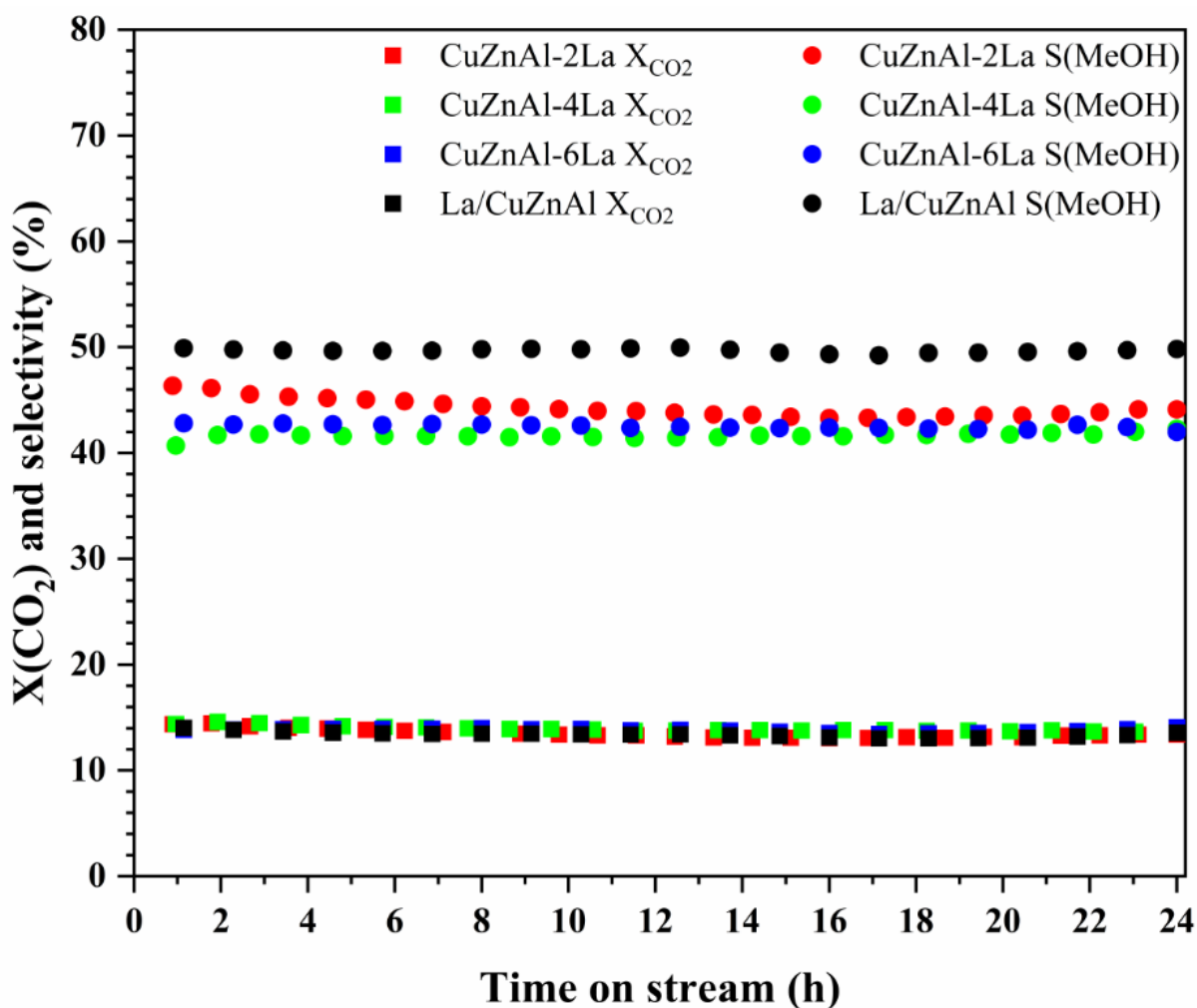


Figure 4.9: CO₂ conversion and Methanol selectivity of promoted CuZnAl catalyst with La

Table 4.3 presents a summary of the CO₂ conversion, methanol selectivity, space-time yield (STY) and turn-over frequency (TOF) of methanol of the catalysts. It also includes the results of the La/CuZnAl catalyst prepared by impregnating the CuZnAl catalyst with the La precursor. The CO₂ conversion and methanol selectivity were used to calculate the STY of methanol. In general, the conversion of CO₂ was lower when the Ce promoter was added as compared to the La promoter. It can also be seen that the promoted catalyst prepared by co-precipitation reduced the STY and TOF of methanol. On the other hand, the La/CuZnAl catalyst exhibited an increase in methanol selectivity from 44% to 50%. Furthermore, the STY of methanol increased from 1222 to 1357 mmol·gcat⁻¹·h⁻¹. The superior performance of the La/CuZnAl catalyst is attributed to the generation of additional surface sites for CO₂ conversion to methanol. This might be related to Cu/LaO_x surface sites, which have been demonstrated to have high methanol selectivity in CO₂ hydrogenation to methanol [182]. The TOF of La/CuZnAl is slightly lower

than that of the CuZnAl-0 catalyst, which might be due to a decrease in the Cu-ZnO interfacial area after the second calcination treatment.

Table 4.2: Summary of CO₂ conversion, CH₃OH selectivity as well as space time yield of different catalysts.

Catalysts	CO ₂ Conversion (%)	Methanol Selectivity (%)	STY (mmol·gcat ⁻¹ ·h ⁻¹)	TOF (s ⁻¹)
CuZnAl-0	13.8	44	1222	0.033
CuZnAl-2La	13.8	42	1112	0.024
CuZnAl-4La	14.3	44	1205	0.022
CuZnAl-6La	13.8	40	1053	0.023
CuZnAl-2Ce	13.4	42	1176	0.026
CuZnAl-4Ce	12.6	45	1108	0.023
CuZnAl-6Ce	12.2	38	905	0.021
La/CuZnAl	13.8	50	1357	0.030

4.2.2 Effect of GHSV

The effect of GHSV on the CO₂ conversion and methanol selectivity was studied by changing the catalyst weight while maintaining the gas flowrate. Three different weights of the catalyst (50, 80, and 100mg) were used. Table 4.2 summarizes the effect of GHSV on the catalyst performance over the CuZnAl-4La catalyst. In addition, a graphical representation of this effect is depicted in Figure 4.10. The STY of methanol increased at higher GHSV. This is expected as the reaction rate decreases gradually as the conversion increases. Furthermore, a higher methanol selectivity is achieved when the GHSV increases.

Table 4.3: The effect of GHSV on CO₂ conversion, methanol selectivity and space time yield of the performance of the CuZnAl-4La catalyst.

GHSV (mL/g _{cat} ·h)	CO ₂ Conversion (%)	Methanol Selectivity (%)	Space Time Yield (mmol·g _{cat} ⁻¹ ·h ⁻¹)
120,000	9.1	54	1537
75,000	14.3	44	1205
60,000	18.4	33	954

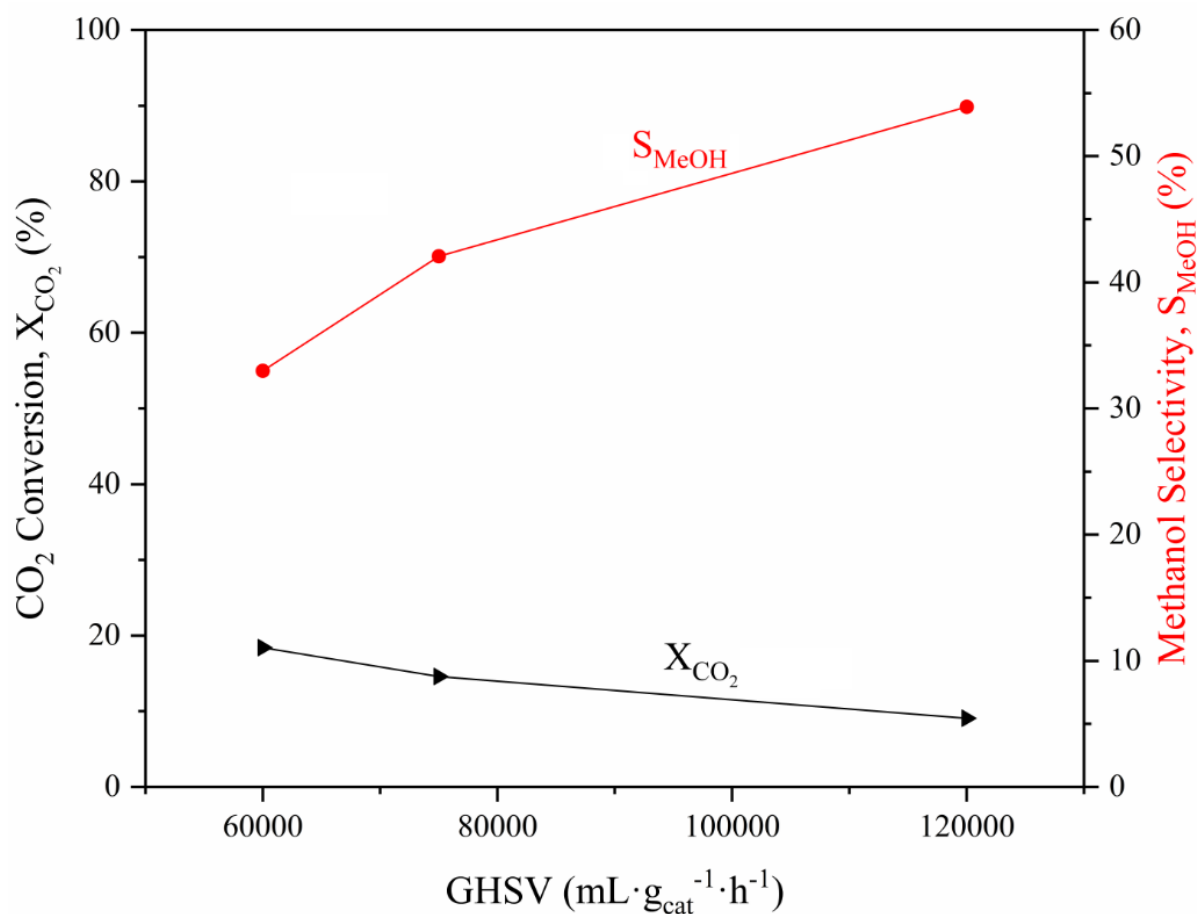


Figure 4.10: Effect of GHSV on CO₂ conversion and Methanol selectivity over CuZnAl-4La catalyst. Reaction conditions: 230°C, 40 bar and H₂/CO₂/N₂ ratio of 3:1:1.

4.2.3 Effect of temperature

The effect of temperature was assessed for the CuZnAl-0, CuZnAl-4Ce and CuZnAl-4La catalysts. The reaction was carried out at 40 bar, 100 mL/min, and 24 h TOS, where the temperature was increased gradually by 20°C every 6 hours. The data was collected between the temperatures of 230 to 290°C. The results are shown in Figure 4.11. All catalysts showed high CO₂ conversion at higher temperatures, and the methanol selectivity decreased with temperature. This can be explained by the fact that the RWGS reaction is favoured at higher temperatures, which will consequently decrease the selectivity for methanol [1]. The influence of temperature was similar on all the catalysts, but the methanol selectivity decreased more strongly for the Ce promoted catalyst when the temperature was increased.

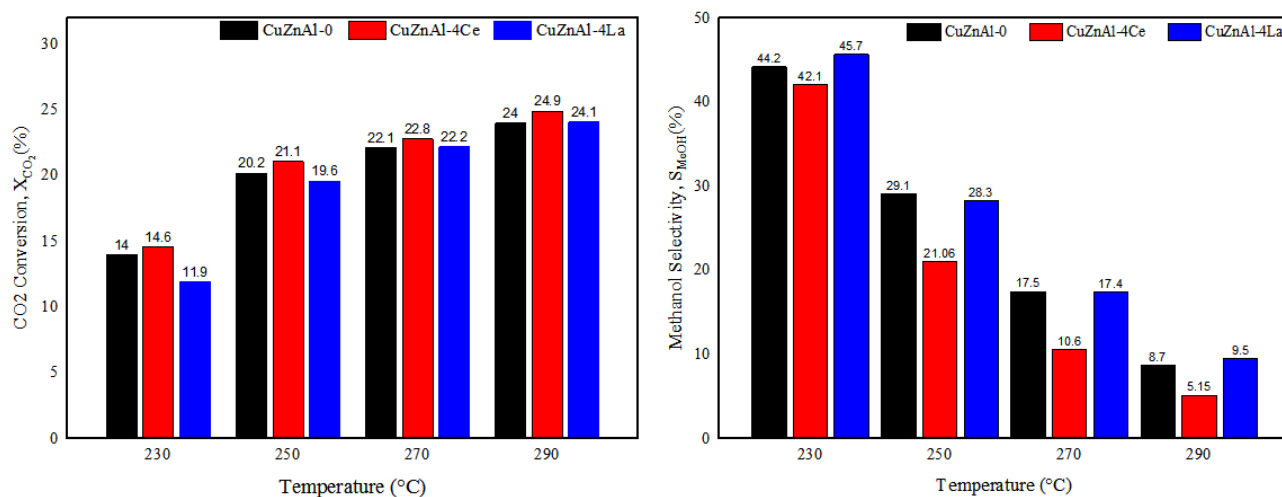


Figure 4.11: The effect of temperature on CO₂ conversion and Methanol selectivity for the CuZnAl-0, CuZnAl-4Ce and CuZnAl-4La catalysts.

4.2.4 The effect of pressure

The pressure used in most of activity tests was 40 bar. We further performed activity tests on the CuZnAl-4Ce catalyst using two different pressures (30 and 35 bar), while maintaining other reaction conditions. The change in pressure had influence on CO₂ conversion as well as methanol selectivity. Figure 4.12 shows the change in CO₂ conversion and methanol selectivity with respect to pressure change. It can be seen from Figure 4.12 that the conversion of CO₂ decreased slightly the pressure was increased. At the same time, the increase in pressure also led to an obvious increase in methanol selectivity. This can be explained by the Le Chatelier principle because the methanol synthesis reaction is favoured at higher pressures but not the

RWGS reaction [67]. The STY of methanol at 30 bar was $920 \text{ mmol} \cdot \text{gcat}^{-1} \cdot \text{h}^{-1}$, which increased to $1108 \text{ mmol} \cdot \text{gcat}^{-1} \cdot \text{h}^{-1}$ at 40 bar.

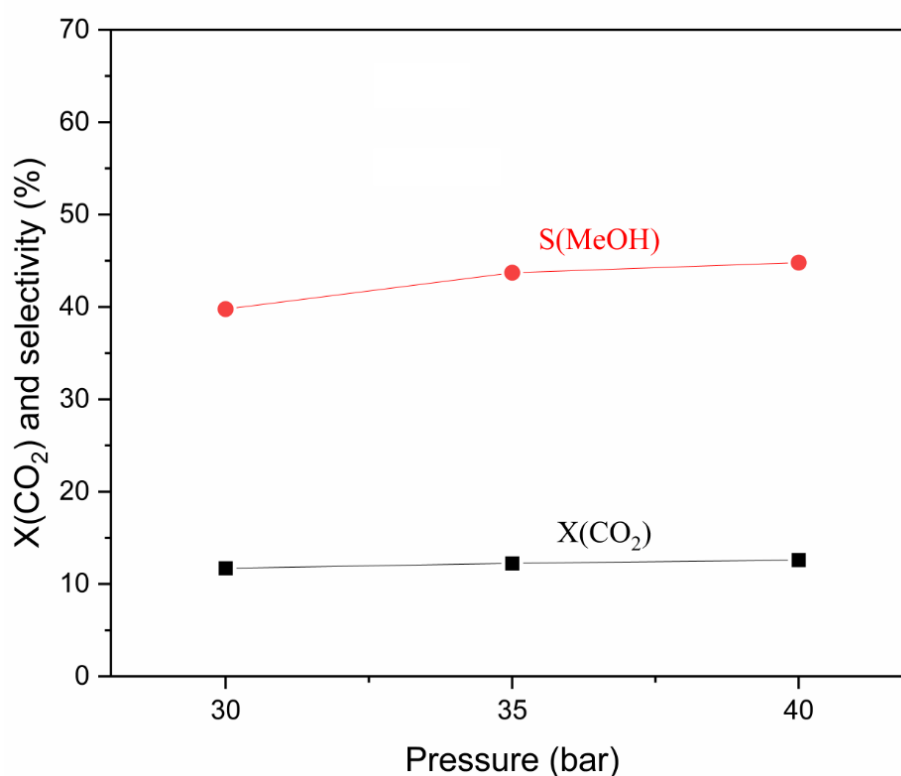


Figure 4.12: Effect of pressure on CO₂ conversion and selectivity over CuZnAl-4Ce Reaction conditions: 230°C, H₂/CO₂/N₂ ratio of 3/1/1.

4.2.5 Long-term activity test

Although the improvement of the catalyst activity and selectivity is essential, developing a catalyst with long-term stability is equally as important to ensure the industrial applicability of the catalyst. The catalysts with the most promising performance were selected from each system for long-term stability tests over 72 h. These tests were conducted under the same reaction conditions as described in Section 4.2.1, except for the reaction time, which was increased from 24 to 72 h. The CO₂ conversion and methanol selectivity for the CuZnAl-0, CuZnAl-4Ce, CuZnAl4La, and La/CuZnAl catalysts are depicted in Figure 4.13a-d. For the unpromoted catalyst, it was observed that the CO₂ conversion and methanol selectivity, for the most part, decreased steadily over the 72 h TOS. Initially, the CO₂ conversion was 14.6%, and after 72 h, the CO₂ conversion decreased to 13.4%. A similar trend was observed in the methanol selectivity, which decreased from 45% to 39% at the end of the reaction. The deactivation of the catalyst might be related to the sintering of the Cu or ZnO phase [172]. The CO₂ conversion

of the CuZnAl-4Ce and CuZnAl-4La catalysts also slightly decreased over the 72h TOS. However, there were small increase in the methanol selectivity of these catalysts. The methanol selectivity of the CuZnAl-4Ce catalyst increased from 45% to 47%, while the selectivity for the CuZnAl-4La increased from 44% to 46%. For the best performing La/CuZnAl catalyst, the CO₂ conversion initially decreased during the first 10 h before it stabilized. The CO₂ conversion was initially 13.8%, and it decreased to 13.3%, which was held stable for over 60 h. The methanol selectivity increased from 47% to 50%, which was the highest for all the catalysts synthesized.

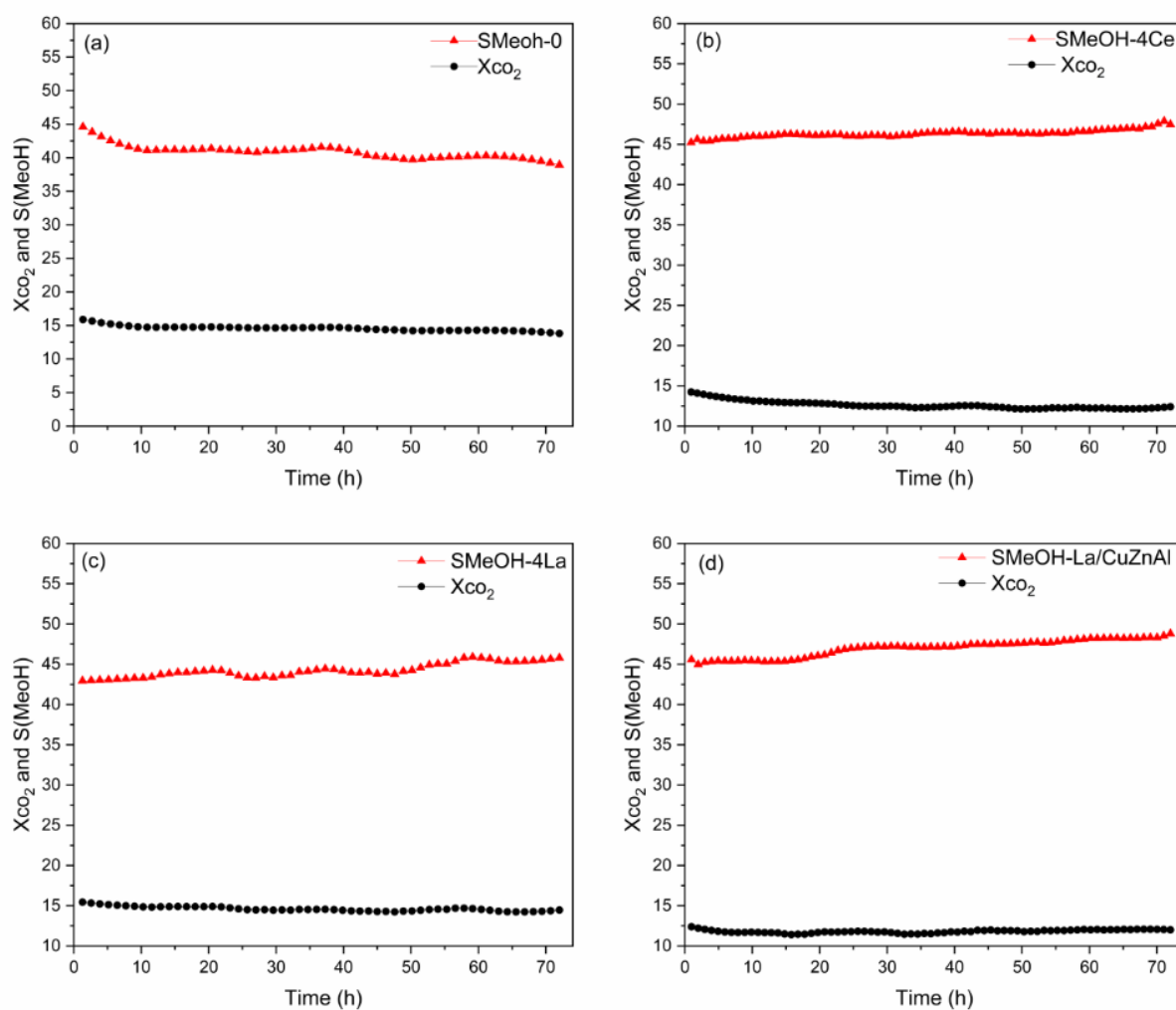


Figure 4.13: CO₂ conversion and methanol selectivity over 72 h for (a) CuZnAl-0; (b) CuZnAl-4Ce; (c) CuZnAl-4La; (d) La/CuZnAl.

The CO₂ conversion, methanol selectivity, and STY of methanol at the start and after 72 h is given in Table 4.4. It can be seen that the STY of methanol decreases for the CuZnAl-0 catalyst. The STY of methanol remained stable for the CuZnAl-4Ce catalyst. Interestingly, the STY of

methanol increased for the CuZnAl-4La and La/CuZnAl catalysts. Thus, the incorporation of both Ce and La seems to improve the catalyst stability. The highest methanol selectivity after 72 h of 1335 mmol·gcat⁻¹·h⁻¹ was obtained over the La/CuZnAl catalyst. Thus, the sequential impregnation of CuZnAl catalyst with La seems a promising approach to enhance the activity, methanol selectivity, and stability of CuZnAl catalysts.

Table 4.4: Methanol selectivity and STY of reaction at 24 h and after 72 h TOS.

Catalyst	Beginning			After 72 h		
	X _{CO2} (%)	Selectivity (%)	STY (mmol·gcat ⁻¹ ·h ⁻¹)	X _{CO2} (%)	Selectivity (%)	STY (mmol·gcat ⁻¹ ·h ⁻¹)
CuZnAl-0	14.6	45	1219	13.4	39	1072
CuZnAl-4Ce	12.6	45	1113	12.3	47	1135
CuZnAl-4La	14.3	44	1210	14	46	1292
La/CuZnAl	13.8	47	1237	13.3	50	1335

5. Conclusions and future work

5.1 Conclusions

In this study, we focused on the performance of enhancing the performance of CuZnAl-based catalysts for the hydrogenation of CO₂ to methanol. The goal of this study was to examine the impact of adding cerium and lanthanum promoters to the CuZnAl catalysts to assess their effect on the CO₂ conversion, methanol selectivity, the overall space time yield, and stability. Different catalysts with various loadings of cerium and lanthanum were prepared (2%, 4%, 6%). Thereafter, a sequential impregnation method was used to prepare a lanthanum-promoted catalyst to compare the two preparation methods.

In order to study the structural and physicochemical properties of the catalysts, several characterization methods were conducted, such as N₂ adsorption-desorption, XRD, TPR, TEM, and N₂O chemisorption. Those characterizations demonstrated the following:

- The developed catalyst precursors exhibited a typical Zincian malachite structure.
- The crystallite size of CuO decreased when the Ce and La promoters were incorporated into the catalyst.
- Promotion with Ce and La enhanced the reducibility and led to the reduction of CuO at lower temperatures.
- The surface area, pore volume and pore size generally first increased then decreased with increased promoter content.
- The addition of promoters increased the Cu surface area

Activity, methanol selectivity, and space time yield of the catalysts were studied at 230°C and 40 bars over a period of 24 hours. It was found that the La and Ce promoted catalysts prepared by co-precipitation had a lower CO₂ conversion and STY of methanol compared to the unpromoted catalyst.

The effects of temperature, pressure and GHSV were also investigated to understand the effect of the reaction conditions.

- The temperature was increased from 230°C to 290°C over 24 hours (+20°C every 6 hours). It showed that the CO₂ conversion increased with temperature, whereas the methanol selectivity significantly decreased with temperature.

- The pressure effect was examined by performing the reaction at three different pressures (30,35,40) bars. The conversion of CO₂ increased slightly, and there was an obvious increase in methanol selectivity with increased pressure.
- The CO₂ conversion increased with the decrease of GHSV, whereas the methanol selectivity and STY of methanol increased with the increasing GHSV.

The impregnation of the CuZnAl-0 catalyst with La was also investigated. This led to a notable improvement in catalytic performance. The methanol selectivity increased from 44 to 50%, and the STY of methanol increased from 1112 to 1357 mmol·gcat⁻¹·h⁻¹. Furthermore, the stability of the impregnated La/CuZnAl catalyst was superior, and the STY of methanol increased over the 72 h TOS. The higher activity could partly be ascribed to a higher Cu surface area, but the generation of Cu-LaO_x interfacial sites might also have contributed to the higher methanol production. Long-term tests were performed on selected Ce and La promoted catalysts prepared by co-precipitation. It was observed that all the promoted catalysts also exhibited improved stability when compared to the reference catalyst (CuZnAl-0). Furthermore, it seems that the sequential impregnation of the CuZnAl catalyst is the most promising approach for enhancing the catalytic performance for CO₂ hydrogenation to methanol.

5.2 Recommendations for future work

Both lanthanum and cerium are promising promoters and therefore different loadings can be tested to optimize the promoter content to achieve the best methanol selectivity and space time yield. A special focus should be put on the sequential preparation method used during synthesis as it showed the best catalytic performance, and further optimization of the preparation conditions might lead to a significant increase in activity and methanol selectivity.

The effect of lanthanum and cerium on the reaction mechanism can be investigated through a detailed kinetic study in combination with in-situ analysis under reaction conditions as well as using DFT calculations. DRIFTS analysis can be applied to directly study the surface species formed during CO₂ hydrogenation to methanol. In addition, it can be used to investigate the influence of the Cu-LaO_x interface in methanol synthesis from CO₂. Furthermore, attention should be put on analysing the spent catalyst after the reaction to gain further insight into the stabilizing effect observed for the La impregnated catalyst.

References

- [1] N. Mota, R. Guil-Lopez, J. Llorente, E. Millán, B. Pawelec, J. L. G. Fierro, and R. M. Navarro, “Methanol Synthesis from CO₂: A Review of the Latest Developments in Heterogeneous Catalysis,” *Materials*, vol. 12, no. 23, Art. no. 23, Jan. 2019, doi: 10.3390/ma12233902.
- [2] X. An, Y. Zuo, Q. Zhang, and J. Wang, “Methanol Synthesis from CO₂ Hydrogenation with a Cu/Zn/Al/Zr Fibrous Catalyst,” *Chinese Journal of Chemical Engineering*, vol. 17, no. 1, pp. 88–94, Feb. 2009, doi: 10.1016/S1004-9541(09)60038-0.
- [3] N. Myhrvold and K. Caldeira, “Greenhouse gases, climate change and the transition from coal to low-carbon electricity,” *Environmental Research Letters - ENVIRON RES LETT*, vol. 7, Mar. 2012, doi: 10.1088/1748-9326/7/1/014019.
- [4] M. Bowker, “Methanol Synthesis from CO₂ Hydrogenation,” *ChemCatChem*, vol. 11, no. 17, pp. 4238–4246, 2019, doi: 10.1002/cctc.201900401.
- [5] F. Lucia, “Global production capacity of methanol 2018-2030,” Statista, Aug. 2021. [Online]. Available: <https://www.statista.com/>
- [6] “IRENA AND METHANOL INSTITUTE (2021), Innovation Outlook: Renewable Methanol, International Renewable Energy Agency, Abu Dhabi.”
- [7] Y.-F. Zhao, Y. Yang, C. Mims, C. H. F. Peden, J. Li, and D. Mei, “Insight into methanol synthesis from CO₂ hydrogenation on Cu(111): Complex reaction network and the effects of H₂O,” *Journal of Catalysis*, vol. 281, no. 2, pp. 199–211, Jul. 2011, doi: 10.1016/j.jcat.2011.04.012.
- [8] X. Tao, J. Wang, Z. Li, and Q. Ye, “Theoretical study on the reaction mechanism of CO₂ hydrogenation to methanol,” *Computational and Theoretical Chemistry*, vol. 1023, pp. 59–64, Nov. 2013, doi: 10.1016/j.comptc.2013.09.002.
- [9] A. Zachopoulos and E. Heracleous, “Overcoming the equilibrium barriers of CO₂ hydrogenation to methanol via water sorption: A thermodynamic analysis,” *Journal of CO₂ Utilization*, vol. 21, pp. 360–367, Oct. 2017, doi: 10.1016/j.jcou.2017.06.007.
- [10] M. Ronda-Lloret, Y. Wang, P. Oulego, G. Rothenberg, X. Tu, and N. R. Shiju, “CO₂ Hydrogenation at Atmospheric Pressure and Low Temperature Using Plasma-Enhanced Catalysis over Supported Cobalt Oxide Catalysts,” *ACS Sustainable Chem. Eng.*, vol. 8, no. 47, pp. 17397–17407, Nov. 2020, doi: 10.1021/acssuschemeng.0c05565.
- [11] S. Kanuri, S. Roy, C. Chakraborty, S. P. Datta, S. A. Singh, and S. Dinda, “An insight of CO₂ hydrogenation to methanol synthesis: Thermodynamics, catalysts, operating

- parameters, and reaction mechanism,” *Intl J of Energy Research*, p. er.7562, Dec. 2021, doi: 10.1002/er.7562.
- [12] K. Stangeland, H. Li, and Z. Yu, “Thermodynamic Analysis of Chemical and Phase Equilibria in CO₂ Hydrogenation to Methanol, Dimethyl Ether, and Higher Alcohols,” *Ind. Eng. Chem. Res.*, vol. 57, no. 11, pp. 4081–4094, Mar. 2018, doi: 10.1021/acs.iecr.7b04866.
- [13] U. J. Etim, Y. Song, and Z. Zhong, “Improving the Cu/ZnO-Based Catalysts for Carbon Dioxide Hydrogenation to Methanol, and the Use of Methanol As a Renewable Energy Storage Media,” *Front. Energy Res.*, vol. 8, p. 545431, Sep. 2020, doi: 10.3389/fenrg.2020.545431.
- [14] G. Patart, “Production of Alcohols, Aldehydes, and Acids. French Patent 540,543, July 12, 1922; appl. filed Aug. 19, 1921. *Ind. Eng. Chem.*, vol. 17, 1925, p. 431; *Chem. Zentralb.*, 1923, II, p. 631.,” vol. 17, 1922.
- [15] I. U. Din, M. S. Shaharun, M. A. Alotaibi, A. I. Alharthi, and A. Naeem, “Recent developments on heterogeneous catalytic CO₂ reduction to methanol,” *Journal of CO₂ Utilization*, vol. 34, pp. 20–33, Dec. 2019, doi: 10.1016/j.jcou.2019.05.036.
- [16] D. Sheldon, “Methanol Production - A Technical History,” *Johnson Matthey Technology Review*, vol. 61, no. 3, pp. 172–182, Jul. 2017, doi: 10.1595/205651317X695622.
- [17] P. Davies and F. F. Snowdon, “Production of Oxygenated Hydrocarbons, US,” *Patent 3,326,956 (June)*, vol. 20, p. 1967, 1967.
- [18] T. Casey and G. Chapman, *Low temperature methanol synthesis catalyst*. Google Patents, 1974.
- [19] D. F. Smith and L. L. Hirst, “Reactions That Occur on a Methanol Catalyst,” *Ind. Eng. Chem.*, vol. 22, no. 10, pp. 1037–1040, Oct. 1930, doi: 10.1021/ie50250a009.
- [20] E. H. Boomer and H. E. Morris, “THE HYDROGEN-CARBON DIOXIDE REACTION,” *J. Am. Chem. Soc.*, vol. 54, no. 1, pp. 407–407, Jan. 1932, doi: 10.1021/ja01340a509.
- [21] V. N. Ipatieff and G. S. Monroe, “Synthesis of Methanol from Carbon Dioxide and Hydrogen over Copper-Alumina Catalysts. Mechanism of Reaction,” *J. Am. Chem. Soc.*, vol. 67, no. 12, pp. 2168–2171, Dec. 1945, doi: 10.1021/ja01228a032.
- [22] M. Porosoff, B. Yan, and J. Chen, “Catalytic reduction of CO₂ by H₂ for synthesis of CO, methanol and hydrocarbons: Challenges and opportunities,” *Energy Environ. Sci.*, vol. 9, Oct. 2015, doi: 10.1039/C5EE02657A.

- [23] W. Zhou *et al.*, “New horizon in C1 chemistry: breaking the selectivity limitation in transformation of syngas and hydrogenation of CO₂ into hydrocarbon chemicals and fuels,” *Chemical Society Reviews*, vol. 48, no. 12, pp. 3193–3228, 2019.
- [24] J. Sehested, “Industrial and scientific directions of methanol catalyst development,” *Journal of Catalysis*, vol. 371, pp. 368–375, Mar. 2019, doi: 10.1016/j.jcat.2019.02.002.
- [25] J. Weigel, R. A. Koeppel, A. Baiker, and A. Wokaun, “Surface Species in CO and CO₂ Hydrogenation over Copper/Zirconia: On the Methanol Synthesis Mechanism,” *Langmuir*, vol. 12, no. 22, pp. 5319–5329, Jan. 1996, doi: 10.1021/la9506990.
- [26] F. Arena, G. Italiano, K. Barbera, G. Bonura, L. Spadaro, and F. Frusteri, “Basic evidences for methanol-synthesis catalyst design,” *Catalysis Today*, vol. 1–2, no. 143, pp. 80–85, 2009, doi: 10.1016/j.cattod.2008.11.022.
- [27] Y. Sun, S. Tian, P. Ciais, Z. Zeng, J. Meng, and Z. Zhang, “Decarbonising the iron and steel sector for a 2°C target using inherent waste streams,” *Nat Commun*, vol. 13, no. 1, Art. no. 1, Jan. 2022, doi: 10.1038/s41467-021-27770-y.
- [28] J. C. Minx *et al.*, “Negative emissions—Part 1: Research landscape and synthesis,” *Environ. Res. Lett.*, vol. 13, no. 6, p. 063001, May 2018, doi: 10.1088/1748-9326/aabf9b.
- [29] Y. Yang, C. A. Mims, R. S. Disselkamp, J.-H. Kwak, C. H. Peden, and C. T. Campbell, “(Non) formation of methanol by direct hydrogenation of formate on copper catalysts,” *The Journal of Physical Chemistry C*, vol. 114, no. 40, pp. 17205–17211, 2010.
- [30] M. B. Fichtl *et al.*, “Kinetics of deactivation on Cu/ZnO/Al₂O₃ methanol synthesis catalysts,” *Applied Catalysis A: General*, vol. 502, pp. 262–270, 2015.
- [31] G. C. Chinchin, P. J. Denny, D. G. Parker, M. S. Spencer, and D. A. Whan, “Mechanism of methanol synthesis from CO₂/CO/H₂ mixtures over copper/zinc oxide/alumina catalysts: use of ¹⁴C-labelled reactants,” *Applied Catalysis*, vol. 30, no. 2, pp. 333–338, Apr. 1987, doi: 10.1016/S0166-9834(00)84123-8.
- [32] P. B. Rasmussen *et al.*, “Methanol synthesis on Cu(100) from a binary gas mixture of CO₂ and H₂,” *Catal Lett*, vol. 26, no. 3–4, pp. 373–381, 1994, doi: 10.1007/BF00810611.
- [33] T. M. Yurieva, L. M. Plyasova, T. A. Kriger, V. I. Zaikovskii, O. V. Makarova, and T. P. Minyukova, “State of copper-containing catalyst for methanol synthesis in the reaction medium,” *React Kinet Catal Lett*, vol. 51, no. 2, pp. 495–500, Dec. 1993, doi: 10.1007/BF02069096.
- [34] V. Ponec, “Cu and Pd, two catalysts for CH₃OH synthesis: the similarities and the differences,” *Surface Science*, vol. 272, no. 1, pp. 111–117, Jan. 1992, doi: 10.1016/0039-6028(92)91427-D.

- [35] J. C. Frost, "Junction effect interactions in methanol synthesis catalysts," *Nature*, vol. 334, no. 6183, Art. no. 6183, Aug. 1988, doi: 10.1038/334577a0.
- [36] F. Liao *et al.*, "Morphology-dependent interactions of ZnO with Cu nanoparticles at the materials' interface in selective hydrogenation of CO₂ to CH₃OH," *Angew Chem Int Ed Engl*, vol. 50, no. 9, pp. 2162–2165, Feb. 2011, doi: 10.1002/anie.201007108.
- [37] J.-D. Grunwaldt, A. M. Molenbroek, N.-Y. Topsøe, H. Topsøe, and B. S. Clausen, "In Situ Investigations of Structural Changes in Cu/ZnO Catalysts," *Journal of Catalysis*, vol. 194, no. 2, pp. 452–460, Sep. 2000, doi: 10.1006/jcat.2000.2930.
- [38] N.-Y. Topsøe and H. Topsøe, "On the nature of surface structural changes in Cu/ZnO methanol synthesis catalysts," *Topics in Catalysis*, vol. 8, no. 3, pp. 267–270, May 1999, doi: 10.1023/A:1019133832569.
- [39] M. Behrens *et al.*, "The active site of methanol synthesis over Cu/ZnO/Al₂O₃ industrial catalysts," *Science*, vol. 336, no. 6083, pp. 893–897, May 2012, doi: 10.1126/science.1219831.
- [40] S. Kuld *et al.*, "Quantifying the promotion of Cu catalysts by ZnO for methanol synthesis," *Science*, vol. 352, no. 6288, pp. 969–974, May 2016, doi: 10.1126/science.aaf0718.
- [41] M. Behrens *et al.*, "The effect of Al-doping on ZnO nanoparticles applied as catalyst support," *Phys. Chem. Chem. Phys.*, vol. 15, no. 5, pp. 1374–1381, Jan. 2013, doi: 10.1039/C2CP41680H.
- [42] N. J. Brown, J. Weiner, K. Hellgardt, M. S. P. Shaffer, and C. K. Williams, "Phosphinate stabilised ZnO and Cu colloidal nanocatalysts for CO₂ hydrogenation to methanol," *Chem. Commun.*, vol. 49, no. 94, pp. 11074–11076, Oct. 2013, doi: 10.1039/C3CC46203J.
- [43] K. Stangeland, F. Chamssine, W. Fu, Z. Huang, and X. Duan, "CO₂ hydrogenation to methanol over partially embedded Cu within Zn-Al oxide and the effect of indium," *10*, Aug. 2021, doi: 10.1016/j.jcou.2021.101609.
- [44] Y. Matsumura and H. Ishibe, "Durable copper–zinc catalysts modified with indium oxide in high temperature steam reforming of methanol for hydrogen production," *Journal of Power Sources*, vol. 209, pp. 72–80, Jul. 2012, doi: 10.1016/j.jpowsour.2012.02.084.
- [45] S. Li, L. Guo, and T. Ishihara, "Hydrogenation of CO₂ to methanol over Cu/AlCeO catalyst," *Catalysis Today*, vol. 339, pp. 352–361, Jan. 2020, doi: 10.1016/j.cattod.2019.01.015.

- [46] S. Li, Y. Wang, B. Yang, and L. Guo, "A highly active and selective mesostructured Cu/AlCeO catalyst for CO₂ hydrogenation to methanol," *Applied Catalysis A: General*, vol. 571, pp. 51–60, Feb. 2019, doi: 10.1016/j.apcata.2018.12.008.
- [47] F. Wang, M. Wei, D. G. Evans, and X. Duan, "CeO₂-based heterogeneous catalysts toward catalytic conversion of CO₂," *J. Mater. Chem. A*, vol. 4, no. 16, pp. 5773–5783, Apr. 2016, doi: 10.1039/C5TA10737G.
- [48] K. Chang, T. Wang, and J. G. Chen, "Methanol Synthesis from CO₂ Hydrogenation over CuZnCeTi Mixed Oxide Catalysts," *Ind. Eng. Chem. Res.*, vol. 58, no. 19, pp. 7922–7928, May 2019, doi: 10.1021/acs.iecr.9b00554.
- [49] J. Graciani *et al.*, "Catalysis. Highly active copper-ceria and copper-ceria-titania catalysts for methanol synthesis from CO₂," *Science*, vol. 345, no. 6196, pp. 546–550, Aug. 2014, doi: 10.1126/science.1253057.
- [50] Z. Shi, Q. Tan, and D. Wu, "Enhanced CO₂ hydrogenation to methanol over TiO₂ nanotubes-supported CuO-ZnO-CeO₂ catalyst," *Applied Catalysis A: General*, vol. 581, pp. 58–66, Jul. 2019, doi: 10.1016/j.apcata.2019.05.019.
- [51] G. Bonura, F. Arena, G. Mezzatesta, C. Cannilla, L. Spadaro, and F. Frusteri, "Role of the ceria promoter and carrier on the functionality of Cu-based catalysts in the CO₂-to-methanol hydrogenation reaction," *Catalysis Today - CATAL TODAY*, vol. 171, pp. 251–256, Aug. 2011, doi: 10.1016/j.cattod.2011.04.038.
- [52] X. Hu, W. Qin, Q. Guan, and W. Li, "The Synergistic Effect of CuZnCeO_x in Controlling the Formation of Methanol and CO from CO₂ Hydrogenation," *ChemCatChem*, vol. 10, no. 19, pp. 4438–4449, 2018, doi: 10.1002/cctc.201800668.
- [53] J. Toyir *et al.*, "Sustainable process for the production of methanol from CO₂ and H₂ using Cu/ZnO-based multicomponent catalyst," *Physics Procedia*, vol. 2, no. 3, pp. 1075–1079, Nov. 2009, doi: 10.1016/j.phpro.2009.11.065.
- [54] M. M.-J. Li *et al.*, "CO₂ Hydrogenation to Methanol over Catalysts Derived from Single Cationic Layer CuZnGa LDH Precursors," *ACS Catal.*, vol. 8, no. 5, pp. 4390–4401, May 2018, doi: 10.1021/acscatal.8b00474.
- [55] M. M.-J. Li, Z. Zeng, F. Liao, X. Hong, and S. C. E. Tsang, "Enhanced CO₂ hydrogenation to methanol over CuZn nanoalloy in Ga modified Cu/ZnO catalysts," *Journal of Catalysis*, vol. 343, pp. 157–167, Nov. 2016, doi: 10.1016/j.jcat.2016.03.020.
- [56] K. Li and J. G. Chen, "CO₂ Hydrogenation to Methanol over ZrO₂-Containing Catalysts: Insights into ZrO₂ Induced Synergy," *ACS Catal.*, vol. 9, no. 9, pp. 7840–7861, Sep. 2019, doi: 10.1021/acscatal.9b01943.

- [57] B. Rungtaweevoranit *et al.*, “Copper Nanocrystals Encapsulated in Zr-based Metal–Organic Frameworks for Highly Selective CO₂ Hydrogenation to Methanol,” *Nano Lett.*, vol. 16, no. 12, pp. 7645–7649, Dec. 2016, doi: 10.1021/acs.nanolett.6b03637.
- [58] J. Słoczyński *et al.*, “Effect of Mg and Mn oxide additions on structural and adsorptive properties of Cu/ZnO/ZrO₂ catalysts for the methanol synthesis from CO₂,” *Applied Catalysis A: General*, vol. 249, no. 1, pp. 129–138, Aug. 2003, doi: 10.1016/S0926-860X(03)00191-1.
- [59] S. Tada *et al.*, “Design of Interfacial Sites between Cu and Amorphous ZrO₂ Dedicated to CO₂-to-Methanol Hydrogenation,” *ACS Catal.*, vol. 8, no. 9, pp. 7809–7819, Sep. 2018, doi: 10.1021/acscatal.8b01396.
- [60] T. Witoon, J. Chalorngham, P. Dumrongbunditkul, M. Chareonpanich, and J. Limtrakul, “CO₂ hydrogenation to methanol over Cu/ZrO₂ catalysts: Effects of zirconia phases,” *Chemical Engineering Journal*, vol. 293, pp. 327–336, Jun. 2016, doi: 10.1016/j.cej.2016.02.069.
- [61] K. et al Samson, ““Influence of ZrO₂ Structure and Copper Electronic State on Activity of Cu/ZrO₂ Catalysts in Methanol Synthesis from CO₂” on Publons.” <https://publons.com/publon/6548611/> (accessed Apr. 15, 2022).
- [62] I. Ro *et al.*, “Role of the Cu-ZrO₂ Interfacial Sites for Conversion of Ethanol to Ethyl Acetate and Synthesis of Methanol from CO₂ and H₂,” *ACS Catal.*, vol. 6, no. 10, pp. 7040–7050, Oct. 2016, doi: 10.1021/acscatal.6b01805.
- [63] Y. Zhu *et al.*, “Copper-zirconia interfaces in UiO-66 enable selective catalytic hydrogenation of CO₂ to methanol,” *Nat Commun*, vol. 11, no. 1, Art. no. 1, Nov. 2020, doi: 10.1038/s41467-020-19438-w.
- [64] B. An, J. Zhang, K. Cheng, P. Ji, C. Wang, and W. Lin, “Confinement of Ultrasmall Cu/ZnOx Nanoparticles in Metal–Organic Frameworks for Selective Methanol Synthesis from Catalytic Hydrogenation of CO₂,” *J. Am. Chem. Soc.*, vol. 139, no. 10, pp. 3834–3840, Mar. 2017, doi: 10.1021/jacs.7b00058.
- [65] E. L. Fornero, A. L. Bonivardi, and M. A. Baltanás, “Isotopic study of the rates of hydrogen provision vs. methanol synthesis from CO₂ over Cu–Ga–Zr catalysts,” *Journal of Catalysis*, vol. 330, pp. 302–310, Oct. 2015, doi: 10.1016/j.jcat.2015.07.025.
- [66] H. Song *et al.*, “Effect of lanthanum group promoters on Cu/(mixture of ZnO and Zn–Al-spinel-oxides) catalyst for methanol synthesis by hydrogenation of CO and CO₂ mixtures,” *Fuel*, vol. 283, p. 118987, Jan. 2021, doi: 10.1016/j.fuel.2020.118987.

- [67] M. Kourtelesis, K. Kousi, and D. I. Kondarides, “CO₂ Hydrogenation to Methanol over La₂O₃-Promoted CuO/ZnO/Al₂O₃ Catalysts: A Kinetic and Mechanistic Study,” *Catalysts*, vol. 10, no. 2, Art. no. 2, Feb. 2020, doi: 10.3390/catal10020183.
- [68] A. Gau, J. Hack, N. Maeda, and D. M. Meier, “Operando Spectroscopic Monitoring of Active Species in CO₂ Hydrogenation at Elevated Pressure and Temperature: Steady-State versus Transient Analysis,” *Energy Fuels*, vol. 35, no. 18, pp. 15243–15246, Sep. 2021, doi: 10.1021/acs.energyfuels.1c02592.
- [69] H. Song *et al.*, “Effect of lanthanum group promoters on Cu/(mixture of ZnO and Zn-Al-spinel-oxides) catalyst for methanol synthesis by hydrogenation of CO and CO₂ mixtures,” *Fuel*, vol. 283, p. 118987, 2021.
- [70] G. Bozzano and F. Manenti, “Efficient methanol synthesis: Perspectives, technologies and optimization strategies,” *Progress in Energy and Combustion Science*, vol. 56, pp. 71–105, 2016.
- [71] J. S. Hayward, P. J. Smith, S. A. Kondrat, M. Bowker, and G. J. Hutchings, “The Effects of Secondary Oxides on Copper-Based Catalysts for Green Methanol Synthesis,” *ChemCatChem*, vol. 9, no. 9, pp. 1655–1662, May 2017, doi: 10.1002/cctc.201601692.
- [72] F. Meshkini, M. Taghizadeh, and M. Bahmani, “Investigating the effect of metal oxide additives on the properties of Cu/ZnO/Al₂O₃ catalysts in methanol synthesis from syngas using factorial experimental design,” *Fuel*, vol. 89, no. 1, pp. 170–175, Jan. 2010, doi: 10.1016/j.fuel.2009.07.007.
- [73] S. Zander *et al.*, “The Role of the Oxide Component in the Development of Copper Composite Catalysts for Methanol Synthesis,” *Angewandte Chemie International Edition*, vol. 52, no. 25, pp. 6536–6540, 2013, doi: 10.1002/anie.201301419.
- [74] Słoczyński *et al.*, “Effect of metal oxide additives on the activity and stability of Cu/ZnO/ZrO₂ catalysts in the synthesis of methanol from CO₂ and H₂,” *Applied Catalysis A: General*, vol. 310, pp. 127–137, Aug. 2006, doi: 10.1016/j.apcata.2006.05.035.
- [75] S. K. Sharma *et al.*, “Design of highly stable MgO promoted Cu/ZnO catalyst for clean methanol production through selective hydrogenation of CO₂,” *Applied Catalysis A: General*, vol. 623, p. 118239, Aug. 2021, doi: 10.1016/j.apcata.2021.118239.
- [76] F. Gallucci, L. Paturzo, and A. Basile, “An experimental study of CO₂ hydrogenation into methanol involving a zeolite membrane reactor,” *Chemical Engineering and Processing: Process Intensification*, vol. 43, no. 8, pp. 1029–1036, 2004, doi: 10.1016/j.cep.2003.10.005.

- [77] C. Tisseraud, C. Comminges, S. Pronier, Y. Pouilloux, and A. Le Valant, “The Cu–ZnO synergy in methanol synthesis Part 3: Impact of the composition of a selective Cu@ZnOx core–shell catalyst on methanol rate explained by experimental studies and a concentric spheres model,” *Journal of Catalysis*, vol. 343, pp. 106–114, Nov. 2016, doi: 10.1016/j.jcat.2015.12.005.
- [78] G. Wang, D. Mao, X. Guo, and J. Yu, “Enhanced performance of the CuO-ZnO-ZrO₂ catalyst for CO₂ hydrogenation to methanol by WO₃ modification,” *Applied Surface Science*, vol. 456, Jun. 2018, doi: 10.1016/j.apsusc.2018.06.090.
- [79] S. Xiao *et al.*, “Highly efficient Cu-based catalysts via hydrotalcite-like precursors for CO₂ hydrogenation to methanol,” *Catalysis Today*, vol. 281, pp. 327–336, Mar. 2017, doi: 10.1016/j.cattod.2016.02.004.
- [80] J. Xiao, D. Mao, X. Guo, and J. Yu, “Methanol Synthesis from CO₂ Hydrogenation over CuO–ZnO–TiO₂ Catalysts: The Influence of TiO₂ Content,” *Energy Technology*, vol. 3, no. 1, pp. 32–39, 2015, doi: 10.1002/ente.201402091.
- [81] F. Zhang *et al.*, “Synthesis of Cu/Zn/Al/Mg catalysts on methanol production by different precipitation methods,” *Molecular Catalysis*, vol. 441, p. 190, 2017.
- [82] V. D. B. C. Dasireddy, S. Š. Neja, and L. Blaž, “Correlation between synthesis pH, structure and Cu/MgO/Al₂O₃ heterogeneous catalyst activity and selectivity in CO₂ hydrogenation to methanol,” *Journal of CO₂ Utilization*, vol. 28, pp. 189–199, Dec. 2018, doi: 10.1016/j.jcou.2018.09.002.
- [83] D. Guse, S. Polierer, S. Wild, S. Pitter, and M. Kind, “Improved Preparation of Cu/Zn-Based Catalysts by Well-Defined Conditions of Co-Precipitation and Aging,” *Chemie Ingenieur Technik*, vol. 94, no. 3, pp. 314–327, Mar. 2022, doi: 10.1002/cite.202100197.
- [84] Y. Bao *et al.*, “Highly efficient Cu/anatase TiO₂ {001}-nanosheets catalysts for methanol synthesis from CO₂,” *Journal of Energy Chemistry*, vol. 27, no. 2, pp. 381–388, Mar. 2018, doi: 10.1016/j.jechem.2017.12.015.
- [85] C. Liu, X. Guo, Q. Guo, D. Mao, J. Yu, and G. Lu, “Methanol synthesis from CO₂ hydrogenation over copper catalysts supported on MgO-modified TiO₂,” *Journal of Molecular Catalysis A: Chemical*, vol. 425, pp. 86–93, Dec. 2016, doi: 10.1016/j.molcata.2016.09.032.
- [86] J. Baima, H.-L. T. Le, J. Goniakowski, C. Noguera, A. Koltsov, and J.-M. Mатаigne, “Theoretical study of metal/silica interfaces: Ti, Fe, Cr and Ni on β -cristobalite,” *Phys. Chem. Chem. Phys.*, vol. 22, no. 37, pp. 21453–21462, Sep. 2020, doi: 10.1039/D0CP03216F.

- [87] E. L. Kunkes, F. Studt, F. Abild-Pedersen, R. Schlögl, and M. Behrens, “Hydrogenation of CO₂ to methanol and CO on Cu/ZnO/Al₂O₃: Is there a common intermediate or not?,” *Journal of Catalysis*, vol. 328, pp. 43–48, Aug. 2015, doi: 10.1016/j.jcat.2014.12.016.
- [88] K. Larmier *et al.*, “CO₂-to-Methanol Hydrogenation on Zirconia-Supported Copper Nanoparticles: Reaction Intermediates and the Role of the Metal–Support Interface - Larmier - 2017 - Angewandte Chemie International Edition - Wiley Online Library.” <https://onlinelibrary.wiley.com/doi/full/10.1002/anie.201610166> (accessed Apr. 18, 2022).
- [89] D. Grandjean *et al.*, “Dynamic Cu/Zn Interaction in SiO₂ Supported Methanol Synthesis Catalysts Unraveled by in Situ XAFS | The Journal of Physical Chemistry C.” <https://pubs.acs.org/doi/10.1021/jp201839s> (accessed Apr. 23, 2022).
- [90] Y. Jiang *et al.*, “Slurry methanol synthesis from CO₂ hydrogenation over microspherical SiO₂ support Cu/ZnO catalysts,” *Journal of CO₂ Utilization*, vol. 26, Jul. 2018, doi: 10.1016/j.jcou.2018.06.023.
- [91] V. Deerattrakul, P. Dittanet, M. Sawangphruk, and P. Kongkachuichay, “CO₂ hydrogenation to methanol using Cu-Zn catalyst supported on reduced graphene oxide nanosheets,” *Journal of CO₂ Utilization*, vol. 16, pp. 104–113, Dec. 2016, doi: 10.1016/j.jcou.2016.07.002.
- [92] Nie, X., et al. (2018) Mechanistic Understanding of Alloy Effect and Water Promotion for Pd-Cu Bimetallic Catalysts in CO₂ Hydrogenation to Methanol. *ACS Catalysis*, 8, 4873-4892.
- [93] “X. Jiang *et al.*, “Origin of Pd-Cu bimetallic effect for synergetic promotion of methanol formation from CO₂ hydrogenation,” *Journal of Catalysis*, vol. 369, pp. 21–32, 2019.
- [94] X. Jiang, N. Koizumi, X. Guo, and C. Song, “Bimetallic Pd–Cu catalysts for selective CO₂ hydrogenation to methanol,” *Applied Catalysis B: Environmental*, vol. 170–171, pp. 173–185, Jul. 2015, doi: 10.1016/j.apcatb.2015.01.010.
- [95] B. Hu, Y. Yu, G. Liu, S. Chen, X. Hong, and S. Tsang, “Hydrogen spillover enabled active Cu sites for methanol synthesis from CO₂ hydrogenation over Pd doped CuZn catalysts,” *Journal of Catalysis*, vol. 359, 2018, Accessed: Apr. 23, 2022. [Online]. Available: <https://ora.ox.ac.uk/objects/uuid:3d0c795a-06ed-4d1d-9346-3129652c03df>
- [96] J. Kugai, J. T. Miller, E. B. Fox, and C. Song, “In-situ X-ray absorption study of ceria-supported Pd-Cu nanoparticles for oxygen-enhanced water gas shift,” *Applied Catalysis A: General*, vol. 528, pp. 67–73, Nov. 2016, doi: 10.1016/j.apcata.2016.09.010.

- [97] E. J. Choi, Y. H. Lee, D. W. Lee, D. J. Moon, and K. Y. Lee, "Hydrogenation of CO₂ to methanol over Pd–Cu/CeO₂ catalysts," *Molecular Catalysis*, vol. 434, pp. 146–153, 2017, doi: 10.1016/j.mcat.2017.02.005.
- [98] E. B. Fox, A. F. Lee, K. Wilson, and C. Song, "In-situ XPS study on the reducibility of Pd-promoted Cu/CeO₂ catalysts for the oxygen-assisted water-gas-shift reaction," *Topics in Catalysis*, vol. 49, no. 1, pp. 89–96, 2008.
- [99] X. Jiang, X. Wang, X. Nie, N. Koizumi, X. Guo, and C. Song, "CO₂ hydrogenation to methanol on Pd-Cu bimetallic catalysts: H₂/CO₂ ratio dependence and surface species," *Catalysis Today*, vol. 316, pp. 62–70, Oct. 2018, doi: 10.1016/j.cattod.2018.02.055.
- [100] Z. Liang, P. Gao, Z. Tang, M. Lv, and Y. Sun, "Three-dimensional porous Cu-Zn/Al foam monolithic catalyst for CO₂ hydrogenation to methanol in microreactor," *Journal of CO₂ Utilization*, vol. 21, pp. 191–199, Oct. 2017, doi: 10.1016/j.jcou.2017.05.023.
- [101] S. Golunski and R. Burch, "CO₂ Hydrogenation to Methanol over Copper Catalysts: Learning from Syngas Conversion," *Top Catal*, vol. 64, no. 17, pp. 974–983, Dec. 2021, doi: 10.1007/s11244-021-01427-y.
- [102] D. S. Marlin, E. Sarron, and Ó. Sigurbjörnsson, "Process Advantages of Direct CO₂ to Methanol Synthesis," *Front Chem*, vol. 6, p. 446, Sep. 2018, doi: 10.3389/fchem.2018.00446.
- [103] S. Dang *et al.*, "A review of research progress on heterogeneous catalysts for methanol synthesis from carbon dioxide hydrogenation," *Catalysis Today*, vol. 330, pp. 61–75, Jun. 2019, doi: 10.1016/j.cattod.2018.04.021.
- [104] S. G. Jadhav, P. D. Vaidya, B. M. Bhanage, and J. B. Joshi, "Catalytic carbon dioxide hydrogenation to methanol: A review of recent studies," *Chemical Engineering Research and Design*, vol. 92, no. 11, pp. 2557–2567, Nov. 2014, doi: 10.1016/j.cherd.2014.03.005.
- [105] H. Lei, R. Nie, G. Wu, and Z. Hou, "Hydrogenation of CO₂ to CH₃OH over Cu/ZnO catalysts with different ZnO morphology," *Fuel*, vol. 154, pp. 161–166, Aug. 2015, doi: 10.1016/j.fuel.2015.03.052.
- [106] A. Karelovic, G. Galdames, J. Medina, C. Yévenes, Y. Barra, and R. Jiménez, "Mechanism and structure sensitivity of methanol synthesis from CO₂ over SiO₂-supported Cu nanoparticles," *Journal of Catalysis*, vol. 369, pp. 415–426, Jan. 2019, doi: 10.1016/j.jcat.2018.11.012.
- [107] Y. Yang, M. G. White, and P. Liu, "Theoretical Study of Methanol Synthesis from CO₂ Hydrogenation on Metal-Doped Cu(111) Surfaces," *J. Phys. Chem. C*, vol. 116, no. 1, pp. 248–256, Jan. 2012, doi: 10.1021/jp208448c.

- [108] C. Tisseraud *et al.*, “The Cu–ZnO synergy in methanol synthesis from CO₂, Part 2: Origin of the methanol and CO selectivities explained by experimental studies and a sphere contact quantification model in randomly packed binary mixtures on Cu–ZnO coprecipitate catalysts,” *Journal of Catalysis*, May 2015, doi: 10.1016/j.jcat.2015.04.035.
- [109] L. Shi, Y. Tan, and N. Tsubaki, “A Solid-State Combustion Method towards Metallic Cu–ZnO Catalyst without Further Reduction and its Application to Low-Temperature Methanol Synthesis,” *ChemCatChem*, vol. 4, Jun. 2012, doi: 10.1002/cctc.201100404.
- [110] L. Shi, K. Tao, R. Yang, F. Meng, C. Xing, and N. Tsubaki, “Study on the preparation of Cu/ZnO catalyst by sol–gel auto-combustion method and its application for low-temperature methanol synthesis,” *Applied Catalysis A-general - APPL CATAL A-GEN*, vol. 401, pp. 46–55, Jul. 2011, doi: 10.1016/j.apcata.2011.04.043.
- [111] X. Dong, F. Li, N. Zhao, F. Xiao, J. Wang, and Y. Tan, “CO₂ hydrogenation to methanol over Cu/ZnO/ZrO₂ catalysts prepared by precipitation-reduction method,” *Applied Catalysis B: Environmental*, vol. 191, pp. 8–17, Aug. 2016, doi: 10.1016/j.apcatb.2016.03.014.
- [112] X. Guo, D. Mao, G. Lu, S. Wang, and G. Wu, “CO₂ hydrogenation to methanol over Cu/ZnO/ZrO₂ catalysts prepared via a route of solid-state reaction,” *Catalysis Communications - CATAL COMMUN*, vol. 12, pp. 1095–1098, Jul. 2011, doi: 10.1016/j.catcom.2011.03.033.
- [113] L. Li, D. Mao, J. Yu, and X. Guo, “Highly selective hydrogenation of CO₂ to methanol over CuO–ZnO–ZrO₂ catalysts prepared by a surfactant-assisted co-precipitation method,” 2015, doi: 10.1016/J.JPOWSOUR.2014.12.142.
- [114] M. Behrens *et al.*, “Understanding the complexity of a catalyst synthesis: Co-precipitation of mixed Cu,Zn,Al hydroxycarbonate precursors for Cu/ZnO/Al₂O₃ catalysts investigated by titration experiments,” 2011, doi: 10.1016/J.APCATA.2010.10.031.
- [115] P. J. Smith *et al.*, “A new class of Cu/ZnO catalysts derived from zincian georgeite precursors prepared by co-precipitation,” *Chem. Sci.*, vol. 8, no. 3, pp. 2436–2447, Feb. 2017, doi: 10.1039/C6SC04130B.
- [116] L. Zwiener *et al.*, “Evolution of zincian malachite synthesis by low temperature co-precipitation and its catalytic impact on the methanol synthesis,” *Applied Catalysis B: Environmental*, vol. 249, pp. 218–226, Jul. 2019, doi: 10.1016/j.apcatb.2019.02.023.
- [117] H. L. Huynh, “Synthesis, characterization, and activity of bimetallic Ni-Fe hydrotalcite-derived catalysts in dry reforming of methane,” Jun. 2018, Accessed: May 07, 2022. [Online]. Available: <https://uis.brage.unit.no/uis-xmlui/handle/11250/2597078>

- [118] S. Velu, K. Suzuki, and C. S. Gopinath, "Photoemission and in Situ XRD Investigations on CuCoZnAl-Mixed Metal Oxide Catalysts for the Oxidative Steam Reforming of Methanol," *J. Phys. Chem. B*, vol. 106, no. 49, pp. 12737–12746, Dec. 2002, doi: 10.1021/jp021003w.
- [119] B. J. Reddy, R. L. Frost, and A. Locke, "Synthesis and spectroscopic characterisation of aurichalcite $(\text{Zn,Cu}_{2+})_5(\text{CO}_3)_2(\text{OH})_6$; implications for Cu–ZnO catalyst precursors," *Transition Met Chem*, vol. 33, no. 3, pp. 331–339, Apr. 2008, doi: 10.1007/s11243-007-9044-9.
- [120] M. Behrens, F. Girgsdies, A. Trunschke, and R. Schlögl, "Minerals as Model Compounds for Cu/ZnO Catalyst Precursors: Structural and Thermal Properties and IR Spectra of Mineral and Synthetic (Zincian) Malachite, Rosasite and Aurichalcite and a Catalyst Precursor Mixture," *European Journal of Inorganic Chemistry*, vol. 2009, no. 10, pp. 1347–1357, 2009, doi: 10.1002/ejic.200801216.
- [121] S. Kaluza *et al.*, "A Novel Synthesis Route for Cu/ZnO/Al₂O₃ Catalysts used in Methanol Synthesis: Combining Continuous Consecutive Precipitation with Continuous Aging of the Precipitate," *ChemCatChem*, vol. 3, Jan. 2011, doi: 10.1002/cctc.201000329.
- [122] E. Frei, A. Schaadt, T. Ludwig, H. Hillebrecht, and I. Krossing, "The influence of the precipitation/ageing temperature on a Cu/ZnO/ZrO₂ catalyst for methanol synthesis from H₂ and CO₂," 2014, Accessed: May 07, 2022. [Online]. Available: <https://publica.fraunhofer.de/entities/publication/7ddea4a6-2e32-4ab4-8a1b-35fa118b827a/details>
- [123] S. Fujita, S. Moribe, Y. Kanamori, M. Kakudate, and N. Takezawa, "Preparation of a coprecipitated Cu/ZnO catalyst for the methanol synthesis from CO₂ — effects of the calcination and reduction conditions on the catalytic performance," *Applied Catalysis A-general - APPL CATAL A-GEN*, vol. 207, pp. 121–128, Feb. 2001, doi: 10.1016/S0926-860X(00)00616-5.
- [124] C. Jeong and Y.-W. Suh, "Preparation of Active Cu/ZnO-based Catalysts for Methanol Synthesis," *Applied Chemistry for Engineering*, vol. 27, no. 6, pp. 555–564, 2016, doi: 10.14478/ace.2016.1109.
- [125] J. Schumann, A. Tarasov, N. Thomas, R. Schlögl, and M. Behrens, "Cu,Zn-based catalysts for methanol synthesis: On the effect of calcination conditions and the part of residual carbonates," *Applied Catalysis A: General*, vol. 516, pp. 117–126, Apr. 2016, doi: 10.1016/j.apcata.2016.01.037.

- [126] A. A. Bunaciu, E. UdriȘtioiu, and H. Aboul-Enein, "X-Ray Diffraction: Instrumentation and Applications," *Critical reviews in analytical chemistry / CRC*, vol. 45, Apr. 2015, doi: 10.1080/10408347.2014.949616.
- [127] T. S. Srivatsan, "Characterization of Minerals, Metals and Materials , edited by Jiann-Yang Hwang, S.N. Monteiro, Chen Guang Bai, John Carpenter, Mingdong Cai, Donato Firrao, and Byoung-Gon Kim," *Materials and Manufacturing Processes*, vol. 29, no. 7, pp. 885–885, Jul. 2014, doi: 10.1080/10426914.2014.905026.
- [128] M. Ermrich and D. Opper, *XRD for the Analyst: Getting Acquainted with the Principles*. PANalytical, 2013.
- [129] U. Holzwarth and N. Gibson, "The Scherrer equation versus the 'Debye-Scherrer equation,'" *Nature Nanotech*, vol. 6, no. 9, Art. no. 9, Sep. 2011, doi: 10.1038/nnano.2011.145.
- [130] J. R. Connolly, *Introduction to X-Ray Powder Diffraction; Spring, 2007*. 2007.
- [131] B. D. Cullity, *Elements of x-ray diffraction*. 2014. [WorldCat.org]."
<https://www.worldcat.org/title/elements-of-x-ray-diffraction/oclc/865160561> (accessed Apr. 24, 2022).
- [132] I. Jendrzewska, P. Zajdel, E. Pietrasik, Z. Barsova, and T. Goryczka, "Application of X-ray powder diffraction and differential scanning calorimetry for identification of counterfeit drugs," *Monatshefte für Chemie-Chemical Monthly*, vol. 149, no. 5, pp. 977–985, 2018.
- [133] A. Ali, Y. W. Chiang, and R. Santos, "X-Ray Diffraction Techniques for Mineral Characterization: A Review for Engineers of the Fundamentals, Applications, and Research Directions," *Minerals*, vol. 12, p. 205, Feb. 2022, doi: 10.3390/min12020205.
- [134] E. M. Gaigneaux *et al.*, *Scientific bases for the preparation of heterogeneous catalysts*. Elsevier, 2002. <https://www.elsevier.com/books/scientific-bases-for-the-preparation-of-heterogeneous-catalysts/gaigneaux/978-0-444-52827-8> (accessed Apr. 28, 2022).
- [135] H. L. Huynh, "Synthesis, characterization, and activity of bimetallic Ni-Fe hydrotalcite-derived catalysts in dry reforming of methane," Z. Yu, Ed., ed: University of Stavanger, Norway, 2018."
- [136] F. Kapteijn, J. A. Moulijn, and A. Tarfaoui, "Temperature programmed reduction and sulphiding," *Studies in Surface Science and Catalysis*, vol. 79, no. 1, pp. 401–401, 1993.
- [137] G. Ertl, H. Knözinger, F. Schüth, and J. Weitkamp, "Handbook of Heterogeneous Catalysis," 2008.

- [138] D. Monti, “Temperature-programmed reduction. Parametric sensitivity and estimation of kinetic parameters,” *Journal of Catalysis*, vol. 83, no. 2, pp. 323–335, Oct. 1983, doi: 10.1016/0021-9517(83)90058-1.
- [139] P. S. Kumar, K. G. Pavithra, and M. Naushad, “Characterization techniques for nanomaterials,” in *Nanomaterials for solar cell applications*, Elsevier, 2019, pp. 97–124.
- [140] A. Parupudi, S. H. R. Mulagapati, and J. A. Subramony, “Chapter 1 - Nanoparticle technologies: Recent state of the art and emerging opportunities,” in *Nanoparticle Therapeutics*, P. Kesharwani and K. K. Singh, Eds. Academic Press, 2022, pp. 3–46. doi: 10.1016/B978-0-12-820757-4.00009-0.
- [141] C. Hacker *et al.*, “Nanoparticle suspensions enclosed in methylcellulose: a new approach for quantifying nanoparticles in transmission electron microscopy,” *Sci Rep*, vol. 6, p. 25275, May 2016, doi: 10.1038/srep25275.
- [142] D. Su, “Advanced electron microscopy characterization of nanomaterials for catalysis,” *Green Energy & Environment*, vol. 2, no. 2, pp. 70–83, Apr. 2017, doi: 10.1016/j.gee.2017.02.001.
- [143] S. Lowell, J. E. Shields, M. A. Thomas, and M. Thommes, *Characterization of porous solids and powders: surface area, pore size and density*, vol. 16. Springer Science & Business Media, 2006.
- [144] M. A. Vannice and W. H. Joyce, *Kinetics of catalytic reactions*, vol. 134. Springer, 2005. Available: <https://link.springer.com/book/10.1007/b136380>
- [145] E. P. Barrett, L. G. Joyner, and P. P. Halenda, “The Determination of Pore Volume and Area Distributions in Porous Substances. I. Computations from Nitrogen Isotherms,” *J. Am. Chem. Soc.*, vol. 73, no. 1, pp. 373–380, Jan. 1951, doi: 10.1021/ja01145a126.
- [146] K. Sing, “The use of nitrogen adsorption for the characterisation of porous materials,” *Colloids and Surfaces A: Physicochemical and Engineering Aspects*, vol. 187–188, pp. 3–9, Aug. 2001, doi: 10.1016/S0927-7757(01)00612-4.
- [147] M. Eddaoudi, “Characterization of Porous Solids and Powders: Surface Area, Pore Size and Density By S. Lowell (Quantachrome Instruments, Boynton Beach), J. E. Shields (C. W. Post Campus of Long Island University), M. A. Thomas, and M. Thommes (Quantachrome Instruments). Kluwer Academic Publishers: Dordrecht, The Netherlands. 2004. xiv + 348 pp. \$159.00. ISBN 1-4020-2302-2.,” *J. Am. Chem. Soc.*, vol. 127, no. 40, pp. 14117–14117, Oct. 2005, doi: 10.1021/ja041016i.
- [148] *Ettre, L.S. (1993). Pure Appl. Chem. 65: 819–872. See also, Ettre, L. S. (1993). LC-GC. 11: 502.*

- [149] I. G. Kolomnikov, A. M. Efremov, T. I. Tikhomirova, N. M. Sorokina, and Y. A. Zolotov, "Early stages in the history of gas chromatography," *J Chromatogr A*, vol. 1537, pp. 109–117, Feb. 2018, doi: 10.1016/j.chroma.2018.01.006.
- [150] H. M. McNair, J. M. Miller, and N. H. Snow, *Basic Gas Chromatography*. Hoboken, NJ, USA: Wiley, 2019. (accessed Apr. 30, 2022).
- [151] J.-F. Portha *et al.*, "Kinetics of Methanol Synthesis from Carbon Dioxide Hydrogenation over Copper–Zinc Oxide Catalysts," *Ind. Eng. Chem. Res.*, vol. 56, no. 45, pp. 13133–13145, Nov. 2017, doi: 10.1021/acs.iecr.7b01323.
- [152] K. Kobl, S. Thomas, Y. Zimmermann, K. Parkhomenko, and A.-C. Roger, "Power-law kinetics of methanol synthesis from carbon dioxide and hydrogen on copper–zinc oxide catalysts with alumina or zirconia supports," *Catalysis Today*, vol. 270, pp. 31–42, Jul. 2016, doi: 10.1016/j.cattod.2015.11.020.
- [153] F. Nestler *et al.*, "Kinetic modelling of methanol synthesis over commercial catalysts: A critical assessment," *Chemical Engineering Journal*, vol. 394, p. 124881, Aug. 2020, doi: 10.1016/j.cej.2020.124881.
- [154] M. Peter, M. B. Fichtl, H. Ruland, S. Kaluza, M. Muhler, and O. Hinrichsen, "Detailed kinetic modeling of methanol synthesis over a ternary copper catalyst," *Chemical Engineering Journal*, vol. 203, pp. 480–491, Sep. 2012, doi: 10.1016/j.cej.2012.06.066.
- [155] K. M. V. Bussche and G. F. Froment, "A Steady-State Kinetic Model for Methanol Synthesis and the Water Gas Shift Reaction on a Commercial Cu/ZnO/Al₂O₃ Catalyst," *Journal of Catalysis*, vol. 161, no. 1, pp. 1–10, Jun. 1996, doi: 10.1006/jcat.1996.0156.
- [156] N. Park, M.-J. Park, Y.-J. Lee, K.-S. Ha, and K.-W. Jun, "Kinetic modeling of methanol synthesis over commercial catalysts based on three-site adsorption," *Fuel Processing Technology*, vol. 125, pp. 139–147, Sep. 2014, doi: 10.1016/j.fuproc.2014.03.041.
- [157] C. V. Ovesen *et al.*, "A Microkinetic Analysis of the Water–Gas Shift Reaction under Industrial Conditions," *Journal of Catalysis*, vol. 158, no. 1, pp. 170–180, Jan. 1996, doi: 10.1006/jcat.1996.0016.
- [158] L. C. Grabow and M. Mavrikakis, "Mechanism of Methanol Synthesis on Cu through CO₂ and CO Hydrogenation," *ACS Catal.*, vol. 1, no. 4, pp. 365–384, Apr. 2011, doi: 10.1021/cs200055d.
- [159] G. H. Graaf, P. J. J. M. Sijtsema, E. J. Stamhuis, and G. E. H. Joosten, "Chemical equilibria in methanol synthesis," *Chemical Engineering Science*, vol. 41, no. 11, pp. 2883–2890, Jan. 1986, doi: 10.1016/0009-2509(86)80019-7.

- [160] G. Schneider, "J. M. Prausnitz: Molecular Thermodynamics of Fluid Phase Equilibria. International Series in the Physical and Chemical Engineering Sciences. Prentice-Hall Inc., Englewood Cliffs, New Jersey, 1969. 523 Seiten Preis: 145 s," 1970. doi: 10.1002/BBPC.19700740327.
- [161] J. G. van Bennekom, J. G. M. Winkelman, R. H. Venderbosch, S. D. G. B. Nieland, and H. J. Heeres, "Modeling and Experimental Studies on Phase and Chemical Equilibria in High-Pressure Methanol Synthesis," *Ind. Eng. Chem. Res.*, vol. 51, no. 38, pp. 12233–12243, Sep. 2012, doi: 10.1021/ie3017362.
- [162] A. Gervasini and S. Bennici, "Dispersion and surface states of copper catalysts by temperature-programmed-reduction of oxidized surfaces (s-TPR)," *Applied Catalysis A: General*, vol. 281, no. 1, pp. 199–205, Mar. 2005, doi: 10.1016/j.apcata.2004.11.030.
- [163] M. Behrens and R. Schlögl, "How to prepare a good Cu/ZnO catalyst or the role of solid state chemistry for the synthesis of nanostructured catalysts," *Zeitschrift für anorganische und allgemeine Chemie*, vol. 639, no. 15, pp. 2683–2695, 2013.
- [164] S. Natesakhawat *et al.*, "Active Sites and Structure–Activity Relationships of Copper-Based Catalysts for Carbon Dioxide Hydrogenation to Methanol," *ACS Catal.*, vol. 2, no. 8, pp. 1667–1676, Aug. 2012, doi: 10.1021/cs300008g.
- [165] C. Vandergrift, "Effect of the reduction treatment on the structure and reactivity of silica-supported copper particles," *Journal of Catalysis*, vol. 131, no. 1, p. 178, 1991.
- [166] B. Liang *et al.*, "Investigation on Deactivation of Cu/ZnO/Al₂O₃ Catalyst for CO₂ Hydrogenation to Methanol," *Ind. Eng. Chem. Res.*, vol. 58, no. 21, pp. 9030–9037, May 2019, doi: 10.1021/acs.iecr.9b01546.
- [167] P. Gao *et al.*, "Influence of modifier (Mn, La, Ce, Zr and Y) on the performance of Cu/Zn/Al catalysts via hydrotalcite-like precursors for CO₂ hydrogenation to methanol," *Applied Catalysis A: General*, vol. 468, pp. 442–452, 2013.
- [168] L. Frusteri, C. Cannilla, S. Todaro, F. Frusteri, and G. Bonura, "Tailoring of Hydrotalcite-derived Cu-based catalysts for CO₂ hydrogenation to methanol," *Catalysts*, vol. 9, no. 12, p. 1058, 2019.
- [169] D. Allam, S. Bennici, L. Limousy, and S. Hocine, "Improved Cu-and Zn-based catalysts for CO₂ hydrogenation to methanol," *Comptes Rendus Chimie*, vol. 22, no. 2–3, pp. 227–237, 2019.
- [170] S. B. Bagherzadeh, M. Haghghi, and N. Rahemi, "Novel oxalate gel coprecipitation synthesis of ZrO₂-CeO₂-promoted CuO-ZnO-Al₂O₃ nanocatalyst for fuel cell-grade

- hydrogen production from methanol: Influence of ceria-zirconia loading,” *Energy Conversion and Management*, vol. 134, pp. 88–102, 2017.
- [171] C.-L. Chiang, K.-S. Lin, and H.-W. Chuang, “Direct synthesis of formic acid via CO₂ hydrogenation over Cu/ZnO/Al₂O₃ catalyst,” *Journal of Cleaner Production*, vol. 172, pp. 1957–1977, 2018.
- [172] P. Gao *et al.*, “Yttrium oxide modified Cu/ZnO/Al₂O₃ catalysts via hydrotalcite-like precursors for CO₂ hydrogenation to methanol,” *Catalysis Science & Technology*, vol. 5, no. 9, pp. 4365–4377, 2015.
- [173] G. R Bertolini, C. P. Jiménez-Gómez, J. A. Cecilia, and P. Maireles-Torres, “Gas-phase hydrogenation of furfural to furfuryl alcohol over Cu-ZnO-Al₂O₃ catalysts prepared from layered double hydroxides,” *Catalysts*, vol. 10, no. 5, p. 486, 2020.
- [174] E. Heracleous, E. T. Liakakou, A. A. Lappas, and A. A. Lemonidou, “Investigation of K-promoted Cu-Zn-Al, Cu-X-Al and Cu-Zn-X (X=Cr, Mn) catalysts for carbon monoxide hydrogenation to higher alcohols,” *Applied Catalysis A: General*, vol. 455, pp. 145–154, Mar. 2013, doi: 10.1016/j.apcata.2013.02.001.
- [175] X. Guo, D. Mao, G. Lu, S. Wang, and G. Wu, “Glycine–nitrate combustion synthesis of CuO–ZnO–ZrO₂ catalysts for methanol synthesis from CO₂ hydrogenation,” *Journal of Catalysis*, vol. 271, no. 2, pp. 178–185, 2010.
- [176] M. Balaraju, V. Rekha, P. S. Sai Prasad, R. B. N. Prasad, and N. Lingaiah, “Selective Hydrogenolysis of Glycerol to 1, 2 Propanediol Over Cu–ZnO Catalysts,” *Catal Lett*, vol. 126, no. 1, pp. 119–124, Nov. 2008, doi: 10.1007/s10562-008-9590-6.
- [177] M. Thommes *et al.*, “Physisorption of gases, with special reference to the evaluation of surface area and pore size distribution (IUPAC Technical Report),” *Pure and Applied Chemistry*, vol. 87, no. 9–10, pp. 1051–1069, Oct. 2015, doi: 10.1515/pac-2014-1117.
- [178] R. Bardestani, G. S. Patience, and S. Kaliaguine, “Experimental methods in chemical engineering: specific surface area and pore size distribution measurements—BET, BJH, and DFT,” *The Canadian Journal of Chemical Engineering*, vol. 97, no. 11, pp. 2781–2791, 2019, doi: 10.1002/cjce.23632.
- [179] N. Mota, R. Guil-Lopez, B. G. Pawelec, J. L. G. Fierro, and R. M. Navarro, “Highly active Cu/ZnO–Al catalyst for methanol synthesis: effect of aging on its structure and activity,” *RSC Advances*, vol. 8, no. 37, pp. 20619–20629, 2018, doi: 10.1039/C8RA03291B.

- [180] J. M. Beiramar, A. Griboval-Constant, and A. Y. Khodakov, "Effects of Metal Promotion on the Performance of CuZnAl Catalysts for Alcohol Synthesis," *ChemCatChem*, vol. 6, no. 6, pp. 1788–1793, 2014, doi: 10.1002/cctc.201402037.
- [181] S. Ali, N. A. Mohd Zabidi, and S. Duvvuri, "Effect of loading on the physicochemical properties of alumina supported Co/Mo bimetallic nanocatalysts," presented at the International Conference on Fundamental and Applied Sciences (ICFAS2010), Convention Centre, Kuala Lumpur, 2010. Accessed: May 18, 2022. [Online]. Available: <http://eprints.utp.edu.my/3848/>
- [182] K. Chen *et al.*, "CO₂ hydrogenation to methanol over Cu catalysts supported on La-modified SBA-15: The crucial role of Cu–LaOx interfaces," *Applied Catalysis B: Environmental*, vol. 251, pp. 119–129, Aug. 2019, doi: 10.1016/j.apcatb.2019.03.059.

Appendices

Appendix A: Calculations of catalysts synthesis

The unpromoted catalyst should contain Cu/ZnO/Al₂O₃ after reduction and calcination. For the catalysts from the promoted systems, they should contain Cu/ZnO/Al₂O₃ – Ce₂O₃ and Cu/ZnO/Al₂O₃ – La₂O₃.

Molecular weights of Precursors used (g/mol):

Precursor	MW
Cu(NO ₃).3H ₂ O	241.6
Zn(NO ₃).6H ₂ O	297.49
Al(NO ₃) ₃ .9H ₂ O	375.13
Na ₂ CO ₃	105.99
La(NO ₃) ₃ .H ₂ O	433.01
Ce(NO ₃) ₃ .6H ₂ O	434.23

Concentrations of solutions used (mol/L)

NaCO ₃	1.2
Metal Nitrate	1

$$V (\text{NaCO}_3)_{\text{used}} = \frac{n(\text{NaCO}_3)}{C(\text{NaCO}_3)} =$$

Where V: Volume of solution used

n: number of moles

C: concentration of solution

M: molecular weight

m: mass

Table A-1. Stoichiometric coefficients of the prepared catalysts

Composition					
Sample	Cu	Zn	Al	La or Ce	Cu/Zn ratio
CuZnAl-0	0.6	0.3	0.1	0	2
CuZnAl-2% La/Ce	0.6	0.3	0.08	0.02	2
CuZnAl-4% La/Ce	0.6	0.3	0.06	0.04	2
CuZnAl-6% La/Ce	0.6	0.3	0.04	0.06	2

Use 0.1 mol of Cu in metal solution and base the mols of metals on the selected Cu mol

Mol of metal based on mol of total Cu				
Sample	Cu ²⁺	Zn ²⁺	Al ³⁺	La ³⁺ /Ce ³⁺
CuZnAl-0	0.1	0.05	0.0167	0
CuZnAl-2% La/Ce	0.1	0.05	0.0133	0.0033
CuZnAl-4% La/Ce	0.1	0.05	0.01	0.0067
CuZnAl-6% La/Ce	0.1	0.05	0.0067	0.01

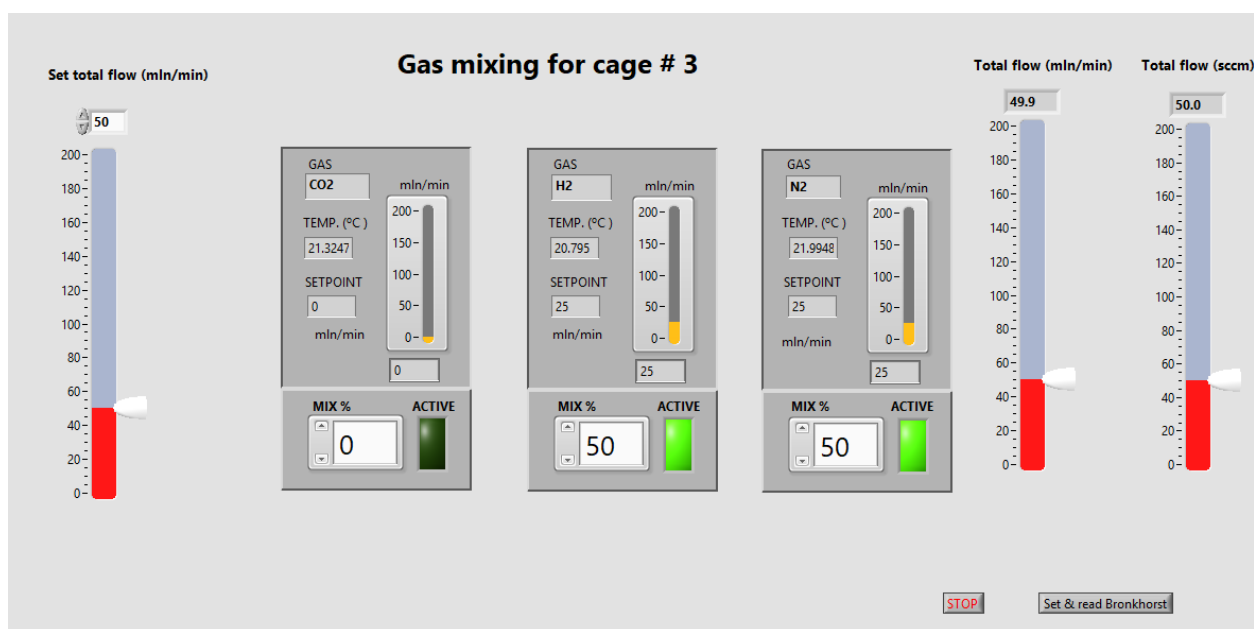
Finally, to calculate the mass of each precursor used: $m = n.M$

Grams of metal precursor based on mol of total Cu				
Sample	Cu nitrate	Zn nitrate	Al nitrate	La ₃ /Ce ₃ nitrate
CuZnAl-0	24.16	14.8745	6.25216667	0
CuZnAl-2% La/Ce	24.16	14.8745	5.00173333	1.44743333
CuZnAl-4% La/Ce	24.16	14.8745	3.7513	2.89486667
CuZnAl-6% La/Ce	24.16	14.8745	2.50086667	4.3423

Appendix B: Description of reaction and data collection procedure

1. Cleaning, reassembling and reduction

- 1) Set Eurotherm to local, take out and clean reactor, discard old catalyst in disposal bottle, use air to remove quartz wool plug and remaining catalyst.
- 2) Place the reactor, put in quartz wool plug.
- 3) weigh 0.050 catalyst and 0.5000 SiC, mix, and put into the reactor.
- 4) Close the reactor with small amount of force.
- 5) Start the N₂ flow at 50 mL/min and increase the flow stepwise to 200 mL/min, then close the exit valve.
- 6) Check for leaks until 40 bar is reached with snoop in relief holes.
- 7) Open exit valve, change the flow to 50/50 H₂/N₂ at 50 mL/min total flow.



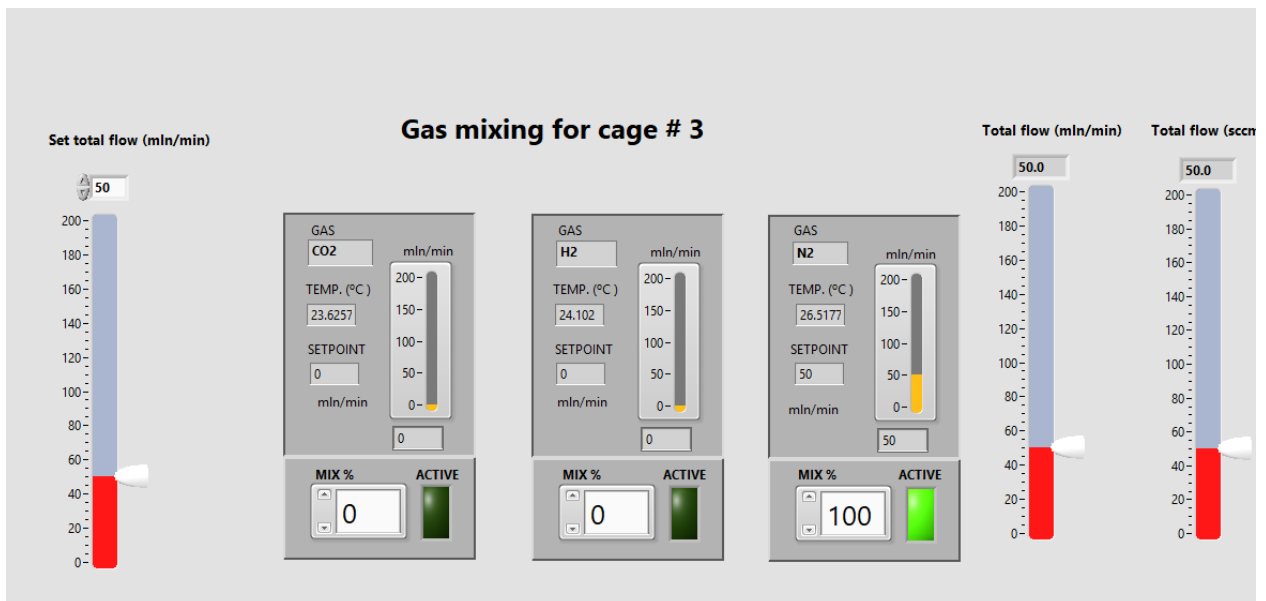
- 8) Set eurotherm to remote, increase temperature to 300°C at 5°C per min, total = 3 hours and cover reactor with insulation.

COM1.ID001-3208 - Watch/Recipe Editor

List	Parameter	Description	Value
INPUT	EMValue	EM Input Value	23.13
SP	SP1	Setpoint 1	300.00
SP	WorkingSP	Working Setpoint	27.35
SP	Rate	Setpoint Rate Limit \	5.00
SP	RampUnits	Setpoint Ramp Units	MIN (0)
CTRL	OutputHighLimit	Output High Limit	10.00
SP	SPHighLimit	Setpoint High Limit	500.00
CTRL	OutputHighLimit	Output High Limit	10.00
CTRL	ActiveOut	Working Output	3.24

2. Cooling down the reactor and starting reaction

1) Switch to N₂ flow at 100% (50 mL/min), then set ramp rate to 0 followed by temperature to 20°C.



Memory Device Panel Terminal Wiring Watch/Recipe OPC Scope

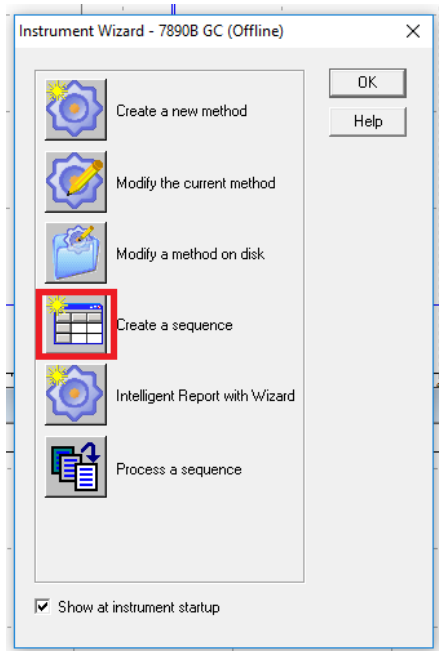
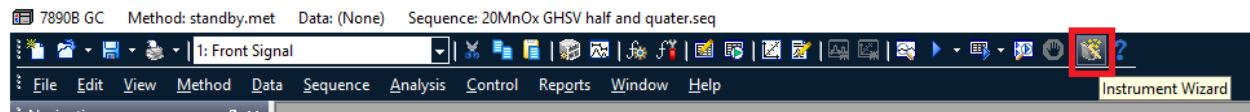
COM1.ID001-3208 - Watch/Recipe Editor

List	Parameter	Description	Value
INPLIT	PVInValue	PV Input Value	247.77
SP	SP1	Setpoint 1	21.00
SP	WorkingSP	Working Setpoint	21.00
SP	Rate	Setpoint Rate Limit \	OFF (0) ▾
SP	RampUnits	Setpoint Ramp Units	MIN (0) ▾
CTRL	OutputHighLimit	Output High Limit	10.00
SP	SPHighLimit	Setpoint High Limit	500.00
CTRL	OutputHighLimit	Output High Limit	10.00
CTRL	ActiveOut	Working Output	0.00

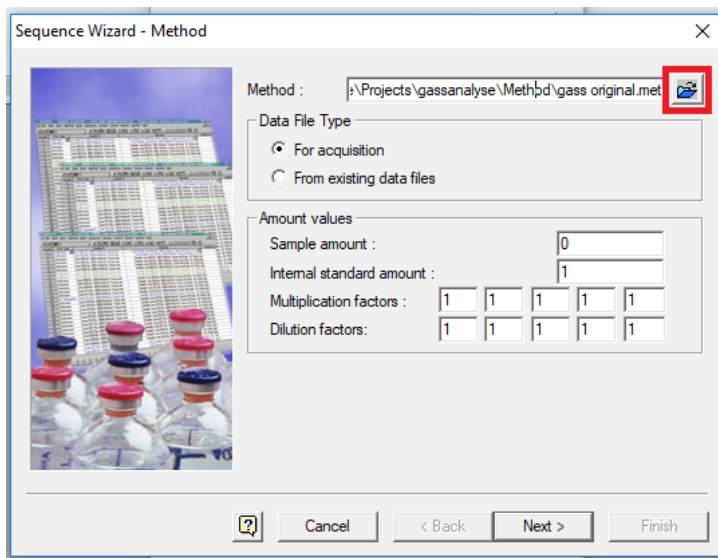
- 2) Remove isolation from the top of the reactor when it is about 200°C.
- 3) Wait for below 60°C, about 30 min.
- 4) Start reactant mixture flow: 27.2% CO₂, 54.2 H₂, 18.6% N₂ (to get close to 1:3:1 ratio (depending on the flow calibration) at total 66 mL/min.
- 5) Wait for 15 min, then close the pressure relief valve and cover the reactor.

3. GC procedure

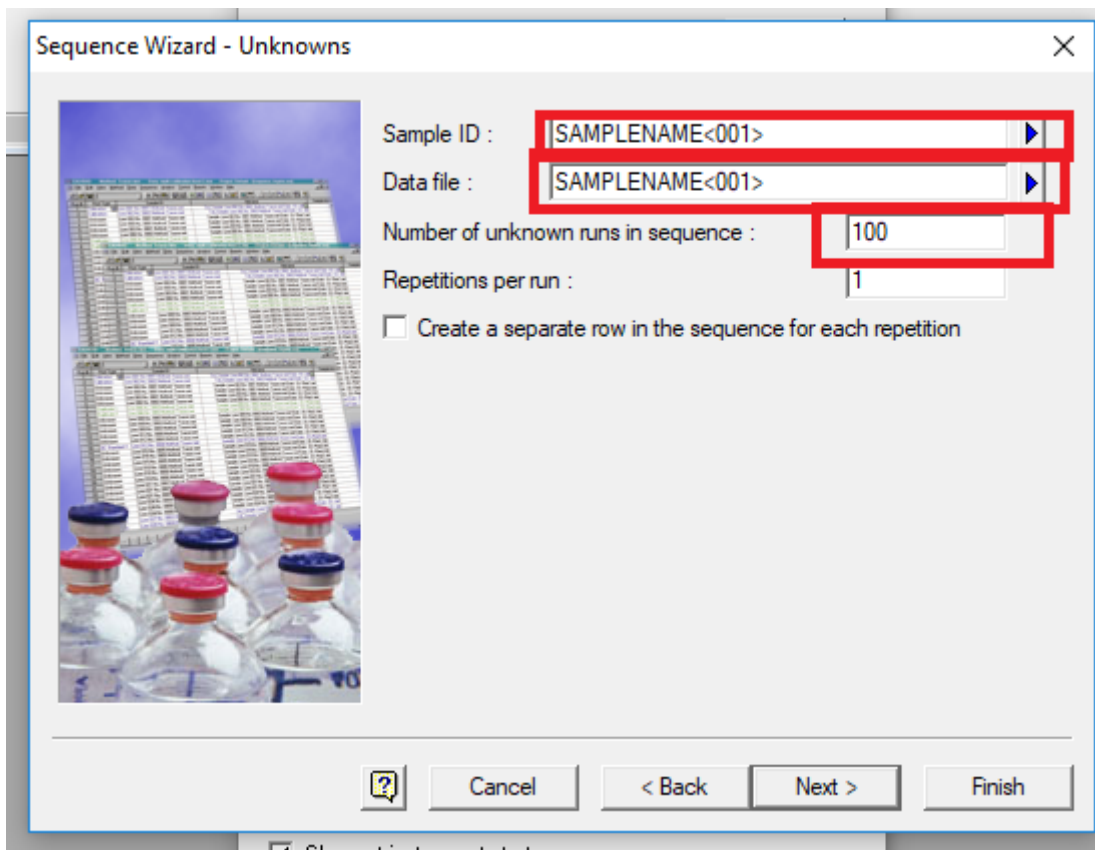
1. Go to instrument wizard -> create sequence



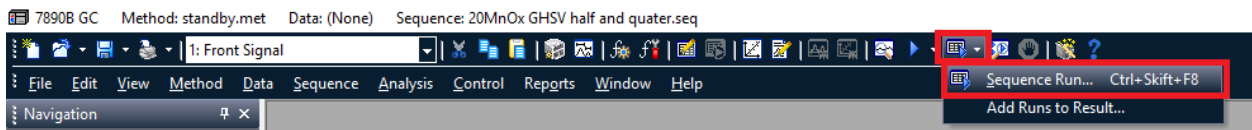
2. Select gas original method -> click next.



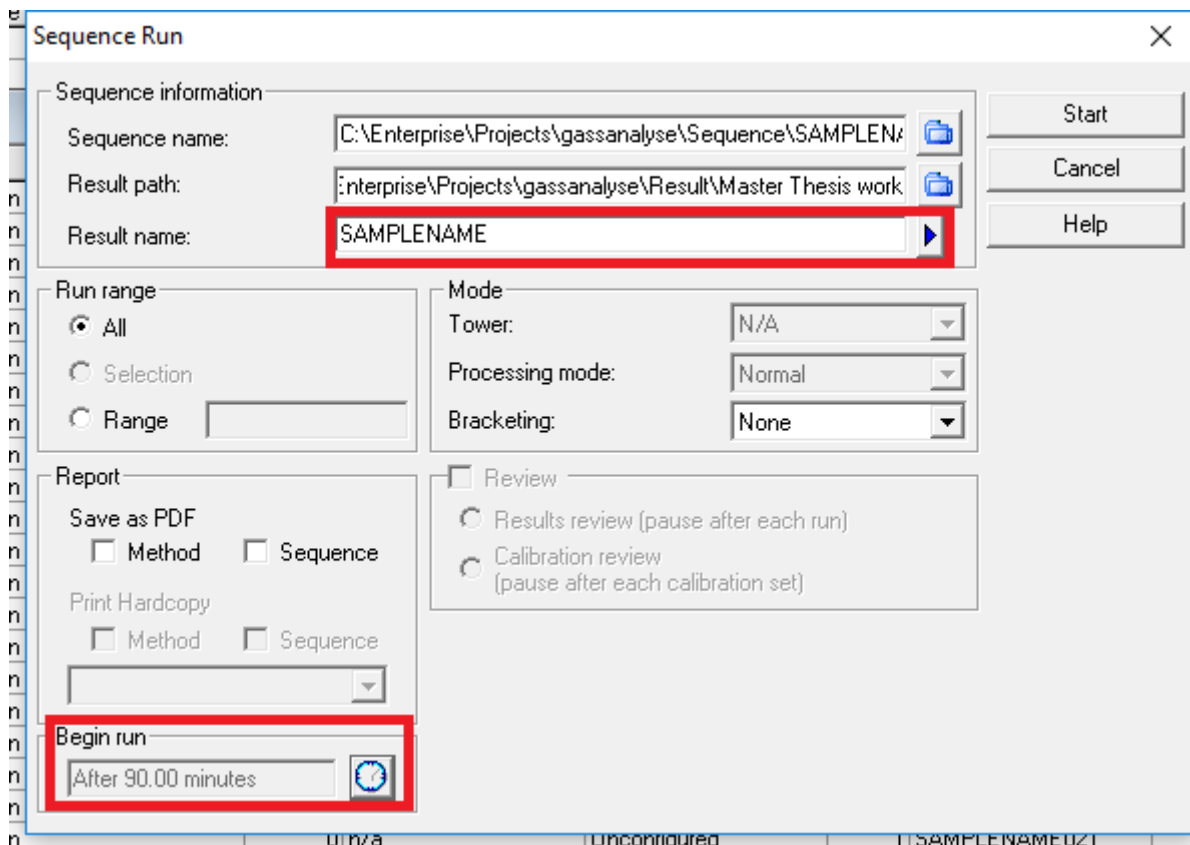
3. Write the same name in sample ID and data file, add increment number (<001>), set number of unknown runs in sequence to 100 (more if long term test) and click finish. NB. Every run takes at least 14 minutes.



4. Go to sequence run -> Click Yes to save sequence -> write name of sample -> click save



5. Write name of the sample in result name -> Change begin immediately to 90 min after closing the relief valve -> click start.



7. Turn on the heating of the wires (white box) and check it is stable at 120°C.

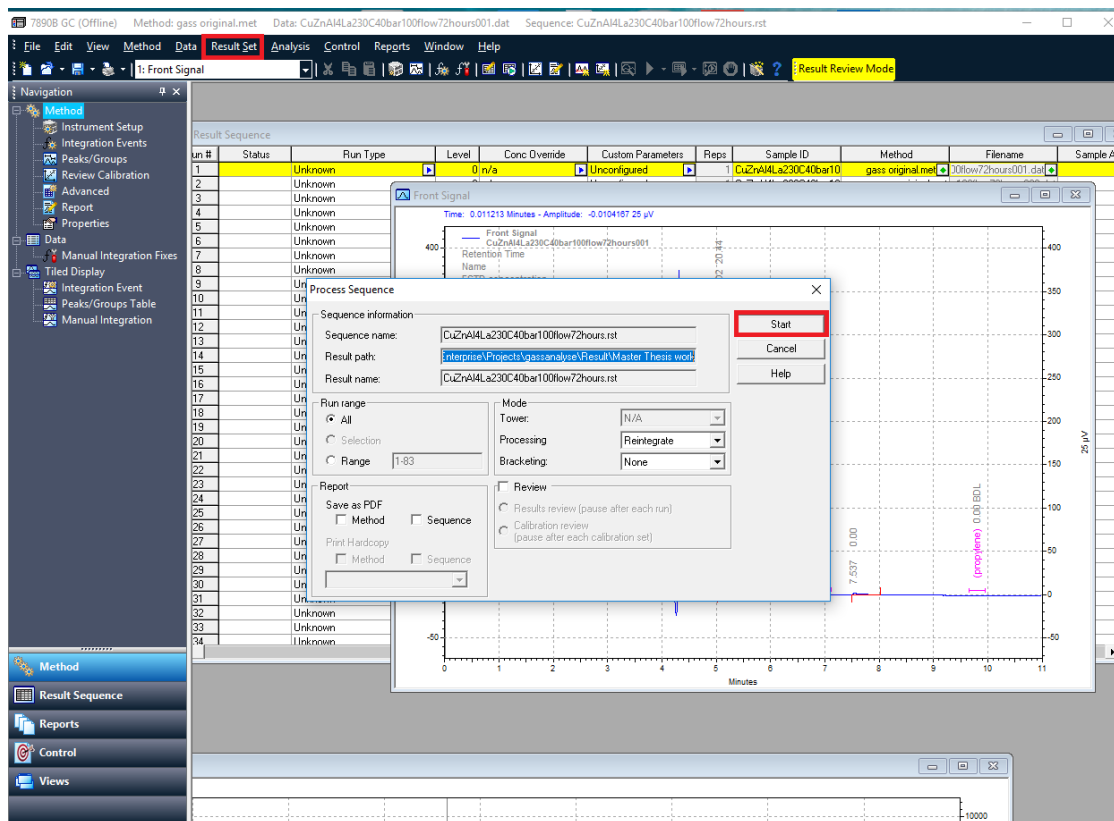
8) Start heating 1 hour after GC starts, 5°C/min and desired reaction temperature

Result extraction

Go to C:\Users\IPT-lab\Desktop\Excel file from GC -> open

Data can also be extracted using the 7890B GC (offline) application.

1. First, click stop run → select stop sequence after current run completes -> click OK
2. Open the 7890B GC (offline) → File → Open → Result Set.
3. Go to result set, select process and start.
4. Results will be found at C:\Users\IPT-lab\Desktop\Excel file from GC.



4. After reaction

1. Click stop run -> select stop sequence after current run completes -> click OK.
2. Switch to N₂ flow, set eurotherm to local, turn off the white box, open relief valve, wait 15 minutes.
3. Turn off the flow.

The screenshot shows a software interface with a menu bar (Analysis, Control, Reports, Window, Help) and a toolbar. A red box highlights a stop button in the toolbar. The main window displays a chromatogram with a y-axis ranging from 6000 to 10000 and a blue signal line. A table on the right lists sample IDs and methods.

Sample ID	Method
CuZnAl50mg230C40bar0	gass origi
CuZnAl50mg230C40bar0	gass origi

A 'Stop Run' dialog box is open, featuring a traffic light icon and five radio button options. The option 'Stop sequence after current run completes' is selected and highlighted with a red box.

- Stop current run only
- Stop current run and sequence run
- Stop sequence after current run completes
- Stop all run queue items you submitted
- Stop all run queue items

Buttons for OK, Cancel, and Help are located at the bottom of the dialog box.